INFORMATION TO USERS

This manuscript has been reproduced from the microfilm master. UMI films the

text directly from the original or copy submitted. Thus, some thesis and

dissertation copies are in typewriter face, while others may be from any type of

computer printer.

The quality of this reproduction is dependent upon the quality of the copy

submitted. Broken or indistinct print, colored or poor quality illustrations and

photographs, print bleedthrough, substandard margins, and improper alignment

can adversely affect reproduction.

In the unlikely event that the author did not send UMI a complete manuscript and

there are missing pages, these will be noted. Also, if unauthorized copyright

material had to be removed, a note will indicate the deletion.

Oversize materials (e.g., maps, drawings, charts) are reproduced by sectioning

the original, beginning at the upper left-hand comer and continuing from left to

right in equal sections with small overlaps.

Photographs included in the original manuscript have been reproduced

xerographically in this copy. Higher quality 6" x 9" black and white photographic

prints are available for any photographs or illustrations appearing in this copy for

an additional charge. Contact UMI directly to order.

Bell & Howell Information and Learning 300 North Zeeb Road, Ann Arbor, MI 48106-1346 USA

800-521-0600

NOTE TO USERS

Page(s) not included in the original manuscript are unavailable from the author or university. The manuscript was microfilmed as received.

5-2

This reproduction is the best copy available.

UMI

Application of the MSR Impact-Echo System for Crack Detection in Concrete Dams

by

Philippe Guevremont

A thesis submitted to the Faculty of Graduate Studies and Research in partial fulfilment of requirements of the Degree of Master of Engineering

Department of Mining and Metallurgical Engineering
McGill University
Montreal, Canada

© Philippe Guevremont, 1997



National Library of Canada

Acquisitions and Bibliographic Services

395 Wellington Street Ottawa ON K1A 0N4 Canada Bibliothèque nationale du Canada

Acquisitions et services bibliographiques

395, rue Wellington Ottawa ON K1A 0N4 Canada

Your file Votre reference

Our file Notre relérence

The author has granted a nonexclusive licence allowing the National Library of Canada to reproduce, loan, distribute or sell copies of this thesis in microform, paper or electronic formats.

The author retains ownership of the copyright in this thesis. Neither the thesis nor substantial extracts from it may be printed or otherwise reproduced without the author's permission.

L'auteur a accordé une licence non exclusive permettant à la Bibliothèque nationale du Canada de reproduire, prêter, distribuer ou vendre des copies de cette thèse sous la forme de microfiche/film, de reproduction sur papier ou sur format électronique.

L'auteur conserve la propriété du droit d'auteur qui protège cette thèse. Ni la thèse ni des extraits substantiels de celle-ci ne doivent être imprimés ou autrement reproduits sans son autorisation.

0-612-37263-4



ABSTRACT

Concrete dams suffer from many forms of deterioration and specifically the presence of internal cracks. Presently, the borehole technique is used to evaluate the orientation of the cracks and the mechanical properties of the concrete. High costs are associated to this method as well as the need to extrapolate results between adjacent boreholes. Nondestructive testing is seen as a possible solution for reducing high inspections costs and increase the precision of crack location. This thesis presents the theoretical and practical aspects of a nondestructive method called the Miniature Seismic Reflection (MSR Impact-Echo) system. The system can evaluate a crack profile and determine the quality of concrete from one test surface. The objective of the research is to extend the capabilities of the system to crack detection in large scale concrete structures. Results are presented with respect to inclined crack detection, the minimum crack thickness detectable, and tests performed on a section of a concrete gravity dam. The experiments are part of a long term research project between McGill University and the "Institut de Recherche en Électricité d'Hydro-Québec (IREQ)".

RÉSUMÉ

Les barrages en béton souffrent de plusieurs formes de détériorations et plus spécifiquement, de fissures internes. La technique du forage est employée pour évaluer ces fissures et déterminer les propriétés mécaniques du béton de masse. Des coûts élevés sont souvent attribués à ses campagnes de forages. Parfois, il est nécessaire d'extrapoler les résultats entre des forages adjacents. L'inspection non destructive est une solution possible pour réduire les coûts d'inspections ainsi qu'augmenter la précision des auscultations. Ce mémoire discute des aspects théoriques et pratiques de la méthode "Miniature Seismic Reflection" (MSR Impact-Echo). Ce système est capable de localiser des fissures et aussi évaluer les propriétés dynamiques du béton. Le but principal de cette recherche est d'augmenter la profondeur d'auscultation du système pour des applications futures sur des barrages en béton. Le mémoire présente des résultats relatifs à des essais pour déterminer l'inclinaison d'une fissure et l'épaisseur minimale détectable par le système. Des essais ont aussi été effectués sur une section de barrage poids. Ce projet de recherche est une collaboration entre l'Université McGill et l'Institue de Recherche en Électricité d'Hydro-Québec (IREQ).

ACKNOWLEDGMENTS

The work presented in this thesis would not have been possible without the support and guidance of my thesis supervisor Professor Ferri P. Hassani. I thank him greatly for the opportunity of working on such an interesting and fulfilling project. I would like to thank Dr. Mohammed Momayezzadeh for his help throughout this project and for always being available to answer technical questions as often as they came. I would also like to sincerely thank him for reviewing the content of this manuscript. The author is grateful to Dr. Afshin Sadri, who never hesitated to help and guide me in the right direction.

Special thanks are extended to Dr. Kaveh Saleh for allowing me to perform the experiments at the Institute of Research of Hydro-Québec (IREQ). His continuous involvement and guidance during the course of the project is also greatly acknowledged. To Mr. Stéphane Tremblay, I wish to sincerely thank for his help throughout all phase of this project. The construction the test samples would not have been possible without his involvement. Everyone of "Equipe Béton" at IREQ is greatly acknowledged for their support during the course of this work.

Sincere thanks are extended to Dr. Parviz Mottahed and Dr. Sharhiar Talebi of CANMET for their involvement and technical support.

I am very grateful to my parents who have always supported me emotionally and financially throughout my studies at McGill. I wish to extend my most sincere thanks to my fiancé, Stamatia Gazetas, for her unconditional support and love during the course of this degree.

Last but not least, the author wishes to acknowledge the help and support of the following people: Mr. Louis-Alexandre Whissell, Mr. Alexander Shinobe, Mr. Richard Lapointe, and Mr. Robert Lapointe.

TABLE OF CONTENTS

ABSTRACT	i
RÉSUMÉ	ii
ACKNOWLEDGMENTS	iii
TABLE OF CONTENTS	iv
LIST OF FIGURES	vii
LIST OF TABLES	ix
CHAPTER 1: INTRODUCTION	1-1
1.1 HYDRO-QUÉBEC'S NEEDS	1-1
1.2 RESEARCH OBJECTIVES	1-2
1.3 OUTLINE OF THE THESIS	1-3
CHAPTER 2: LITERATURE REVIEW	2-1
2.1 NONDESTRUCTIVE TESTING (NDT) METHODS	2-1
2.1.1 Electrical Methods	2-2
2.1.2 Electromagnetic Methods	2-3
2.1.3 Magnetic Methods	2-4
2.1.4 Infrared Thermography	2-5
2.1.5 Nuclear Methods	2-6
2.1.6 Acoustic Emission Methods	2-8
2.1.7 Ultrasonic Methods	2-9
2.1.8 Mechanical Methods	2-16
2.2 NDT METHODS USED AT HYDRO-QUÉBEC	2-19
2.2.1 Case study: Acoustic Emission test at the Paugan Dam	2-19
2.2.2 Laboratory NDT testing and Hydro-Québec	2-20
2.3 APPLICATIONS OF MININATURE SEISMIC TECHNOLOGY	2-25
2.3.1 Mine Shafts and Circular Structures	2-26
2.3.2 Concrete Slabs	2-26
2.3.3 Concrete Parking Structures	2-27
2.3.4 Concrete Dams, Bridges, Walls, and Pre-stressing Ducts	2-27
2.3.5 Concrete Beams and Columns	2-29
2.3.6 Other Concrete Structures	2-29
2.4 FINAL NOTES	2-30

CHAPTER 3: THEORETICAL NOTIONS OF THE	
MSR IMPACT-ECHO METHOD	3-1
3.1 FUNDAMENTALS OF ELASTIC WAVE PROPAGATION IN SOLIDS	3-1
3.1.1 P-waves	3-1
3.1.2 S-waves	3-2
3.1.3 R-waves	3-3
3.1.4 Seismic Wave Velocities	3-4
3.1.5 Reflection and Refraction	3-5
3.1.6 Diffraction	3-8
3.1.7 Attenuation of Waves in Heterogeneous Solids	3-9
3.2 THE MINIATURE SEISMIC REFLECTION (MSR) METHOD	3-10
3.2.1 Theoretical Background	3-11
3.2.2 Instrumentation of the MSR Impact-Echo System	3-14
3.3 DATA ACQUISITION AND DATA ANALYSIS USING THE	
FAST FOURIER TRANSFORM (FFT)	3-22
3.3.1 Signal Conditioning	3-23
3.3.2 Signal Recording	3-23
3.3.3 Data Analysis by the Fast Fourier Transform (FFT)	3-26
3.4 FINAL NOTES	3-29
CHAPTER 4: RESEARCH OBJECTIVES	4-1
4.1 SCOPE OF WORK	4-1
4.2 RESEARCH NEEDS AND OBJECTIVES	4-2
4.2.1 Research needs for the MSR Impact-Echo System	4-2
4.2.2 Research objectives	4-3
4.2.3 Summary of Research Needs and Objectives	4-4
4.3 TEST BED CONFIGURATIONS AND DESCRIPTIONS	4-5
4.3.1 Inclined Crack Detection	4-5
4.3.2 Crack Thickness Investigation	4-9
4.3.3 Investigation of a Section of a Concrete Gravity Dam	4-14
CHAPTER 5: TEST RESULTS AND DISCUSSION	5-1
5.1 INCLINED CRACK DETECTION	5-1
5.1.1 Test Methodology	5-2
5.1.2 Static Material Tests and Results	5-2

5.1.3 Dynamic Material Tests and Results	5-7
5.1.4 Initial Crack Detection Results and Discussion	5-7
5.1.5 Final Crack Detection Results and Discussion	5-18
5.1.6 Conclusions of the Inclined Crack Detection Tests	5-21
5.2 CRACK THICKNESS INVESTIGATION	5-24
5.2.1 Test Methodology	5-24
5.2.2 Static Material Tests and Results	5-24
5.2.3 Dynamic Material Tests and Results	5-25
5.2.4 Dry Crack Test Results and Discussion	5-26
5.2.5 Saturated Crack Test Results and Discussion	5-27
5.2.6 Conclusions of the Crack Thickness Investigation Tests	5-28
5.3 INVESTIGATION OF A SECTION OF A CONCRETE	
GRAVITY DAM	5-29
5.3.1 Test Methodology	5-29
5.3.2 East Face Testing Results and Discussion	5-32
5.3.3 South Face Testing Results and Discussion	5-35
5.4 FINAL NOTES	5-38
CHAPTER 6: SOFTWARE DEVELOPMENT	6-1
6.1 SOFTWARE MODIFICATIONS	6-1
6.2 COMPUTER PROGRAM DESCRIPTION	6-2
6.3 FINAL NOTES	6-3
CHAPTER 7: CONLUSIONS	7-1
7.1 SUMMARY OF THE RESEARCH	7-1
7.2 CONCLUSIONS	7-2
7.2.1 Inclined Crack Detection	7-2
7.2.2 Crack Thickness Investigation	7-3
7.2.3 Investigation of a Section of a Concrete Gravity Dam	7-3
7.3 FUTURE WORK	7-4
REFERENCES	R-1
APPENDIX A	A-1

LIST OF FIGURES

Figure 2.1	Application of the electrical resistivity method	2-3
Figure 2.2	Nuclear radiometry of concrete samples	2-7
Figure 2.3	Suggested test configurations for ultrasonic testing	2-11
Figure 2.4	Schematic of Pulse-Echo and Pitch-Catch ultrasonic methods	2-13
Figure 2.5	Sonic tomography testing	2-16
Figure 2.6	Principle and test Configuration of the SASW method	2-17
Figure 2.7	Three dimensional view of crack surface found by Impact-Echo	2-22
Figure 2.8	Ray paths for sonic tomography tests	2-24
Figure 2.9	Tomographic image of P-waves velocities	2-25
Figure 3.1	P-wave propagation inside and elastic material	3-2
Figure 3.2	S-wave propagation inside and elastic material	3-3
Figure 3.3	R-wave propagation inside and elastic material	3-3
Figure 3.4	Reflection and refraction of an incident P-wave	3-7
Figure 3.5	Angles of reflected and refracted body waves	3-8
Figure 3.6	Incident wave diffraction caused at a crack tip	3-8
Figure 3.7	P-wave reflections from concrete-steel and concrete-air interfaces	3-13
Figure 3.8	Schematic of the MSR Impact-Echo system	3-14
Figure 3.9	Propagation of P-, S-, and R-waves after initial impact	3-15
Figure 3.10	Waveform generated on the surface of a concrete test object	3-16
Figure 3.11	Estimation of the contact time by looking at the R-wave	3-17
Figure 3.12	Polar axes of a quartz crystal	3-19
Figure 3.13	Deformation of and X-cut quartz plate	3-19
Figure 3.14	Flowchart of the FFT algorithm developed on the GAUSS system	3-30
Figure 4.1	Schematic placement of the artificial cracks in the concrete slabs	4-7
Figure 4.2	Photos of placement of the artificial cracks in the formwork	4-8
Figure 4.3	Concrete slab showing the profile of the artificial crack	4-9
Figure 4.4	Schematic of the experimental setup of the crack thickness tests	4-10
Figure 4.5	Formwork used to mold the concrete blocks	4-11
Figure 4.6	Rigid metal frame used to support the two concrete blocks	4-12
Figure 4.7	Adjustment assembly used to align both concrete blocks	4-12
Figure 4.8	Clamping assembly anchored to each side of the concrete blocks	4-13
Figure 4.9	Dimensions of the concrete gravity dam section built at IREO	4-15

Figure 4.10	Construction of the concrete foundation slab	4-16
Figure 4.11	Formwork used to build the concrete gravity dam section	4-17
Figure 5.1	Flowchart of experimental procedure for inclined crack tests	5-3
Figure 5.2	Test grid placed on the impact surface of all three slabs	5-8
Figure 5.3	Results from initial test at point C3 on slab 1	5-11
Figure 5.4	Top view of a concrete slab with actual depths of internal crack	5-12
Figure 5.5	Results of initial MSR Impact-Echo tests on slabs 1,2, and 3	5-16
Figure 5.6	Results of final MSR Impact-Echo tests on slabs 1,2, and 3	5-22
Figure 5.7	MSR Impact-Echo test equipment used on the concrete blocks	5-25
Figure 5.8	Dry crack condition time domain waveform and frequency spectrum	5-26
Figure 5.9	Top view of the blocks showing saturation of the crack interface	5-27
Figure 5.10	Saturated crack time domain waveform and frequency spectrum	5-28
Figure 5.11	Test grids placed on the concrete gravity dam section	5-30
Figure 5.12	MSR Impact-Echo test equipment used on the dam	5-30
Figure 5.13	Scaffolding used to access the higher sections of the dam	5-31
Figure 5.14	P- and S- wave velocities obtained on the east face of the dam	5-33
Figure 5.15	Dynamic material properties determined on the east face of the dam	5-34
Figure 5.16	P- and S- wave velocities obtained on the south face of the dam	5-36
Figure 5.17	Dynamic material properties observed on the south face of the dam	5-37
Figure 6.1	Flowchart of new program for defect depth location	6-4
Figure 6.2	Flowchart of new program for determining dynamic properties	6-5

LIST OF TABLES

Table 3.1	Specific acoustic impedance of various common material	3-6
Table 3.2	Relationships between elastic wave velocities and dynamic elastic material properties	3-13
Table 4.1	Research needs and objectives	4-5
Table 4.2	Artificial crack materials	4-6
Table 5.1	List of ASTM standards used for testing concrete test cylinders	5-4
Table 5.2	Physical dimensions of the concrete test cylinders	5-5
Table 5.3	Physical dimensions of the cylinders used for tensile resistance tests	5-5
Table 5.4	Results of static testing on concrete cylinders	5-6
Table 5.5	Dynamic properties of the concrete cylinders	5-7
Table 5.6	Specifications of the MSR Impact-Echo impact devices	5-9
Table 5.7	Initial P-wave velocities for each concrete slab	5-10
Table 5.8	Initial test results for slabs 1,2, and 3	5-17
Table 5.9	Final test results for slabs 1,2, and 3	5-23
Table 5.10	Dynamic properties of the concrete blocks	5-25

INTRODUCTION

The main objective of the work presented in this thesis is to develop a nondestructive testing (NDT) method that will locate cracks in concrete dams. The intention is to create an affordable, continuous, and user friendly method designed to investigate large scale concrete structures. The use of miniature seismic reflection (MSR) theory is at the basis of this study. For almost a decade, the Sub-Surface Sensing Laboratory of McGill University has been developing a nondestructive method called the MSR Impact-Echo technique. The system was initially designed to evaluate the thickness of concrete linings in mine shafts and tunnels. The aim of the research is to adapt this technique for use on concrete dams.

The information found in the present chapter reflects the needs of Hydro-Québec in finding a reliable and efficient testing method for their concrete infrastructure. The following pages also present the main research objectives of the work and a summary of the content and organization of the thesis.

1.1 HYDRO-QUÉBEC'S NEEDS

Hydro-Québec is a state run agency and a major provider of electricity in the province of Quebec and elsewhere. The company concentrates its research in many fields related to the production of hydroelectric power. A majority of the research work is performed at the "Institut de Recherche en Électricité d'Hydro-Québec" (IREQ). Research related to concrete technology is conducted principally by the Concrete Research Team that is based at IREQ. The research team concentrates its work on finding effective repair methods and materials for use on Hydro-Québec's vast concrete infrastructure.

Presently, Hydro-Québec uses boreholes to investigate the condition of their concrete structures. The study of the extracted cores allows professionals to detect the orientation and continuity of internal cracks. Degradation processes that affect the concrete can also be determined. The static material properties and the chemical content

of concrete is performed when required. Borehole investigation is a widely accepted technique for testing concrete structures according to related international standards.

However, there are some drawbacks associated to boreholes such as high costs and limited information from the cores. High costs are linked to the time needed to extract and analyze the cores which involve high labour costs and the use of specialized laboratories.

The information obtained from the cores is generally related to a small region surrounding the borehole. The distance separating a series of boreholes is often substantial when testing large concrete dams. In some instances, the results are interpolated between adjacent boreholes. The accuracy of the interpolation is therefore very important and, consequently, difficult. In order to increase the validity of the results, research at IREQ has focused on the use of robotics, modeling, and water pressure testing. Research is driven by the need to increase the safety level of the concrete infrastructure and develop economical inspection and repair methods.

In 1995, Hydro-Québec approached McGill University to develop an NDT method based on MSR technology. The project objective focuses on replacing existing destructive techniques that are costly and slow with a quick and precise method that can locate cracks in concrete dams of various shapes.

1.2 RESEARCH OBJECTIVES

The research discussed in the next chapters focuses on determining the capabilities of the MSR Impact-Echo system. Once the capabilities of the system are known, it will be possible to modify the system in order to reach the main goal of finding cracks in concrete dams.

The first objective of the tests is to determine if the system can map the inclined profiles of cracks in concrete. Most cracks in concrete dams have inclined surfaces. The second objective of the research is to evaluate the minimum crack thickness detectable with the MSR Impact-Echo system. The third objective is to assess the penetration depth of the system with the current instrumentation.

Laboratory and field tests were performed on small and large scale concrete elements to help evaluate the preceding objectives. A complete description of the research objectives is given in Chapter 4 of the thesis.

1.3 OUTLINE OF THESIS

The following paragraphs outline the main composition and organization of the thesis. Chapter 2 is an overview of NDT methods used on concrete elements and structures. The focus is on each method's ability to detect cracks in concrete.

Chapter 3 describes the MSR Impact-Echo system and presents the theory behind its operation. As previously mentioned, the system is based on miniature seismic reflection in elastic media. The piezoelectric effect of materials and initial concepts of the Fast Fourier Transform (FFT) technique are also presented in this chapter.

Chapter 4 discusses in detail the research needs and objectives related to the evaluation of the MSR Impact-Echo system for use on large concrete structures. The chapter focuses on the experimental setup of three test beds.

Chapter 5 presents results obtained from investigating three different test beds. Tests performed were inclined crack detection, minimum crack thickness tests, and the evaluation of a section of a concrete gravity dam. Investigations of the first two experiments were in laboratory conditions. The third experiment was performed in field conditions.

Chapter 6 discuses software development that was required for the analysis of vast amounts of data that originated from investigating the concrete gravity dam discussed in Chapter 4 and Chapter 5.

Chapter 7 summarizes the results, presents conclusions, and suggests further development of the MSR Impact-Echo system.

LITERATURE REVIEW

Nondestructive technology has come a long way since the 1980's. There has been developments in the medical, metallurgical, and mining industries and most recently in civil engineering. Notable technological achievements stem from the use of microseismics for internal investigations of materials. Recent developments mainly focus on solving specific problems with the appropriate techniques and methodologies. It is difficult to find an NDT method capable of solving a multitude of problems. Most methods concentrate on measuring one of many physical or chemical properties of a material. Accordingly, it is easier to investigate homogeneous materials such as metals. Concrete is a heterogeneous material composed of water, cement, sand, aggregates, and often reinforcement bars. The internal matrix of the concrete paste partially explains the difficulty to detect internal anomalies in that material.

There are a multitude of NDT applications that involve the use of complex methodologies. To obtain a better grasp of these methods, a brief literature review is presented in the following sections. A complete discussion of the various NDT methods is found in an exhaustive literature review published at "l'Institut de Recherche en Électricité d'Hydro-Québec" (IREQ) in November 1996 [see Hassani et al., 1996a]. The work was co-authored by the author of this thesis. The review that follows focuses on each method's ability to detect cracks in large scale concrete structures.

Section 2.1 describes NDT methods other than the *MSR Impact-Echo* method. Section 2.2 is an overview of NDT methods used at Hydro-Québec. The last section explains current work on *MSR Impact-Echo* technology with respect to scientific research and practical applications.

2.1 NONDESTRUCTIVE TESTING (NDT) METHODS

It is important to point out that there are many NDT techniques used in various industries that do not apply to concrete investigation. Most technical developments for heterogeneous materials stem from the mining and geophysics industries. Researchers have always tried to adapt NDT applications from one industry to another. The concrete

industry is of no exception and widespread NDT research in concrete is relatively recent. Many researchers view NDT as the wave of the future for in situ and laboratory investigations. Presently, instrumentation is available on the market for many types of concrete testing. However, each of these techniques have their limitations. The following sections describe these techniques with respect to their capability for crack detection in concrete structures such as dams.

2.1.1 Electrical Methods

Concrete exhibits an electrical nature and hence possesses electrical properties. Electrical conduction in humid concrete is essentially an electrolytic phenomenon. An electrolyte is a material or a solution that can be subjected to electrical conductivity [Nikkanin, 1962]. The resistance of an electrolyte is directly proportional to its length and inversely proportional to its cross sectional surface area. The passage of direct current through an electrolytic material polarizes its particles. The polarization effect creates a readable potential at electrodes placed on the test element. Electrical potential differences at the electrodes is an indication of a material's internal electrical resistance.

The dielectric constant of a material is a fundamental part of this method. The dielectric constant is an indication of the alignment velocity of molecular dipoles in a magnetic field. In concrete pores or cracks, free water has a dielectric constant superior to the cement, sand, and aggregates. The average value of the dielectric constant of concrete is a function of these elements and that of the free water content. Electrical methods serve to evaluate the free water content of concrete. The water content is used to determine the shrinkage level and the thermal conductivity of the material. It also indicates the cracking potential of concrete elements. A high water content may lead to an increase in cracking due to the expansion of ice crystals in the pore structure of the concrete. The result is an increase in the internal stresses in the medium.

Electrical methods can also yield the humidity profiles inside concrete samples. According to Bracs et al. (1970), by analyzing the local electrical resistance of concrete samples, it is possible to detect a reduction in electrical resistance caused by the presence of humidity in the concrete. The reduction can be measured by inserting electrical resistance probes in the concrete.

Electrical resistivity techniques have been used for a long time for geophysical exploration purposes. In civil engineering, the technique is mainly used to measure the thickness of pavements. In 1968, Moore developed the first in situ application of the electrical resistance technique on pavements. Pavements often have an electrical

resistance that is different from those encountered underneath the pavement itself. Pavement thickness measurement consists of placing four (4) electrodes in a straight line on the surface (see Figure 2.1). The distance separating the electrodes is the same. For practical reasons, the current is assumed to penetrate to a depth equal to the spacing between the electrodes D1 and D4. Changes in the current and potential readings allow the users to determine the depths of subsurface materials.

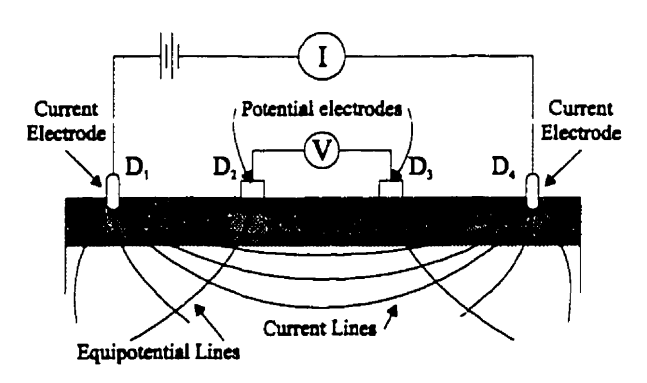


Figure 2.1

Application of the electrical resistivity method to a section of concrete pavement [after Robertshaw and Brown, 1955].

It is important to note that every electrical resistivity analysis technique assumes that the resistivity of each layer is constant and slightly varies with depth. This concept is actually very far from reality [Hassani et al., 1989]. Presently, there is very little information in the literature regarding the potential use of this technique for crack or surface delamination detection in concrete. However, research indicates the possibility of using linear polarization to calculate the corrosion rate of steel reinforcement bars. Due to a lack of information, it is difficult to recommend this method as a possible solution for crack detection in large scale concrete structures.

2.1.2 Electromagnetic Method

The following discussion will concentrates on the radar inspection method. It is based on the propagation of electromagnetic (EM) waves inside a material. When testing concrete, it is common to use short-pulse radar. Ground Probing Radar (GPR) is a commercially available system that can be used on concrete. The methodology of this system is comparable to ultrasonic and stress-wave reflection methods, except for the use of EM waves. The radar system transmits a pulse followed by a timed pause. During the pause, the system acquires the reflected EM pulse from the test medium. A typical radar system includes a control unit, a monostatic antenna that transmits and receives signals,

an oscillograph, and an energy source. When testing concrete, it is best to use a high resolution antenna (short-pulse) with maximum pulse time of 1 nanosecond. It is possible to test thin concrete slabs with this type of antenna. Clemeña (1991) states that if concrete has a dielectric constant of 6, it is possible to measure a thickness of 31 to 61 millimeters.

When a monostatic antenna generates an EM pulse, many wave reflections occur inside the material. Interfaces with different dielectric constants, other than that of concrete, cause the reflections. Each reflected EM wave reaches the antenna at different times. The depth of the interfaces and their respective dielectric constants govern the arrival times of the EM waves.

Radar applications on concrete include delamination detection, thickness measurement and also the location of internal defects and steel reinforcement. Recent research on the applications of GPR to concrete show promising results. Not long ago, the Sub-Surface Sensing Laboratory of McGill University used a GPR system to detect honeycombing in concrete walls used to support a multi-ton press. GPR can also monitor cement hydration, concrete resistance development, concrete admixture effects, and water content [Clemeña, 1991]. The main limitations of this system are the penetration depth of the EM waves in concrete and the resolution of the acquisition system for precise crack location. The principal advantages are the rapid data processing techniques, real time observation of subsurface defects, and the ease of use of the system.

2.1.3 Magnetic Methods

Magnetic nondestructive techniques find their applications mainly on metal elements. For example, they essentially depend on the magnetic properties of concrete reinforcement and the response of hydrogen nuclei in concrete when subjected to magnetic fields. These techniques are used to locate reinforcement bars and evaluate the water content of concrete [Lauer, 1991]. There are three main magnetic nondestructive testing methods: a) magnetic induction, b) flux leakage, and c) nuclear magnetic resonance (NMR).

Magnetic induction only applies to applications on ferromagnetic materials such as reinforcement. In general, reinforcement location is the main application of this technique. Crack detection is not yet possible. The instrumentation includes two coils. One of the coils is connected to an electrical source. Closely placing the coils together induces a small voltage in the other coil. When they pass over a ferromagnetic material such as reinforcement bars, a significant voltage increase occurs in the second coil. The amplitude of this voltage is a function of the position, geometry, and magnetic

characteristics of the ferromagnetic material. The precision of these instruments is $\pm 2\%$ up to a concrete thickness of 152 mm [Lauer, 1991].

Flux Leakage is another application for ferromagnetic materials. When a ferromagnetic material is magnetized, magnetic flux lines propagate through the material and complete a trajectory between two magnetic poles. Typically, there is no flux leakage in a uniform material. In the case of a cracked reinforcement bar, the magnetic permeability changes. Flux leakage occurs at the discontinuity. It is possible that cracked reinforcement is an indication of concrete cracking in the surrounding area [Lauer, 1991].

Nuclear Magnetic Resonance (NMR) methods are base on the interaction between magnetic dipole moments and magnetic fields. The technique helps determine the water content of concrete. Lauer (1991) mentions that the the water content precision of this method is ± 2 % for a 70 mm thick concrete sample. Crack location in concrete is not possible for the moment.

In the literature, there is very little information on crack detection in concrete structures with these methods. Material characterization remains the essential application of these techniques. At this time, it is not possible to consider these methods as realistic solutions for crack detection in concrete structures.

2.1.4 Infrared Thermography

Infrared thermography has become a common method for large surface investigations Since the 1980's, . Applications of this technique include bridge decks, expressways, garages, and airport taxi ways [Weil, 1991].

The basics behind this technique depend greatly on the circulation of heat in a material. An anomaly inside this material affects the internal heat flow. Variation in heat circulation result in temperature differences on the material's surface. A great advantage to this system is its speed. For example, the Dan Ryan Expressway in Chicago, Illinois, underwent infrared thermography testing. It took approximately 14 hours spread over a 5 day period to investigate a distance of 17.6 km [Weil, 1991].

The temperature on a concrete surface depends essentially on 3 factors: a) local subterranean geology, b) surface conditions, and c) environmental considerations.

It is very difficult to prevent heat propagation from a warm region to a cold region. Insulating properties of a material may in some cases hinder heat circulation within the material. Anomalies in concrete generally possess different thermal conductivity constants.

The main source of heat for these tests is the sun. The sun allows for a constant energy distribution on large surfaces. It is possible to detect surface delaminations and other anomalies found in concrete. To this date it is very difficult, if not impossible, to determine the depth and thickness of cracks. It is common, however, to detect only the perimeter of the crack or surface delamination.

This technique is fast and to some degree accurate, depending on the use of the system and information desired. A typical system includes infrared optical sensors, computers, and a data acquisition system with storage capability. Weil (1991) recommends using infrared thermography with GPR.

2.1.5 Nuclear Methods

Testing concrete with nuclear methods is a relatively new NDT application. There are two general techniques used on concrete: radiography and radiometry. Radiography uses a special film to capture emerging radiation from a concrete sample. Radiometry uses Geiger or similar counters to capture the radiation. Both techniques use X-rays or Gamma (G) rays as radiation sources. When X- or G-rays bombard a concrete sample, the material absorbs a portion of the radiation and disperses another radiated portion inside the sample. The remaining radiation emerges from the sample. The objective is to capture the emerging radiation.

Radiography methods use either X-rays or G-rays. The methodology consists of generating X- or G-rays, bombarding the test sample, and storing the image on a special film. The quality of a radiography depends on the penetration characteristics of the X- or G-rays. The image definition captured on film relies on the strength of the source, the distance between the source and the sample, and the distance separating the sample and film.

In concrete testing, it is common to use maximum X-ray energy levels of 30 to 125 keV. In this energy output range, X-ray attenuation is a factor of the atomic number of absorbent materials such as metal reinforcement [Foster, 1968]. Typical G-ray energy levels vary between 0.3 to 0.33 meV. In the preceding energy level range, attenuation is relatively independent of the atomic number of the absorbing materials. For G-rays, attenuation is proportional to material density.

Most research work on concrete occurred between the 1940's and 1960's. Mullins and Pearson performed the first documented nuclear tests on concrete in 1949. Their objective was to find density variations in a concrete slab and to locate reinforcement bars. Other work focused on the evaluation of reinforcement bond stress

inside prestressed beams [Evans and Robinson, 1955]. Since the work performed by Mullins and Pearson, there has not been significant research conducted on concrete. High instrumentation costs, portability problems, and on site equipment manipulation difficulties account for the limited research on this subject.

A G-ray radiography is produced by an interaction between the escaping radiation from a test sample and a photographic film. This method There is frequently used in the United Kingdom and in Europe. Most applications are on construction sites. The test equipment is portable, affordable, and concrete testing is possible up to a thickness of 450 mm.

Radiometry techniques generally use G-rays. As previously mentioned, radiometry does not use special photographic film. Instead, the escaping radiation from a test sample is captured by a Geiger counter. There are two main radiometry techniques: the backscatter method and the direct transmission method. The backscatter method requires access to only one source of a test sample. The other method uses two surfaces, as its name suggests. Figure 2.2 illustrates both techniques [Mitchell, 1991].

With limited literature information available with respect to crack location by nuclear methods, it is impractical to recommend these methods. The limited penetration depth and the equipment costs remain major obstacles for further development of these techniques.

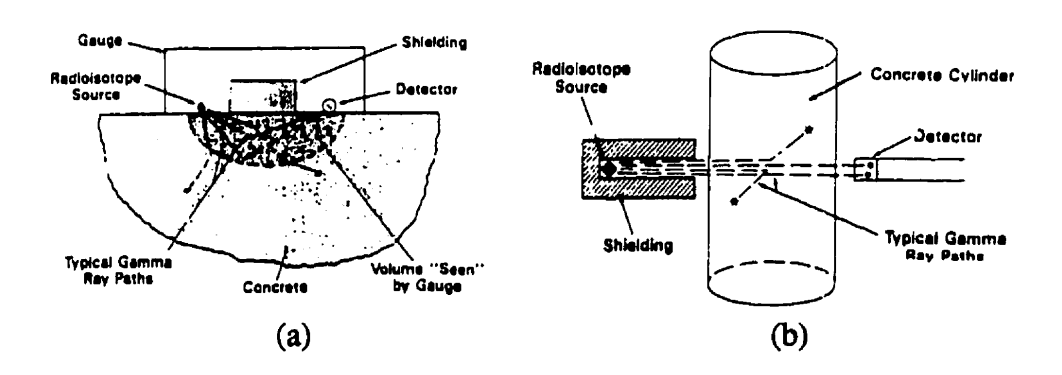


Figure 2.2

Nuclear radiometry of concrete samples:

(a) the backscatter method and (b) the direct transmision method [Mitchell, 1991].

2.1.6 Acoustic Emission Methods

When a material is under stress due to dynamic or static loads, it may plastically deform. The deformation generally causes inaudible sounds that are of microseismic nature. It is currently possible to detect sounds at 10% of the ultimate compressive resistance of concrete [Mindess, 1991]. Acoustic emission is the general term used to identify the inaudible events. Detection of acoustic emissions is performed with accelerometers, geophones, or piezoelectric transducers. Mindess (1991) suggests that acoustic emissions in concrete are the result of microscopic or macroscopic cracking processes, reinforcement slip, fiber reinforcement slip, and failure in composite concrete.

An important phenomenon to discuss is the Kaiser Effect. In 1950, Kaiser explained the irreversibility of acoustic emissions [Lim et al., 1989]. ASTM E610-82 defines the Kaiser Effect as "the absence of detectable acoustic emission at a fixed sensitivity level, until previously applied stress levels are exceeded". Rüsch discovered in 1959, that the Kaiser Effect occurs up to 70-85% of the ultimate resistance of concrete. Green (1970) is the first researcher to use the Kaiser Effect to conclusively prove that acoustic emissions from concrete emanate from internal ruptures.

There are two types of acoustic emission signals: continuous emissions and burst emissions. Continuous emissions are typical of plastic material deformations. Burst emissions occur from failures of brittle materials. Researchers establish the frequency content of acoustic events to be 2 to 400 kHz when testing concrete [Robinson, 1968; Wells, 1970; Green, 1970]. The easiest way to characterize an acoustic emission event is by ring-down counting. This method counts the number of times an acoustic event exceeds a pre-established threshold level [Hassani et al., 1996a]. Many other characterization methods are available. They are discussed in detail in the previous reference. Acoustic emissions suffer attenuation due to many factors such as sample geometry, aggregate type, and concrete resistance. Typical instrumentation for this system includes transducers, preamplifiers and amplifiers, frequency filters, voltage regulator, and computers.

A complete summary of laboratory experimentation on concrete is found in Hassani et al. (1996a). Laboratory experimentation is the main use of acoustic emissions. Research subjects studied with acoustic emission include the rupture mechanism of concrete, crack types, crack location, concrete shrinkage, and other similar areas.

The in situ use of acoustic emission has increased in recent years. However, this method is best suited for controlled experiments where the origin of most acoustic events are known. In situ applications involve very complex signal analysis. It is often difficult

to determine the origin of arbitrary acoustic emissions. Mindess (1991) mentions two main advantages of using acoustic emission on concrete. Firstly, the method allows for a better understanding of the internal structure of concrete. It also helps to evaluate internal changes due to loading. Secondly, one could eventually determine if structures were built as designed on construction sites.

If a structure produces continuous acoustic emissions, the condition may suggest a need for frequent inspections. McCabe et al. (1976) suggest that if a structure exhibits no acoustic events, the structure may be sound. However, the same structure can be heavily stressed and not exhibit acoustic emissions. In this case, it is difficult to determine the actual damage in the structure.

Another inconvenience of the acoustic emission method is the need to apply a load to the test material or structure. Evidently, this is a difficult task to conduct on a concrete dam. Note that the oscillation of the reservoir water level may induce stresses into the structure. In this situation, the problem becomes very complex because of the difficulty of determining the origin of the acoustic emissions. Therefore, acoustic emission is still in its infancy with respect to in situ applications. At this time it is not possible to recommend this method for crack detection in large structures such as concrete dams.

2.1.7 Ultrasonic Methods

In the manufacturing industry, ultrasonic testing occasionally serves as an important step during the fabrication of goods. The main purpose for these tests is quality control. Ultrasonic testing is very well suited for investigating metallic parts of a product. This is due to the use short ultrasonic wavelengths and the homogeneous nature of metals.

Ultrasonic techniques can determine the location, the dimension, and the form of defects in a material [Hassani et al., 1989]. The heterogeneous nature of concrete motivated many researchers to investigate possible practical applications on concrete. Many solutions and techniques are available today on the market, but most apply to specific test conditions.

The density and elastic properties of concrete affect the ultrasonic pulse velocity in concrete. However, pulse attenuation leads to a significantly reduced ultrasonic signal energy at the receiver end of the system. Generally, ultrasonic applications require two test surfaces. Naik and Malhotra (1991) suggest it is possible to use ultrasonic methods on only one surface. However, they report a 97% loss of ultrasonic wave energy with this type of test configuration. The high energy loss eliminates many possible applications of

ultrasonic testing on concrete. The energy loss is a result of ultrasonic wave interaction with the aggregates and boundaries of the test sample. In other words, wave dispersion seriously affects the strength of the ultrasonic pulse in concrete.

There are four general ultrasonic methods used to test concrete: Pulse Velocity, Pulse-Echo, Frequency Response, and Sonic Tomography. The following sections discuss these methods in detail and mention their advantages and disadvantages.

2.1.7.1 The Pulse Velocity Method

The Pulse Velocity method involves the generation of ultrasonic pulses into the test medium. Ultrasonic pulses are generally imperceptible by the human ear. The time a pulse takes to propagate from the source to the receiver is an important measure for these tests. By accurately measuring the time and by knowing the travel distance of the pulse, one can determine the pulse velocity.

Present technology allows the user to measure the arrival time of the first pulse. This first pulse is commonly known as a P-wave pulse. Chapter 3 initiates the reader to theoretical notions of stress wave propagation in elastic solids. If the determined Poisson's ratio has an error of 0.05, the P-wave velocity varies about 6% [Naik, 1979].

The equipment needed to accomplish these tests is a pair of piezoelectric transducers (often of a frequency of 54 kHz), coupling agents, a pulse generator, a signal amplifier and a time analysis system. Rough surfaces occasionally require surface preparation for an adequate transducer coupling. Pulse velocity tests generally produce P-wave velocities in the range of 3700 m/s in concrete of ordinary quality (i.e., density (ρ) of 2350 kg/m³). This technique is very susceptible to arbitrary vibration sources. It is important to eliminate all possible sources before testing.

The following list indicates factors that affect the pulse velocity in concrete [after Naik and Malhotra, 1991]:

- Cement type
- Admixtures
- Curing conditions
- Concrete temperature
- Water/cement ratio
- Consolidation level
- Path length of the pulse
- Stress location on the test element
- Age of the concrete
- Humidity conditions in concrete
- Sample dimensions
- Reinforcement bars

There are three common transducer arrangements: direct transmission, semi-direct transmission, and indirect transmission. Figure 2.3 illustrates the positioning of each arrangement.

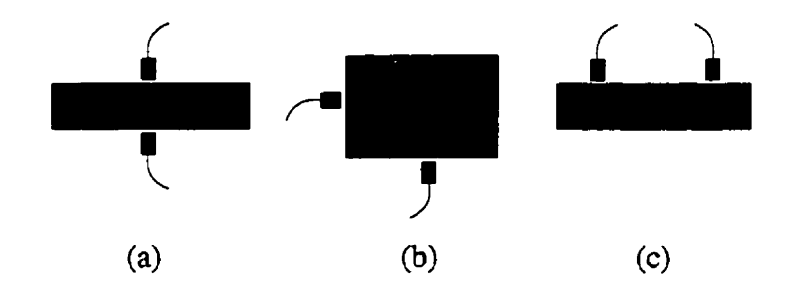


Figure 2.3
Suggested test configurations for ultrasonic testing; (a) direct transmission, (b) semi-direct transmission, and (c) indirect transmission
[after Naik and Malhotra, 1991]

The Pulse Velocity method allows one to evaluate concrete quality and analyze its deterioration process. Many published research papers discuss the capability of determining the dynamic Young's Modulus and the Poisson's ratio of concrete. Researchers strongly suggest that only after testing concrete cylinders from the field and establishing a calibration curve, can one estimate in situ concrete resistance [Naik and Malhotra, 1991]. Many international standards recommend procedures to determine the calibration curves.

Concrete homogeneity is another concern that can be addressed by the Pulse Velocity method. A very heterogeneous concrete, such as one suffering from honeycombing, produces wave dispersion. The result is long pulse travel times inside the material. One can then determine the locations of internal voids.

McHenry and Oleson (1967) mention ten cases where pulse velocity measurements on concrete dams help determine repair procedures. The objective presented in the report was to evaluate the maximum range of a device called the Soniscope. The instrument was developed by Ontario Hydro at the end of the 1940's [Leslie and Cheesman, 1950]. The Soniscope measures the propagating wave's time interval between two points. The precision of this system is of the order of a millionth of a second or better.

Between 1948 and 1965, thousands of tests were conducted on more than 30 concrete dams by the Portland Cement Association in the United States and Ontario Hydro in Canada. In most cases, concrete quality evaluation was the objective of the

tests. Gravity, arched, and buttress dams figured in these tests. The concrete quality in most of the dams was adequate. However, some dams were afflicted with alkali-silica reaction and surface cracking [McHenry and Oleson, 1967]. The authors state that measurement through good quality concrete is possible up to a thickness of 23 m. They also note that for these distances the accuracy level of the measurements is $\pm 2\%$. For short path lengths, the accuracy may increase. Internal abnormalities in concrete usually cause low pulse velocities. There is no mention of the Soniscope's ability to accurately locate internal defects.

As discussed, the pulse velocity method is a simple and effective technique to analyze the uniformity of concrete. The test procedure is simple and the equipment widely available. This test is also standardized under ASTM C597-83 in the United States and A23.2-24C in Canada. The two limitations of this system are the point by point application and the need for two test surfaces. Internal defect location remains difficult at this time.

2.1.7.2 The Pulse-Echo Method

Applications of the Pulse-Echo method include concrete slab thickness determination, defect location and pile monitoring. This method is at the basis of the Impact-Echo method treated in detail in Chapter 3 [Carino and Sansalone, 1984].

The Pulse-Echo method requires only one surface of the test object. A transmitting transducer generates a pulse that reflects off internal flaws in the material. The reflected pulse can be detected either by the same transmitting transducer or by a separate receiver. The use of a separate receiver is referred to as the *pitch-catch* method. Figure 2.4 illustrates these two methods.

In both cases, the methods require an oscilloscope to visualize the transmitted and received pulses. The oscilloscope displays the pulses in the time domain. The propagation time of the pulse is determined. The principal components of the systems include transmission and reception transducers, an oscilloscope, and a data acquisition and analysis system. Most transducers are of the piezoelectric type. Section 3.2 discusses the theory behind piezoelectric materials and their uses in detail. To ensure adequate transmission of the pulse into the test object the transmitter requires a coupling agent. For testing concrete specimens, instrument manufacturers and researchers suggest using low

Alkali-silica reaction is the attack of alkali solution found in concrete pores on silica-containing aggregates in the concrete mix. The result is an expanding silica gel which forms around the aggregate and creates internal stresses in the concrete element [CEB, 1993].

frequency transducers. To build such transducers, the surface area dimensions must be significantly increased. The increased dimensions add to the manufacturing costs and limits the applications to large test surfaces.

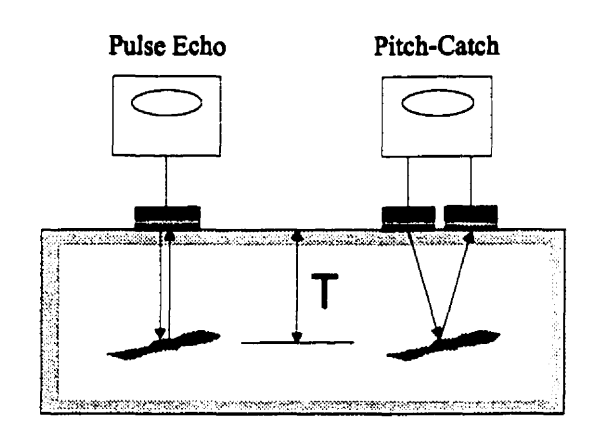


Figure 2. 4
Schematic of the Pulse-Echo and the Pitch-Catch ultrasonic methods [after Sansalone and Carino, 1991].

Pile monitoring with ultrasonic methods began in the early 1970's. The purpose of this work was to evaluate the integrity of slender concrete members with the use of stress waves [Carino and Sansalone, 1984]. Researchers have long understood stress wave behavior in long slender members of this type. The slender structure acts as a waveguide because of the transformation of initial spherical waves into plane waves. Plane wave reflection occurs between the surface and the end of the pile. As a result, signal analysis of the captured waveform on the pile surface is significantly simpler. Partial and complete discontinuities in the pile can be detected. Other forms of anomalies found by this technique include voids, cross sectional area variations, poor concrete quality, and soil intrusions.

In the literature there is a limited number of reports regarding in situ Pulse-Echo tests on concrete. In 1967, an earthquake hit India and produced large horizontal cracks in the Koyna Dam. Pulse-Echo was used to evaluate the extent of those fractures. A free falling hammer served as the impact source. The hammer generated 200 to 600 Hz frequency stress waves. In this frequency range it is possible to detect 15 m crack surfaces. It was possible to detect cracks 100 m from the point of impact. Pulse-Echo tests were later performed to qualitatively assess the successful attempt at grouting the internal cracks in the dam [Carino and Sansalone, 1984].

Other applications include pavement thickness measurements on roads and bridge decks [Muenow, 1963], safety investigations of concrete structures built for reactor cores [Sutherland and Kent, 1976], and the thickness measurement of refractory concrete [Claytor and Ellingson, 1983].

2.1.7.3 The Resonance Frequency Method

The resonance frequency of an elastic element is an important dynamic property. The resonance frequency is influenced by the dynamic elastic modulus, the density, and the support conditions of the test element. It is principally a laboratory test method. Mathematical relationships exist regarding the resonance frequency of solid, homogeneous, isotropic, and perfectly homogeneous materials. The same relationships can be applied to concrete specimens. It is possible to do so since the dimension of a concrete test sample is usually significantly larger than the constituents that form concrete [Malhotra and Sivasundaram, 1991]. Concrete prisms and cylinders are common elements used to evaluate dynamic properties and damage progression during durability tests.

Two test methodologies can help determine the resonance frequency of a concrete sample: the forced resonance method and the impact resonance method. During the forced resonance test, vibrations are induced into the test object with the help of an electro-mechanical source. A pickup unit placed on the top of the specimen captures its response. The frequency responsible for maximum response is considered to be the resonance frequency of the test object. The impact resonance method uses an impact source that strikes the test element. Accelerometers, placed on the test element, measure the response. The fundamental frequency of the specimen is obtained with the use of digital signal processing methods. Counting zero crossings in the time domain waveform is another technique used to evaluate the resonance frequency by the impact resonance method [ASTM C215-91, 1991].

Equipment currently available on the market typically include the following set of components: oscillators linked to amplifiers, oscilloscopes, data acquisition systems and additional amplifiers, and transducers. Transverse, longitudinal, and torsional frequencies are obtained when testing a concrete sample. The fundamental transverse and longitudinal frequencies yield the dynamic Young's Modulus. The modulus of elasticity of each constituent in the concrete mix influences the overall dynamic modulus of elasticity. The torsional frequency helps determine the dynamic modulus of rigidity. Research shows that specimen dimension plays a significant role during the testing

process. Large specimens generally exhibit lower resonance frequencies compared to smaller specimens of the same material [Malhotra and Sivasundaram, 1991].

In the literature, there is very little discussion of in situ applications of resonance frequency testing. Therefore, it is currently a laboratory testing technique. Since the laboratory specimens are typically small, one cannot suggest this method for use on concrete dams. Researchers usually caution users of this method to not overstate the usefulness of dynamic values as a design parameter.

2.1.7.4 Sonic Tomography

Sonic tomography is an imaging technique based on the analysis of seismic P-wave velocities. The principle of the technique is similar to the ultrasonic pulse velocity method. Both methods require access to more than one side of the test sample, and both study the velocity of a seismic wave traveling through a medium. Sonic tomography can use a large number of transmitters and receivers at the same time. This technique is used in geophysics and mining engineering applications and has recently been used on civil engineering structures such as dams [Kharrat et al., 1993].

Due to the high sensitivity of this method, researchers can differentiate internal anomalies that possess various seismic wave velocity characteristics. Sonic tomography tests can be conducted on concrete structures up to a thickness of 10 m. The test depth depends on the objectives of the tests and the image resolution that is required.

Instrumentation consists of a multitude of receptors and transmitters, data acquisition cards and a portable computer. The method is essentially a numerical technique for data analysis. Each transmitter is triggered consecutively and signals are recorded by the receivers. The P-wave travel times are obtained by analyzing all possible P-wave travel path combinations between the transmitters and the receivers. The data is processed by an inverse modeling software based on an iterative process that manipulates the data. Geometric iterative reconstruction techniques have been found to be faster than other methods for this type of analysis. All the data undergoes a tomographic reconstruction, followed by a computer generation of a P-wave velocity tomography of the section. The P-wave velocity distribution has a direct relationship with the discontinuity distribution in the tested medium. Figure 2.5 shows the application of sonic tomography on a concrete gravity dam.

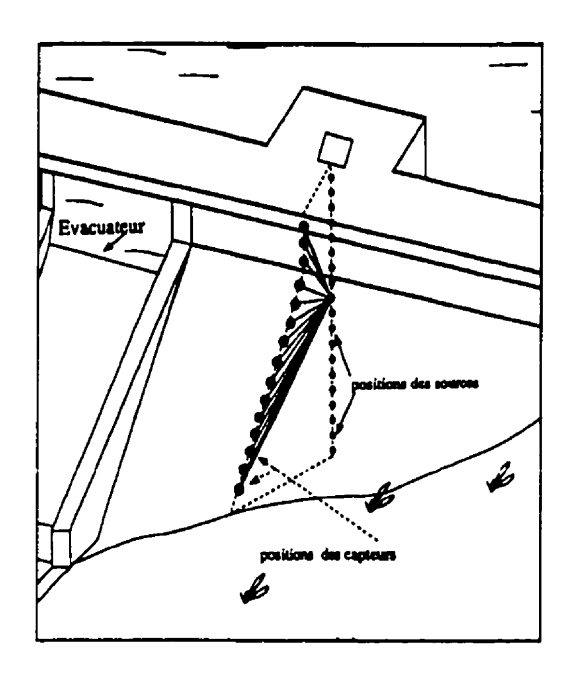


Figure 2.5

Position of transmitters and receivers on a concrete gravity dam for sonic tomography testing [Kharrat et al., 1993].

Sonic tomography testing is relatively recent in the civil engineering industry. This method is still in the experimental stage and continuously under development. Crack detection in concrete structures requires a precise technique. This method has yet to prove this capability, therefore a better seismic technique may be preferable.

2.1.8 Mechanical Methods

NDT methods based on mechanical energy sources are generally considered as mechanical methods. Techniques used on concrete structures and based on mechanical devices have been developed for a long time. The MSR and Impact-Echo methods are both considered as mechanical methods since they are both dependent upon spring loaded impact sources. Chapter 3 relates the theory and methodology of both systems in detail.

There are six major categories of mechanical NDT methods for concrete structures: surface hardness, penetration resistance, pullout systems, the SASW technique, Impulse-Response, and Impact-Echo. The first three categories deal with techniques that give users an approximate compressive resistance of concrete elements in laboratory and in situ conditions. Typically, they are not used for crack detection in concrete and thus are not relevant to the discussion in this thesis. The author refers the reader to a book edited by Malhotra and Carino (1991) for further information on these techniques (see

references). The following sections discuss the last three mentioned methods used on concrete structures.

2.1.8.1 The Spectral Analysis of Surface Waves (SASW) Method

The SASW method uses Rayleigh waves generated on the surface of a material by a mechanical impact device. This system was first developed to assess the rigidity of concrete pavements [Carino, 1992]. Figure 2.6 illustrates the main components and test configuration of the SASW technique.

Typically, two receptors are used to capture surface displacements. The receptors capture propagating Rayleigh waves[†] caused by an impact on a surface. Often, the receptors consist of geophones or accelerometers. Two channel oscilloscopes are used to record the waveforms. The waveforms undergo complex signal analysis that can yield the rigidity of concrete pavement. When there is a need to investigate a layered pavement system, one may use phase velocities. The layered condition causes complex surface wave dispersions. In this case, each dispersed wave has a different phase and travels at different velocities. Therefore phase velocity values help distinguish dispersed waves.

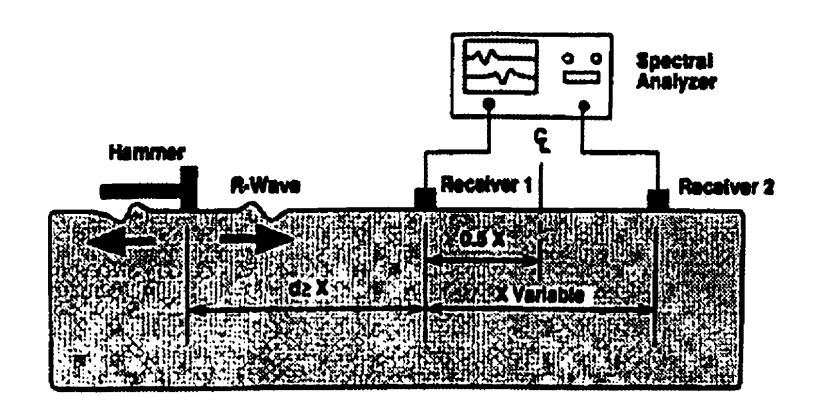


Figure 2.6
Principle and typical test configuration of the SASW method [Carino, 1992].

A surface wave contains a range of frequencies. In other words, there are a multitude of components with different wavelengths generated after the initial contact. Each wave dispersion has a different wavelength and hence a different phase velocity. Often, a plot of the phase velocity versus the wavelength helps to analyze data and obtain the stiffness profile of the layered system. The penetration depth limits applications of

^{*} Rayleigh waves or R-waves are one of many types of surface waves. For more information, Chapter 3 introduces some theoretical aspects of R-waves which may be of interest to the reader.

this system. Discrepancies between field and laboratory data are also a disadvantage of the method.

Olson and Sack (1995) report using the SASW method on the Rogers Dam Hydroelectric Generating Plant in Michigan, with satisfying results. This method was chosen to evaluate the spillway structure of the dam. Of interest was the determination of the thickness of surface shotcrete and the evaluation of an underlying layer of eroded and deteriorated concrete. Tests were performed on piers, abutments, walls, and long chute walls. The results showed the presence of delaminations on the majority of the piers and walls and also a sound concrete core. Ensuing hydroblasting operations helped verify these results.

2.1.8.2 The Impulse-Response Method

The Impulse-Response method is very similar to the Impact-Echo method. An hammer generates the force time function of the impact. The impact generates a stress pulse that propagates into the test object just as in the case of the Impact-Echo method. A transducer positioned near the impact source monitors the surface vibration velocities. The waveforms obtained from the transducers undergo signal processing. Information relating to the condition of the tested structure is obtained [Sansalone and Carino, 1991].

In situ concrete pile monitoring is the main application of this method. Davis and Dunn (1974) report that results obtained from piles become complex due to variations in pile diameter with respect to depth, concrete quality, stiffness, soil damping characteristics and in situ conditions of the pile cap. Higgs (1979) reports that when the length to diameter (L/D) ratio of the pile is greater then 20, the results must be viewed with a critical eye, except when a pile is surrounded by soft soil and is supported by a rigid layer. Higgs discusses how the pile length, dynamic stiffness, and the geometric mean of the mobility interrelate with one another.

2.1.8.3 The Impact-Echo Method

In the 1980's, the National Bureau of Standards (NBS) in the United States undertook a large scale investigation on applications of NDT methods. The main focus was to determine the thickness of concrete slabs, and detect delaminations and other anomalies in this heterogeneous material. After an investigation of the Pulse-Echo method, Carino and Sansalone (1986) developed a test method based on the propagation of seismic waves. They pointed out the usefulness of frequency spectrum analysis over

time domain analysis. Typical configurations include spring loaded impact sources, a broadband vertical displacement transducer and a digital waveform analyzer with accompanying analysis software. The main drawback of this system is that only slabs thicker than 10 cm can be tested [Sadri, 1996]. The theory behind this technique is discussed solely in Chapter 3. Section 2.3 discusses current research topics undertaken in the area of Impact-Echo testing.

2.2 NDT METHODS USED AT HYDRO-QUÉBEC

This section highlights the past work on projects involving nondestructive testing on concrete structures and dams at Hydro-Québec. Although most of the information is confidential, some information can be discussed here. The first part of this section mentions applications conducted on the Paugan Dam situated in the province of Quebec and nondestructive laboratory investigations previously conducted on concrete slabs at IREQ.

2.2.1 Case study: Acoustic Emission and Microseismic Testing at the Paugan Dam

Hydro-Québec was interested in finding an affordable solution to an important problem afflicting one of its dams. The suggested solutions involved nondestructive testing. The two retained methods were based on acoustic emission testing. A private firm was retained by Hydro-Québec to carry out this work. The main objectives of the investigation were to locate, qualify, and if possible quantify water leaks inside this dam. Another aspect to this project involved finding the probable causes of the deformations sustained by the dam and thought to be at the root of the preceding problem.

The Paugan Dam is located about 50 km from Ottawa, Canada in the town of Low. This dam was built between 1927 and 1929 by the Gatineau Power Company. The main client for the hydroelectric facility was the Canadian International Paper Company (CIP). The dam is the third of a series of three dams on the Gatineau River, downstream from the Chelsea and Farmers Dams.

The Paugan Dam is a concrete gravity dam and possesses a different geometry than the upstream dams on the Gatineau River. It was necessary to construct four dikes to contain the increased water level upstream from the dam. The maximum discharge recorded on the river is 2150 m³/s.

Inverse pendulums, piezometers, and discharge meters were placed on the dam. The instrumentation helped to confirm the magnitude of displacements at the top and underneath the dam. In 1988, a project was undertaken to reduce the internal stresses in the structure and reduce its deformations. NDT tests were concentrated on the areas subjected to deformations.

When using these nondestructive methods on concrete dams, it is essential that the receivers be broadband, robust, and of a high sensitivity level. During signal analysis, the personnel must take into account signal attenuation, background noise, electromagnetic interference, signal distortion, and electrical noise caused by the instrumentation.

The devices used for the acoustic emission tests are described in Section 2.1.6. The private firm used a commercially available instrument for these tests. The microseismic investigation involved the use of geophones and seismometers as wave receptors. The firm proceeded to evaluate both methods in a first series of tests on the dam. Four accelerometers used for acoustic emission tests and four geophones were placed on the dam. Their sensitivity and reception quality were evaluated. According to the firm, 350 acoustic events were recorded and only 59 were found useful for interpretation. The acoustic events were continuously recorded over a 30 day period.

After the data analysis period, the firm concluded that the commercial unit that was used for acoustic emission testing was useful for determining the movements of the dam. It was also found that the accelerometers yielded better information due to their higher sensitivity compared to geophones. It is important to note that geophones cost less than accelerometers and economics figure highly in this investigation project. Presently, the private firm is trying to perfect the acoustic emission system.

Other nondestructive projects were conducted on Hydro-Québec dams. The information relating to these tests was very difficult to obtain by the author and therefore cannot be published here. There seems to be a general consensus in the industry that nondestructive technology is still in its infancy with respect to investigating large concrete structures, such as gravity dams.

2.2.2 Laboratory NDT testing at Hydro-Québec

Crack injection is a common solution to problems afflicting concrete structures. This technique has been used on concrete dams in the past. However, the propagation of injection products and their behavior inside a crack is still misunderstood. Therefore, a long term research program to determine the effectiveness of cement grouts injected in

concrete dams was initiated by IREQ in 1986. To investigate the effectiveness of the grouts, three nondestructive methods based on seismic wave propagation were recently applied to concrete slabs. The concrete slabs had the following typical dimensions: $2.6 \text{ m} \times 1.4 \text{ m} \times 0.4 \text{ m}$.

The slabs were dotted with linear variable displacement transducers (LVDTs) and pressure meters. The pressure meters were placed on a grid, on top of the slab and were used to measure the variations in pressure at different points as the crack was being injected. By analyzing the pressure variations and the grout take, one can determine if the grout hole had been completely injected. However, it may be difficult do determine if the grout had traveled between the pressure meters. This is where NDT techniques can be used to enhance the information obtained during an injection test.

The Impact-Echo method was used to determine the crack profile before the injection process began in one of the slabs. This method was used successfully and the detected internal crack depths agreed well with crack depths measured on the sides of the concrete slab. Acoustic Emission was used to monitor the penetration of the grout inside the crack. This method also allowed the researchers to determine at which moment, during the injection test, the cement grout mixture needed to be changed. Sonic Tomography was used to produce a tomographic image of the internal seismic wave velocities which traveled through the slab before and after the injection tests. Two different transmitter and receiver arrangements were used to determine the best measurement configuration [Saleh et al., 1997].

With the Impact-Echo results obtained after scanning a grid placed on the concrete slabs, it was possible to draw a crack profile along the test lines. In Figure 2.7, the crack profile is shown in a three dimensional representation of the slab. This was obtained by interpolating the results between the test points. It is important to note that this is not a true three dimensional image, since no tests were carried out on the bottom surface of the slab (i.e., the crack width cannot be determined in this case). This is an example of an application of the Impact-Echo method which helps assess the condition of the slab before the injection tests are conducted.

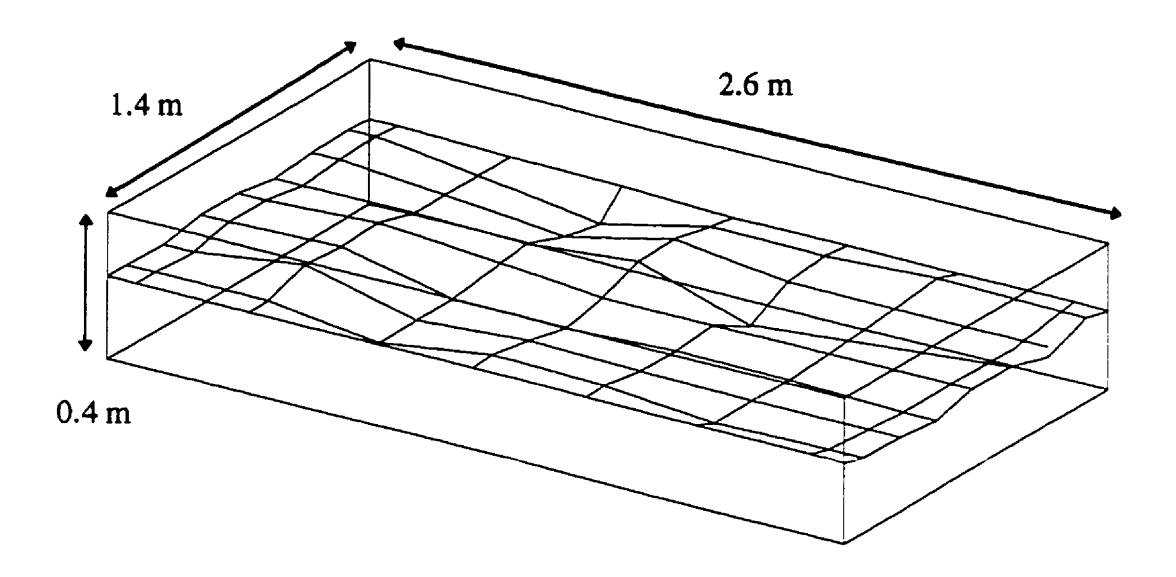


Figure 2.7

Three dimensional view of the crack surface as determined by the Impact-Echo method [Saleh et al., 1997].

Acoustic emission (AE) tests were performed to evaluate the injection process. Tests were conducted during the grouting periods. It is possible to locate the origin of these sounds and determine the progression of cracks or of an injection grout. Tests were performed with a SPARTAN data acquisition system manufactured by the Physical Acoustic Corporation. It is used for locating and analyzing, in real time, acoustic emission events. It is a high speed acquisition system which is capable of a sampling rate up to 10 MHz. The analysis of AE signals is conducted in real time and involves a statistical analysis of parameters such as: amplitude, duration, rise time, energy analysis, and event counting.

In order to correlate AE activity to injection flow parameters, the evolution of the AE signals was compared to water pressure during a water test and at different crack positions. It was found that the detected AE signals were not due to constant pressure flow, but to the acceleration and deceleration of the injected product, and to the mechanisms resulting from the variations of pressure and flow in the fluid [Saleh et al., 1997].

The number of AE events from each transducer gives an indication of the success of the injection in each area of the slab and also offers a qualitative analysis of the injection product. The general evolution of the signals indicated an increase in AE activity during approximately the first 90 minutes of an injection test. After this period,

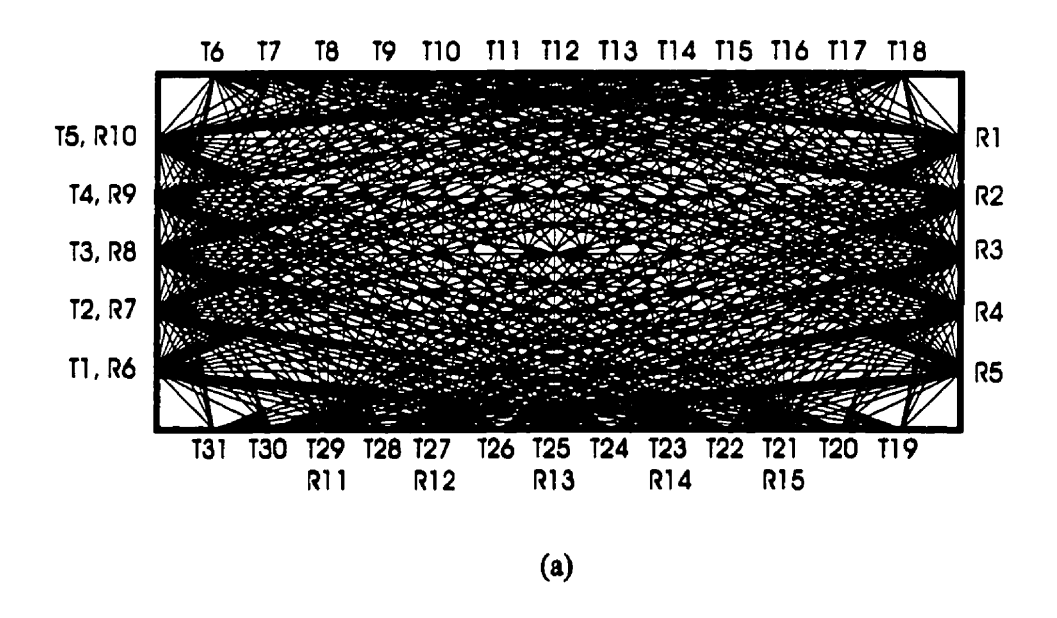
the activity generally decreased with only occasional increases. This activity tends to be representative of the injection procedure used during the tests [Saleh et al., 1995].

During the tests it was shown that the AE method can help determine the time to change the injection mix and also find areas where the injection grout has penetrated into the slab. It was also possible to locate events with the AE method by applying what is called linear location [Saleh et al., 1995]. This technique helps determine what activity is occurring between two receivers, and it allows the users to define the linear distribution of the grout penetration into the slab. This is accomplished by analyzing information retrieved between two adjacent receivers.

Sonic tomography tests were conducted on some concrete slabs to asses the internal soundness of the injection process. As previously discussed, this method uses a multitude of receivers and transmitters. Two test configurations were used on the concrete slabs. The first configuration consisted of sounding the slab with sensors on every side. The second configuration consisted of sounding the slab with sensors placed on only three faces because the bottom face was not accessible. The first configuration used 31 transmitters and 15 receivers. This generated 350 ray combinations between the receivers and transmitters for a very dense ray field. The second configuration consisted of 18 transmitters and 10 receivers. This arrangement allowed for 155 ray combinations. The ray fields for both configurations are shown in Figure 2.8. In this figure, the R stands for receivers and T stands for transmitters.

This method is essentially a numerical technique for data analysis. Each transmitter is triggered consecutively and recorded by the receivers. The P-wave travel times are obtained by using all possible P-wave path combinations between the transmitters and the receivers. All the data undergoes a tomographic reconstruction, and the P-wave velocity tomography of the section is displayed on a computer screen. The velocity distribution is in direct relation with the distribution of the discontinuities of the medium being tested. Figure 2.9 shows the P-wave velocity distribution in the concrete slab before and after the injection process for the low density ray path configuration [Saleh et al., 1997].

Notice in Figure 2.9 (b) the almost uniform nature of the cross section of the injected slab. This indicates a constant wave velocity and a successful injection test.



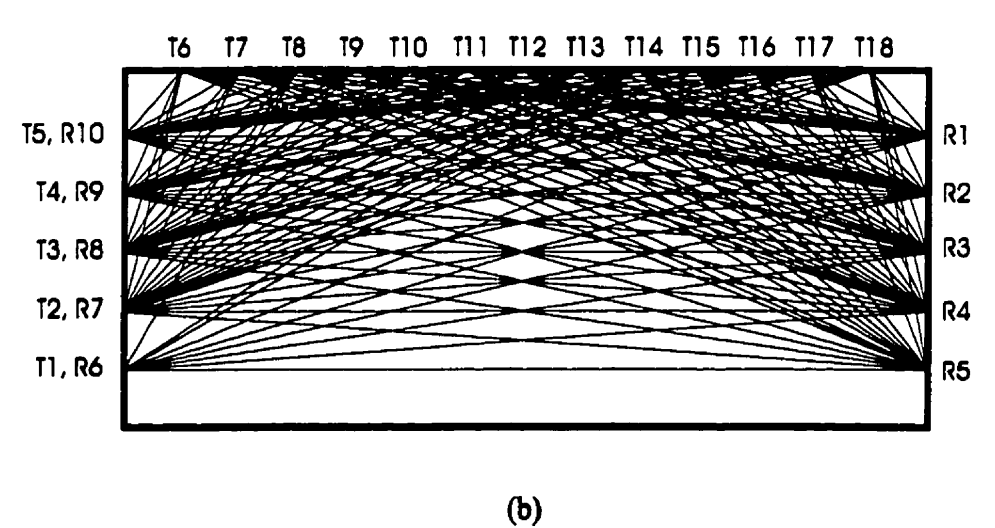


Figure 2.8

Ray paths for sonic tomography tests:
(a) setup 1, and (b) setup 2 [Saleh et al., 1997].

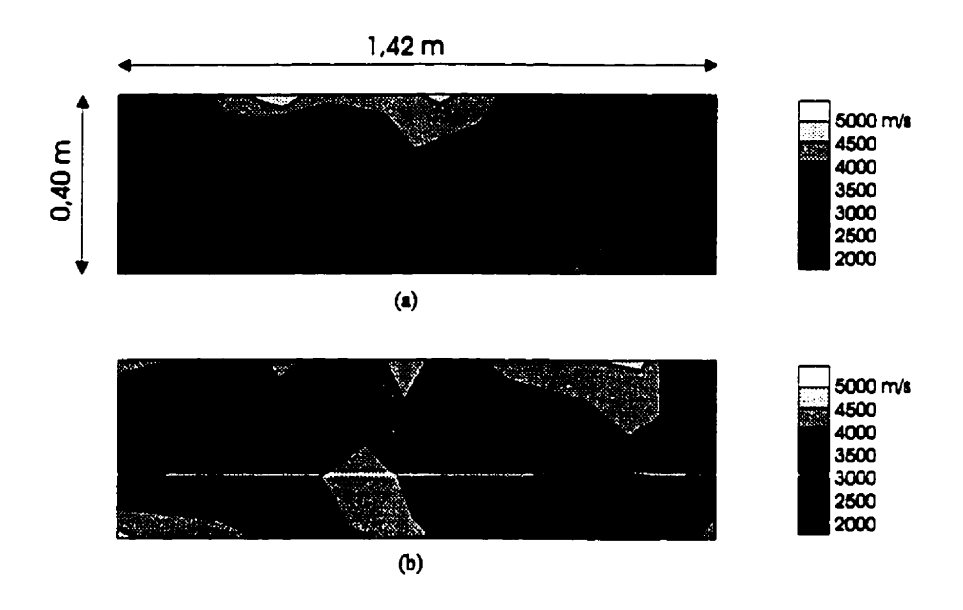


Figure 2.9

Tomographic image of the P-wave velocities for the low density ray path configuration:

a) before grouting, and b) after grouting [Saleh, et al., 1997].

2.3 APPLICATIONS OF MINIATURE SEISMIC TECHNOLOGY

The following section discusses initial and current work undertaken in the field of nondestructive testing. The section focuses on work based on the propagation of miniature seismic waves. The intent is to offer a brief overview of the research and practical aspects of the theoretical notions described in Chapter 3. From the mid 1980's to this date, the main focus of the research was a better theoretical understanding of stress wave propagation in concrete due to an impact by a spherical object. Most of the research was conducted at the National Bureau of Standards under the supervision of Dr. N.J. Carino and at Cornell University under the supervision of Dr. M. Sansalone. References to research conducted by Drs. Carino and Sansalone can be found at the end of the thesis. Theoretical notions are described in Chapter 3. An important portion of the theoretical development concentrated on using finite element analysis for a better understanding of stress wave propagation in solids.

The research described here refers to work carried out between 1990 and 1997 with a focus on the practical applications of the Impact-Echo (IE) and MSR Impact-Echo methods in in situ conditions. In 1990, the first practical applications of the (IE) method

were reported in the literature. This represents a transition from laboratory testing to in situ validation and practice.

2.3.1 Mine Shafts and Circular Structures

Lin and Sansalone (1994) reported conducting research on the use of the IE method to investigate the integrity of concrete pipes and mine and tunnel shaft liners. Field studies involved assessing the influence of a concrete-soil interface on transient wave propagation. The results show that the IE response depends upon the acoustic impedance of the soil and the concrete. As well, voids and cracks are located without difficulty. The presence of delaminations at concrete to rock interfaces was also noticed.

Hassani et al. (1996b) discuss using the newly developed MSR Impact-Echo system to evaluate excavated tunnel and shaft linings. The MSR Impact-Echo method is capable of determining the dynamic elastic properties of materials. The system can also perform defect location and thickness measurement. The system was first developed to assess the physical properties of rocks [Momayez et al., 1995]. Tests were conducted at the CPP Mine which is operated by Central Canada Potash Inc. Other tests were performed at the Allen Mine which is operated by the Potash Corporation of Saskatchewan Inc. The thickness of the shaft lining in both mines was measured along with the position of reinforcement bars. The dynamic elastic properties were also evaluated at both sites. At the Allen Mine, concrete cores were taken at the same locations as the MSR tests. Ultrasonic pulse velocity (UPV) tests were performed by an independent laboratory. It was shown that the MSR results are consistently lower than the UPV tests except for Poisson's ratio and the Bulk modulus.

2.3.2 Concrete Slabs

Carino and Sansalone (1990) report using the Impact-Echo (IE) method in "blind" tests to experimentally validate this method. Part of the study focused on detecting anomalies and delaminations in a reinforced concrete slab. During the tests, the positions of the defects were not known. The concrete slab was cast with imbedded polyurethane disks positioned at different locations and at different angles. The defects were found at their expected locations. For the delamination detection test, a 0.20 m thick reinforced concrete slab was constructed. Plastic sheets were imbedded in the concrete to simulate the delaminations. They were successfully detected in the upper and lower

sections of the slab. The perimeter of the delaminations was determined by reducing the dimensions of the test grid.

Prior to these tests, the IE method was applied to skating rink concrete slabs. Unconsolidated concrete under the cooling pipes was successfully detected. The pockets were generally 50 to 100 mm in length. In order to detect small voids, a 20 µs contact time was used for the tests. The low contact time helped to detect successfully the small voids [Sansalone and Carino, 1991; Sansalone and Carino, 1989].

Sack et al. (1995) report the development of a scanning IE testing apparatus capable of performing 3000 IE tests per hour. The rapidity of the tests depends on new rolling transducers, water coupling, and solenoid-driven impactors. Software development was necessary in order to take advantage of the fast scanning rate. On smooth slab surfaces, tests have rendered 600-800 IE tests in 5 minutes in a straight distance of 50 feet. The system is sensitive to 2.5 mm thickness variations. This accuracy is dependent upon the measurement accuracy of the P-wave velocity found before tests are performed. This system has been successfully used in a number of applications on different types of concrete slabs such as floor slabs, slabs on grade, and elevated floor slabs with imbedded joists.

2.3.3 Concrete Parking Structures

Olson and Wright (1990) discuss using the IE method for crack detection in a concrete parking garage deck. The purpose of the test was to find spalled and delaminated concrete caused by reinforcement corrosion in the decks. The asphalt overlay averaged a 2 cm thickness. Due to the asphalt overlay, chain dragging was not a feasible method. The IE tests were conducted from the underside of the deck, thus avoiding the influence of the asphalt overlay. Test results showed a variety of conditions including sound concrete to asphalt adhesion, top and bottom delaminations, unbonded concrete to asphalt interfaces. Fifteen (15) concrete cores were taken from the deck. The cores confirmed the IE results.

2.3.4 Concrete Dams, Bridges, Walls, and Pre-stressing Tendon Ducts

The Canadian Center for Mineral and Energy (CANMET) decided to conduct tests to assess the ability of NDT techniques to detect voids in tendon ducts. The Impact-Echo method was retained as a possible solution. A section of a post-tensioned concrete ice wall that is typically used for an arctic structure was built as a test bed. Voids were

introduced into the structure during the duct grouting operations. The location of the voids were not known by the investigators. During the IE tests, it was necessary to repeatedly strike the surface until the desired amplitude spectrum was obtained. The results obtained showed that all the detectable voids, however discrepancies did occur. The detected voids tended to appear larger than the actual ones and the Impact-Echo method found more than the actual number of voids in the tendon ducts [Carino and Sansalone, 1990; 1992].

Olson (1991) discusses using the IE method on box girder bridge walls with success. Extensive honeycombing and voids were found after the concrete forms were removed. These problems were apparently caused by the placement sequence of the concrete inside the forms. The IE method was used to identify honeycombing and void areas impossible to detect on the surface. The contractor was faced with the possibility of replacing the entire structure. Therefore, the objective of the evaluation was to reduce the contractor's repair costs. IE tests were conducted on sound concrete surfaces where visible and hidden anomalies were known to exist. These tests allowed the contractor to identify areas where cement-based patches shrank and did not adhere to the concrete. Several hundred locations on the box girder walls were investigated. Unobserved honeycombing and internal voids were detected. The contractor made the necessary repairs based on the IE test results.

Ghorbanpoor et al. (1992) report using the IE method to evaluate the condition of grout in ducts of a two-span continuous box girder type post-tensioned concrete bridge. By analyzing the frequency peaks in the spectrum it was possible to determine the position of suspected unfilled portions of the post-tensioning ducts. However, there was no physical validation of the results by coring the box girder or by other methods.

The Humphrey's thin-arched concrete dam situated in Colorado, USA, recently underwent IE testing. The dam is 6 m to 26 m in height and has a crest length of 49 m. The wall thickness ranges from 1.1 m to 4.9 m. The objectives of the IE tests were to evaluate from the downstream face of the dam, the concrete condition and to detect the position of vertical internal cracks parallel to the test surface. Due to freeze-thaw cycles, the dam suffers from excess seepage and other forms of damage. Distressed and sound concrete areas were detected. The test results indicated that the vertical cracks were in partial contact with the concrete at the interface. This was observed in the frequency spectrum by an additional frequency peak which corresponded to the thickness of the dam. The iests corresponded fairly well with results obtained from cores taken at the dam. The results served as the basis for a rehabilitation strategy for the damaged concrete dam [Olson, 1992].

Henrickson (1995) discusses successfully using the IE method to investigate the asphalt deck on a 25 year old bridge. The deck was also layered with a waterproofing membrane. The signs of distress on the bridge were evident just from looking at the cracks formed on the edge beams. The cause of the problems was associated to alkaliaggregate reaction that suggested that the waterproofing membrane needed to be replaced at a very large cost. The entire bridge deck was investigated. IE results were compared to results obtained from areas where the asphalt layer was reduced. A maximum of 10% of the total surface area showed damage. It was decided that the waterproofing membrane would not have to be replaced for an extra period of 10 years.

Grouted pre-stressing ducts in concrete girders from the Champlain Bridge in Montreal were recently evaluated by the IE method [Sadri et al., 1995]. In these tests, a Schmidt Hammer was used to generate low frequency impacts. The tests were hindered to a certain level by the background noise caused by continuous traffic on the bridge. Out of the possible six ducts to be detected, four ducts were located with an accuracy of $\pm 6\%$. The two remaining ducts could not be located due to their proximity to the test surface. The generated wavelengths by the impactors were too long to detect these grouted ducts.

2.3.5 Concrete Beams and Columns

Sansalone et al. (1991) mention results obtained from testing rectangular and circular concrete columns with the IE method. Some of the columns were solid and the others had artificial internal voids. The voids were detected by selecting frequency peaks in the frequency spectrums. Relationships have been developed for the fundamental modes of columns with circular, square, and rectangular cross-sections. The fundamental modes produce specific frequency peaks in the frequency spectrum. Internal anomalies correspond to the other peak frequencies in the spectrum (see Chapter 3 for a discussion of the frequency spectrum of a signal).

2.3.6 Other Concrete Structures

Henrikson (1995) mentions using the IE method for evaluating a concrete sludge basin built at a water treatment plant. Heavy rain falls seriously damaged the structural integrity of the basin. After draining the basin, it was important to determine if there were any voids created by a loss of a sand layer placed between the concrete bottom and a clay/chalk substratum. The voids could seriously affect the load carrying capacity of the

basin and promote the infiltration of sludge into the lower substrata. The IE test results discovered only a limited amount of voids. The results were compared to cores drilled at the suspected sites of the voids. These tests resolved a dispute about which repair strategy to use: complete rebuilding or injecting the voids. The later solution was retained.

2.4 FINAL NOTES

Chapter 2 reviewed past and current work performed in nondestructive testing on concrete. Section 2.1 discussed many of the NDT techniques that may eventually be useful for crack detection in concrete. Most techniques are not fully adapted for crack location. Section 2.2 presented NDT applications performed for Hydro-Québec. A case study concerning acoustic emission tests performed at the Paugan Dam was discussed. Laboratory experiments conducted at IREQ were also mentioned.

Section 2.3 focused the discussion on work performed with miniature seismic systems. A brief introduction to each test system was given. Tests conducted on a variety of concrete structures was presented. A complete discussion on the theoretical notions of the MSR Impact-Echo system is given in Chapter 3.

THEORETICAL NOTIONS OF THE MSR IMPACT-ECHO METHOD

The present chapter describes the theory behind the MSR Impact-Echo method. The beginning of this section focuses on general miniature seismic reflection (MSR) theory followed by a discussion of theoretical considerations related to the methodology of the MSR system. The ensuing sections present an overview of the instrumentation of this system.

3.1 FUNDAMENTALS OF ELASTIC WAVE PROPAGATION IN SOLIDS

When an object impacts a solid, three types of seismic waves are generated: compression waves, shear waves, and Rayleigh waves. Common terms associated to these types of waves are:

- a) Compression waves: longitudinal or primary (P) waves.
- b) Shear waves: transverse or secondary (S) waves.
- c) Rayleigh waves: surface or (R) waves.

For the purpose of easing the text throughout the chapter and the manuscript, the terms P-, S-, and R-waves are used to designate each type of seismic wave. The following paragraphs describe in detail the three wave types.

3.1.1 P-waves

The oscillation of a material's particles in a direction parallel to the direction of propagation characterizes these waves. Compression and tension movement of the material will distinguish the particle's oscillation. The particles remain in place and oscillate about their initial positions. In this case, no particle rotations occur in an elastic medium [Telford et al., 1990]. Of the three types of seismic waves discussed here, P-waves have the highest velocities. P-waves are capable of traveling in water, however they sustain an important energy loss. Figure 3.1 illustrates the phenomenon of a

P-wave traveling through an elastic medium. Notice the alternating compression and tension zones in this figure. The wave length refers to the distance between particles in the same state of oscillation. That is, at the length between the center of compression or tension zones. The wave length is inversely proportional to the frequency of the wave [Krautkrämer and Krautkrämer, 1983].

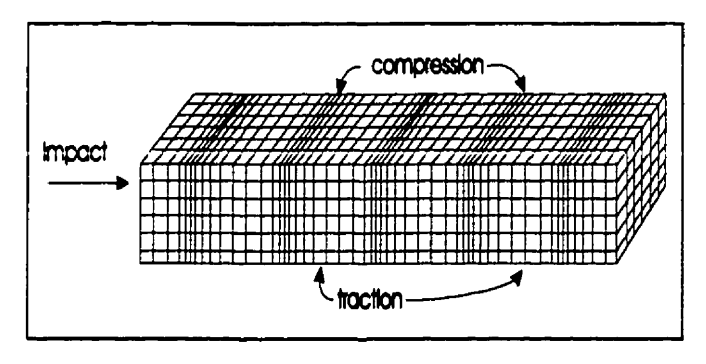


Figure 3.1
P-wave propagation inside an elastic material [after Bolt, 1976].

3.1.2 S-waves

A perpendicular particle motion distinguishes S-wave propagation in a material. Rotation and shearing of the particles occurs as the S-wave travels through an elastic medium. S-waves do not produce a volume change [Telford et al., 1990]. The waves do not travel through water because water does not possess shear resistance. Figure 3.2 demonstrates particle motion caused by an S-wave traveling through a material. The distance between two planes of particles at the same vertical positions defines the wave length. Krautkrämer and Krautkrämer (1983) explain that the shear stress is greatest where the particles pass through their rest position because the displacement between these particles and the adjoining particles is the greatest. Zero shear stress occurs at maximum amplitude.

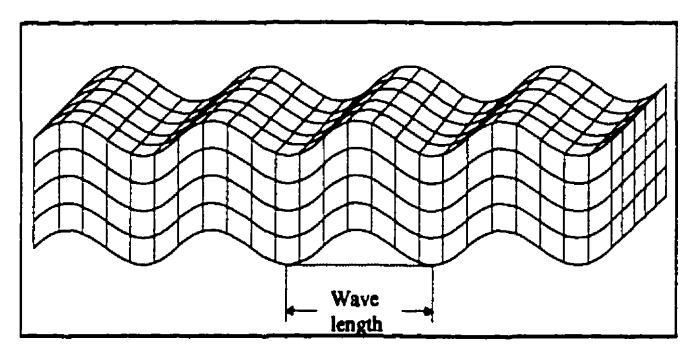


Figure 3.2
S-wave propagation inside
an elastic material [after Bolt, 1976].

3.1.3 R-waves

R-waves propagate on the surface of a material after the initial impact. The propagation is in a radial projection, parallel to the plane of the surface of the material. These waves highly attenuate (loss of energy) with depth [Telford et al., 1990]. Theoretically, these waves sustain almost full attenuation at depths equal to their wavelengths [Krautkrämer and Krautkrämer, 1983]. When R-waves travel on the surface of a material, an elliptical rotation of particles occurs. The motion is in part perpendicular and in part parallel to the surface. The deformation on the surface is therefore not uniquely sinusoidal. It is important to note that the R-wave is one of many types of surface waves. Figure 3.3 illustrates this phenomenon.

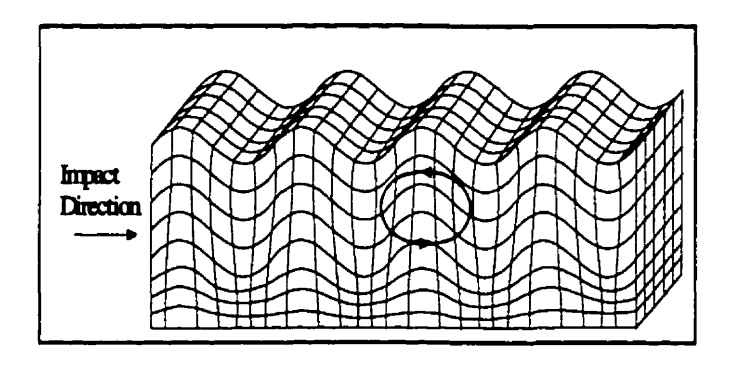


Figure 3.3

R-wave propagation on the surface of an elastic material [after Bolt, 1976].

3.1.4 Seismic Wave Velocities

A body wave is another term associated to P- and S-waves. typically travel along hemispherical wavefronts and when reflected from edges they may travel along spherical wavefronts. Each of the three wave propagation types result in a temporary and almost instantaneous displacement of the particles in a specimen. In the case of a vertical impact on a surface, P-waves possess a vertical velocity component. S-waves exhibit horizontal and vertical velocity components (SH and SV, respectively), as do R-waves due to the elliptical motion of the particles. P- and SV-waves propagate along hemispherical wavefronts. SV-waves produce vertical surface displacements on the surface, as do P-waves. SV-waves may be confounded with P-waves in a time domain spectrum. Upon arrival at the surface, the SV-wave creates horizontal displacements parallel to the surface that create a horizontal velocity component of the SV-wave. In other words, upon collision with an interface, SH-waves are produced. The horizontal velocity components at the surface of a material is used with the MSR Impact-Echo system. The SV horizontal velocity is used to assess the dynamic properties of materials.

The P-, S-, and R-wave velocities are a function of various dynamic elastic properties of the tested material. The velocities depend on the dynamic Young's Modulus (E), the dynamic Poisson's Ratio (v), and the material density (ρ) . For v = 0.2, P-waves are approximately 1.61 times faster than S-waves [Carino and Sansalone, 1984]. In 1970, Timoshenko and Goodier associated the dynamic material properties of a material to P- and S-waves velocities. The material was a homogeneous, linear elastic, and isotropic solid. The velocity equations below show these relationships:

P-wave velocity:
$$C_p = \sqrt{\frac{E(1-\nu)}{\rho(1+\nu)(1-2\nu)}}$$
 (3.1a)

$$C_p = \sqrt{\frac{E}{\rho}}$$
 (3.1b)

S-wave velocity:
$$C_s = \sqrt{\frac{E}{2\rho(1+\nu)}} = \sqrt{\frac{G}{\rho}}$$
 (3.2)

R-wave velocity:
$$C_R = \frac{0.87 + 1.12\nu}{1 + \nu} C_s$$
 (3.3a)

$$C_R = \frac{0.87 + 1.12\nu}{1 + \nu} \sqrt{\frac{(1 - 2\nu)}{2(1 - \nu)}} C_p$$
 (3.3b)

where G is the shear modulus of elasticity, C_p , C_s , and C_r are in m/s, E in GPa, the density (ρ) in T/m³, and Poisson's Ratio (ν) is non dimensional. The P-wave velocity in a bounded medium, such as in a concrete pile or a long rod, is independent of Poisson's ratio (ν) if the wave length is a few times the rod diameter. Equation 2.1b illustrates this relationship [Timoshenko and Goodier, 1970]. The S- and P-wave velocities relate to the surface wave velocity by equations 3.3a and 3.3b, respectively. If $\nu = 0.2$, the R-wave velocity is 56 % of the P-wave velocity.

3.1.5 Reflection and Refraction

Specular reflection of an incident wave occurs when wavefronts strike an interface of two dissimilar mediums. Specular reflection is analogous to the reflection of light off a mirror [Carino and Sansalone, 1984]. Dissimilar mediums are referred to as mediums which possess a different acoustic impedance. The amount of energy of an incident P-wave reflected off an interface is dependent on the difference in acoustic impedance. Equation 3.4a is the specific acoustic impedance of a medium:

$$Z = \rho \times C_p \tag{3.4a}$$

where the acoustic impedance Z is in T/m^2s , the density ρ in T/m^3 , and the P-wave velocity C_p is in m/s. In the case of long rods and concrete piles, the acoustic impedance of a medium is:

$$Z = \sqrt{E \times \rho} \tag{3.4b}$$

where Young's Modulus (E) is in GPa. If the shear wave velocities (C_s) are known, equation 3.1a is still valid. The acoustic impedance of each material is expressed as a function of C_s [Carino and Sansalone, 1984].

The incidence angle of the seismic wave is a major factor that affects the amplitude of the reflected wave. Maximum amplitude specular reflection occurs when the incident wave is perpendicular to the interface of two mediums. A coefficient of reflection determines the amount (percentage) of wave energy reflected from an interface. Equation 3.5 shows the relationship between the acoustic impedance of each material at the interface.

$$R_c = \frac{Z_2 - Z_1}{Z_2 + Z_1} \tag{3.5}$$

where R_c is a dimensionless parameter. At an interface with two very dissimilar materials, such as concrete and air, virtually all the incident wave energy (about 99%) reflects back into the concrete according to values in Table 3.1 and by using equation 3.5. The reason related to this effect is the different acoustic impedance of each material. In the case of a concrete to water interface, approximately 72% of the incident wave energy reflects back into the concrete. Table 3.1 gives the specific acoustic impedance of many common materials and rocks.

If an incident wave has an angular trajectory with respect to the plane of an interface, the incident wave may go through mode conversion. That is, an incident P-wave may split into reflected P- and S-waves. This transpires also with incident S-waves. If this occurs, the reflected energy of the incident wave divides between both reflected waves.

Table 3.1
Specific Acoustic Impedance of various common materials
[after Carino and Sansalone, 1984].

Materials	Density (p) (kg/m²)	P-wave Velocity (C,) (m/s)	Specific Acoustic Impedance (Z) (kg/m²s)
Air -	1.205	343	0.413
Water	1000	1480	1.48 E+06
Concrete	2300	3000 - 4500	6.9 - 10.4 E+06
Steel	7850	5940	46.6 E+06
Granite	2750	5500 - 6100	15.1 - 16.8 E+06
Marble	2650	3700 - 6900	9.8 - 18.3 E+06
Quartzite	2620	5600 - 6100	14.7 - 16.0 E+06
Soils	1400 - 2150	200 - 2000	0.28 - 4.3 E+06

[•] This is representative of normal weight concrete only.

As previously discussed, when a wave is incident on a concrete to air interface, only a portion of the wave reflects back into the concrete. The other portion of energy from the incident wave transfers into the second media in this case, water. This phenomenon is wave refraction (see Figure 3.4).

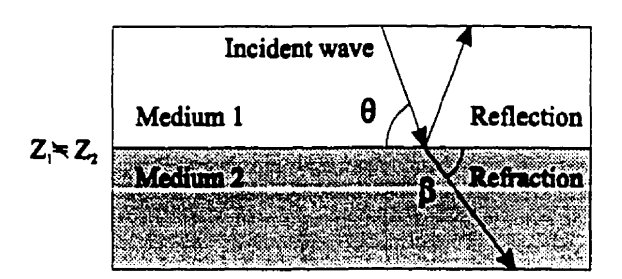


Figure 3.4

Reflection and refraction of an incident P-wave at the interface of two materials with different acoustic impedance.

With respect to the orientation of the flaw, the refracted wave is at angle β . This angle is a function of the angle of incidence θ of the initial wavefront, along with the P-wave velocity of each medium. Snell's Law governs the refraction angle β in the second media as shown in equation 3.6a [Carino and Sansalone, 1984]. Snell's Law is also applicable to mode converted incident waves. Figure 3.5 illustrates the above phenomena for a mode converted incident P-wave.

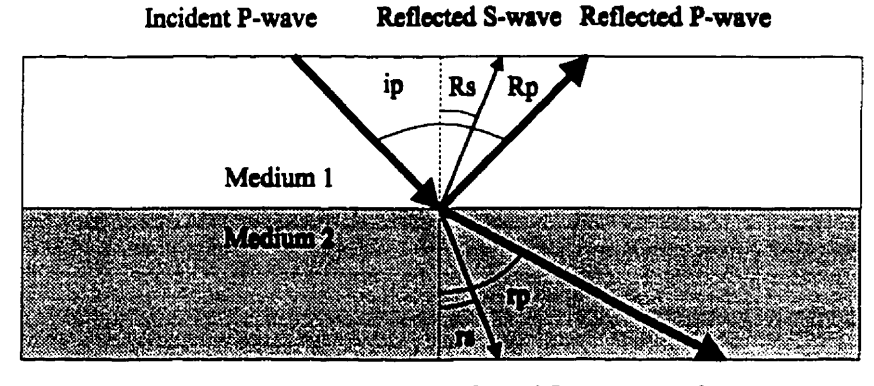
$$\sin \beta = \frac{C_{p2}}{C_{p1}} \sin \theta \tag{3.6a}$$

In this case Snell's Law will take the following form:

$$\frac{\sin i_p}{C_{p1}} = \frac{\sin R_p}{C_{p1}} = \frac{\sin R_s}{C_{s1}} = \frac{\sin r_p}{C_{p2}} = \frac{\sin r_s}{C_{s2}}$$
 (3.6b)

where R is the reflection angle, i is the incidence angle, r is the refraction angle, and C_p and C_s are the P- and S-wave velocities, respectively.

A wavefront occurs on a surface (or planes) in a material where the wave motion is the same. In other words, at the position where the phase has the same value. For P-waves, the wavefronts are perpendicular to the direction of propagation. This notion holds for all types of waves in an isotropic medium [Telford et al., 1990]. A line showing the propagation direction of a wave is called a raypath.



Refracted S-wave Refracted P-wave

Figure 3.5

Angles of reflected and refracted body waves due to an incident P-wave impacting an interface of two dissimilar media at an oblique angle.

3.1.6 Diffraction

Diffraction of an incident wave occurs when the wavefronts intercept the edge of a crack oriented at an acute angle as shown in figure 3.6. In this case, the edge of the crack reflects back a spherical wave. Theoretically, the reflected energy of a diffracted wave is an order of magnitude less than the incident wave energy [Carino et al., 1986]. These waves allow the detection of crack tips. A later chapter of this thesis discusses this phenomenon by experimental evaluation. Figure 3.6 illustrates this effect in concrete.

As previously mentioned, specular reflection creates the most powerful response on the surface of a material and is the easiest to examine. Specular reflection is highly dependent on the orientation of a defect in a material. Therefore, for specular reflection to occur, the orientation of the crack is preferably perpendicular to the incident wave.

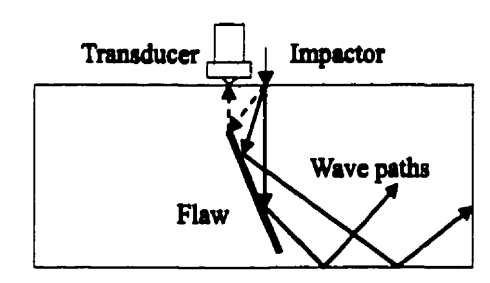


Figure 3.6
Incident wave diffraction caused at a crack tip. The dotted lines indicate the diffracted path of the incident wave [after Carino et al., 1986].

3.1.7 Attenuation of Waves in Heterogeneous Solids

In an ideal homogeneous material, the energy of a spherical wave would inversely decrease at an exponential rate with the distance from the impact source. Natural materials, on the other hand, create a more or less noticeable effect that lowers the wave energy. This also occurs in man-made materials such as concrete. There are two general reasons for this phenomenon: *scattering* and *absorption*. Attenuation is in essence, the loss of energy of a seismic wave [Krautkrämer and Krautkrämer, 1983]. Scattering is the result of wavefronts intercepting boundaries of different acoustic impedance inside a medium.

In the case of concrete, boundaries are between the cement paste and the aggregates. Scattering occurs if the aggregate size is much larger than the wave length. The wave splits in two at the interface of the first cement/aggregate interface, repeating this process at each subsequent interface. Therefore, the incident wave divides constantly into other waves that eventually convert into. It is therefore essential that the wave length be longer than the minimum aggregate size of the concrete member or structure to be tested [Krautkrämer and Krautkrämer, 1983]. The same researchers state that for ultrasonic testing of heterogeneous materials, scattering is almost negligible for grain sizes of $1/1000^{th}$ to $1/100^{th}$ of the wave length. Scattering can be clearly observed at about $1/10^{th}$ to the full value of the wave length.

The second source of attenuation is absorption. In essence, absorption is the natural conversion of energy into heat. After excitation, the particles suffer a dampening effect. This after effect makes it clear why a high frequency-low energy wave attenuates faster than the inverse type of wave. Typically, the absorption of a wave is proportional to its frequency increase. Low frequency-high energy waves are ideal for concrete testing waves. Note that in this case, the use of a low frequency increases the dimensions of the detectable flaw. In other words, short wave lengths help find small objects at short distances and vice versa for long wave lengths.

The acoustic pressure (or energy) of miniature seismic waves decreases as a result of attenuation at great depths [Krautkrämer and Krautkrämer, 1983]:

Note that ultrasonic testing uses a higher frequency stress pulse which is more susceptible to scattering in concrete compared to the stress pulse generated by the MSR Impact-Echo system.

Acoustic pressure is a general term used for ultrasonic testing of materials. This term is used to describe the pressure change of an oscillating particle. For instance, a motionless particle of a material is at normal pressure. Once the particle is excited, it begins to oscillate between other particles. Pressure is higher in denser material and vice versa [Krautkrämer and Krautkrämer, 1983].

$$P = P_o e^{-\alpha t} \tag{3.7}$$

where P_o and P are respectfully the initial and subsequent acoustic pressures, α is the attenuation coefficient (dB/m), and d is the path length of the wave (m). Scattering is the leading cause of attenuation. Therefore, the value of α relates to the wave length of the propagating wave. In this case, increasing the frequency content of the wave will cause a higher attenuation in any given material and in particular concrete [Carino and Sansalone, 1983]. According to Rothing (1974) and also Claytor and Ellington (1983), the values of the attenuation coefficient, α , for concrete are of the order of 0.3 to 30 dB/m. These values are for wave frequencies of 100 to 200 kHz (as used for ultrasonic testing).

Attenuation has an effect on the frequency content of a wave pulse that travels through a heterogeneous material. A transmitted pulse does not contain one single frequency but a frequency range that forms the frequency content. When testing concrete, the higher frequency (small wave length) pulses attenuate first with respect to propagation depth. In this case, the lower frequencies of a pulse propagating in concrete dominate the frequency spectrum. For the nondestructive methods discussed in this thesis, typical frequencies are in the range of 0 to 15 kHz.

The MSR method discussed in this thesis is based on the propagation of non-planner, hemispherical, and spherical waves. These types of waves do not only attenuate by the preceding phenomena, but also by *spreading* away from the impact source as they propagate through an infinite medium. This is called wave *divergence*. For a point source impactor, divergence causes the acoustic pressure to vary as the inverse of the distance from the source [Carino and Sansalone, 1984].

The pulse generated at the surface of a medium undergoes attenuation and divergence in both directions between a surface boundary and an internal flaw. Therefore, the amplitude of the received signals at the surface of a medium decrease significantly with the total travel distance. Thus, the energy loss of the propagating wave depends on both the test medium characteristics and the type of seismic wave under investigation [Krautkrämer and Krautkrämer, 1983].

3.2 THE MINIATURE SEISMIC REFLECTION (MSR) METHOD

The following sections describe in detail the MSR Impact-Echo method with respect to its technical aspects and test methodologies. It is important to note that the MSR method's defect location capability is based on the IE method hence its inclusion in the name of the MSR Impact-Echo system. The IE system was developed for concrete in

the 1980's by Drs. Sansalone and Carino at the National Bureau of Standards in the United States [Sansalone and Carino, 1986]. Both of these test systems use miniature seismic waves which propagate in a medium. Both systems incorporate piezoelectric transducers, impact sources, data acquisition hardware, and data analysis software. However, the Impact-echo system is based solely on the analysis of P-wave reflections and was developed to investigate thin concrete slabs. The MSR Impact-Echo system is based on the analysis of both P- and S-wave reflections and for possible applications on large concrete elements and shaft linings. Therefore in order to eliminate repetition and to simplify the text, the ensuing sections discuss the fundamentals of the MSR Impact-Echo system. This system is a more recent development of the use of miniature seismics in an elastic medium.

3.2.1 Theoretical Background

Wave reflections occur due to a sudden change in elastic property or density of a medium (i.e., a change in acoustic impedance). A variation in acoustic impedance is the result of internal flaws or voids. The angle of incidence, radiation pattern, elastic material properties, and acoustic properties of the second medium all contribute to the amplitude of the reflected waveform received at the surface of the tested object. Piezoelectric transducers, which respond to surface displacements and translate the deformations into electrical signals, record the sinusoidal pattern of the reflected waves. The reflected P- and SV-waves create a periodical waveform at the surface (vertical and tangential, respectively). Vertical and tangential displacement transducers capture the periodical deformations on the surface and transform them into electrical signals. An oscilloscope displays the electrical signals in the time domain (i.e., the waveform). The time domain signals are converted separately to the frequency domain by applying the Fast Fourier Transform (FFT) technique. In the resulting frequency spectrums (one each for the P- and SV-waves), the dominant peek reflection frequencies are determined. The frequency peaks are the result of multiple P- and SV-wave reflections between the surface and a boundary.

The periods of P- and SV-wave arrivals at the surface of a medium (Δt_p and Δt_s) are related to the travel path length and their respective velocities C_p and C_s . In equations 3.8a and 3.8b, 2T is to account of twice the propagation distance between the interfaces as shown in Figure 3.9 [Sansalone and Carino, 1988].

$$\Delta t_p = \frac{2T}{C_p}$$
 and $\Delta t_s = \frac{2T}{C_s}$ (3.8a), (3.8b)

Knowing that the period and the frequency of multiple P- and SV-wave arrivals have an inverse relationship, the frequencies of these arrivals are written as:

$$f_p = \frac{C_p}{2T}$$
 and $f_s = \frac{C_s}{2T}$ (3.9a), (3.9b)

The P- and SV-wave velocities C_p and C_s in an elastic medium can therefore be determined by the following equations:

$$C_n = 2T \times f_n$$
 and $C_r = 2T \times f_r$ (3.10a), (3.10b)

From equations 3.10a and 3.10b, the thickness of concrete sections and elements can be determined from the following relationships:

$$T = \frac{C_p}{2f_p}$$
 or $T = \frac{C_s}{2f_s}$ (3.11a), (3.11b)

Relationships have been established in order to take into account the difference in acoustic impedance of two dissimilar media. For example, if one looks at the conversion from compression to tension and vice-versa of a propagating P-wave in concrete which intercepts another medium with lower acoustic impedance, equation 3.11a is valid (see Figure 3.7a). However, if a P-wave is incident upon an interface with a higher acoustic impedance such as a steel reinforcement bar (see Table 3.1), conversion from compression to tension and vice-versa only occurs at the concrete to air interface (i.e. the surface of the media as shown in Figure 3.7(b)). In this case, equation 3.11a is written as [Lin et al., 1990]:

$$T = \frac{C_p}{4f_s}$$
 ; for $Z_1 < Z_2$ (3.12)

The Sub-Surface Sensing Laboratory of McGill University assembled the first prototype of the MSR Impact-Echo system. The applications of the system include testing circular and arch shaped concrete structures, evaluating rock masses in the field, and laboratory investigation. The principal purpose of developing system was to

nondestructively determine the dynamic properties of concrete and rock. In situ and laboratory investigations are now possible. The dynamic properties of interest are the dynamic Young's Modulus (or Modulus of elasticity), the dynamic Poisson's ratio, the dynamic Shear Modulus, and the dynamic Bulk Modulus. Table 3.2 shows the general relationships between P-and S-wave velocities and the dynamic properties of a material [Telford, 1996].

An analysis software, developed on the GAUSS mathematical and statistical system, provides a tool for the evaluation of these properties. Of interest in this application are body waves namely, the P- and SV-waves. By determining their propagation frequencies between two boundaries and by knowing the P- and S-wave velocities in the same medium, it is possible to determine the dynamic elastic properties of a medium. The following sections describe the MSR system in detail.

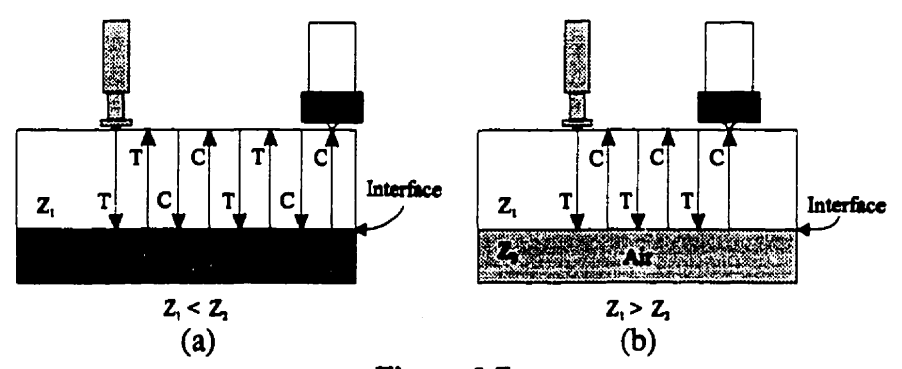


Figure 3.7
P-wave reflections from (a) concrete to steel interface, and (b) concrete to air interface.

Table 3.2

Relationships between elastic wave velocities and dynamic elastic properties of materials [Telford, 1990].

Young's Modulus (GPa)	Shear Modulus (GPa)	Bulk Modulus (GPa)	Poisson's Ratio
$E = C_p^2 \rho \frac{(1+\nu)(1-2\nu)}{(1-\nu)}$	$G = \rho C_s^2$	$K = \rho \left(C_p^2 - \frac{4}{3}C_s^2\right)$	$v = \frac{\binom{C_p}{C_s}^2 - 2}{2\binom{C_p}{C_s}^2 - 2}$
$E=C_s^22\rho(1+\nu)$	$G = \frac{K}{\begin{pmatrix} C_p^2 / -4/3 \end{pmatrix}}$	$K = G\left(\frac{C_p^2}{C_s^2} - \frac{4}{3}\right)$	

3.2.2 Instrumentation of the MSR Impact-Echo system

The hardware for this nondestructive testing system consists of the following essential elements:

- a series of impact sources
- a set of broadband piezoelectric displacement transducers
- an oscilloscope or analog to digital signal converter
- an analysis software
- and a portable computer.

The ensuing sections describe the impact sources and the piezoelectric displacement transducers in detail. Section 3.3 presents a complete discussion of the data acquisition principles used with this technique. The Fast Fourier Transform (FFT) is also discussed in this section. Figure 3.8 illustrates the principle of the MSR Impact-Echo system.

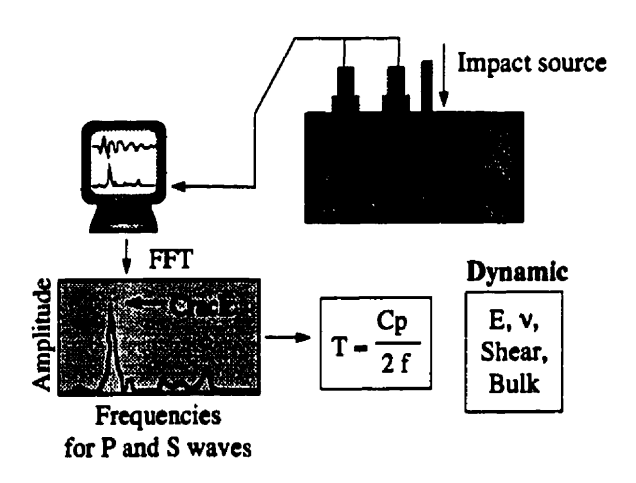


Figure 3.8
Schematic of the MSR Impact-Echo system.

3.2.2.1 Impact Sources

The impact source generates miniature seismic waves by the release of a spherically tipped mass onto the test surface. The impact generates low frequency stresses into the media. The initial dynamic point load then travels through the medium as hemispherical P- and S-waves (see Figure 3.9). The P- and S- waves travel inside the solid and reflect back from free boundaries and internal interfaces.

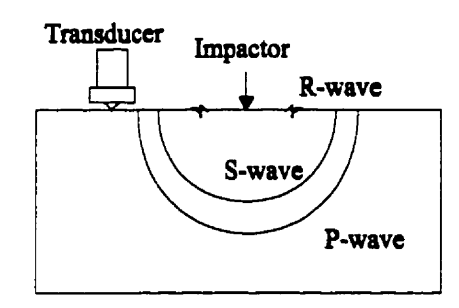


Figure 3. 9
Propagation of P-, S-, and R-waves after initial impact.

As previously discussed, the frequency content of a wave is of great importance. There are many factors that affect the frequency content of the wave. For concrete testing, it is essential to match the desired frequencies of the wave with the internal characteristics of the material. The main factor that governs the frequency content is the contact time of the spherical tip on the material surface. The ensuing section describes this subject in detail.

3.2.2.2 The Contact Time

The contact time of a sphere falling on a concrete surface is key to the success of both the MSR and Impact-Echo methods. In effect, the contact time determines the frequency content of the waves generated by the impact source. Therefore, the contact time limits the dimensions of detectable defects as well as their depth relative to the surface. In essence, the shorter the contact time, the higher the frequency content of the wave. Note however, that the wavelengths are shorter. This allows for detection of small objects and defects at relatively short distances. It is important to use short contact times when testing concrete slabs since they typically thin concrete elements. In theory, the contact time of the impact of a spherical object on concrete is approximately equivalent to the elastic solution of a sphere colliding with a thick plate. Equations 3.13 (a to c) shows this elastic solution and the relationship between contact time and material properties [Goldsmith, 1965].

$$t_c = 5.97 \left[\left[\rho_s \left(\delta_s + \delta_p \right) \right]^{2/5} R \right] / (h)^{0.1}$$
 (3.13a)

$$\delta_p = \left(1 - \nu_p^2\right) / \left(\pi E_p\right) \tag{3.13b}$$

$$\delta_{\epsilon} = (1 - v_{\epsilon}^2) / (\pi E_{\epsilon}) \tag{3.13c}$$

where

 t_c = contact time (seconds)

 v_p = Poisson's ratio for the plate

 ρ_s = density of the sphere (kg/m³)

 v_r = Poisson's ratio for the sphere

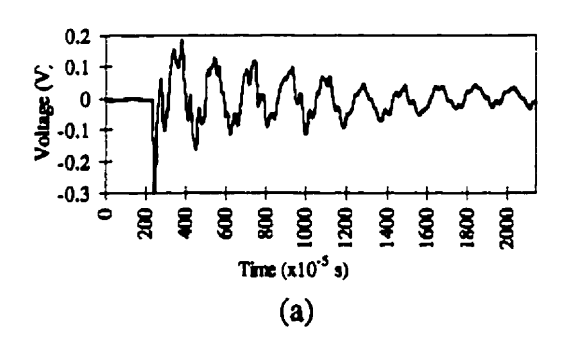
R - radius of the sphere (m)

 E_p = Young's modulus for the plate (N/m²)

h = drop height (m)

 E_r = Young's modulus for the sphere (N/m²)

Figure 3.10 illustrates a typical waveform captured by a vertical displacement piezoelectric transducer along with its frequency spectrum. Notice the sinusoidal pattern that results from the surface displacements. The maximum frequency produced by the impact is equal to the inverse of the contact time. The application of the Fast Fourier Transform (FFT) technique to a digitized time domain waveform generates the frequency content of a wave. The typical maximum input frequency is equal to $1.5/t_c$, where t_c is the contact time [Sansalone and Carino, 1987]. Analyzing the first portion of the waveform in the time domain can give an approximation of the contact time (see figure 3.11). Since the material properties of concrete are not taken into account, this method is only an approximation of the real contact time. Note however, that the resulting contact time is typically inferior to the time shown in figure 3.11. Contact times of 20 to 100 μ s are typical for applications of the MSR and Impact-Echo methods.



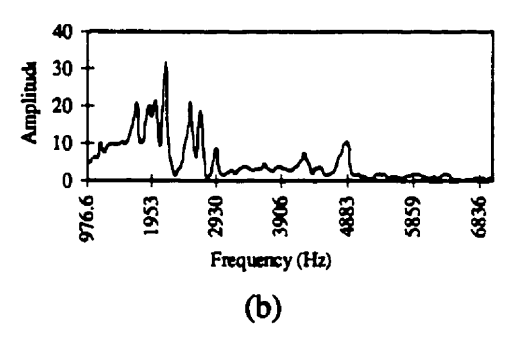


Figure 3.10

Waveform generated on the surface of a concrete test object

(a) time domain waveform; (b) frequency spectrum of the waveform.

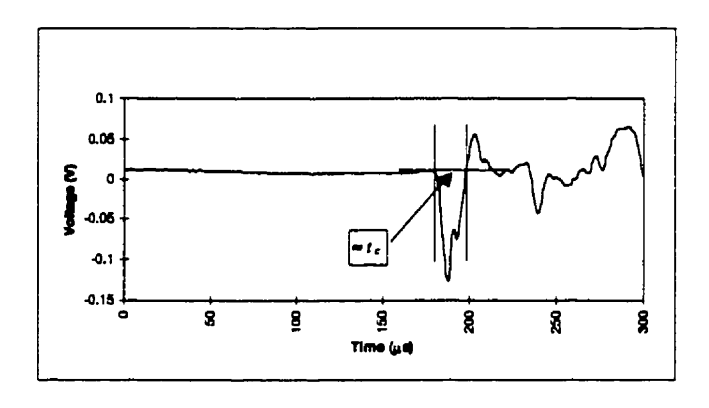


Figure 3.11
Estimation of the contact time by analyzing the first arrival of the Rayleigh wave.

It is interesting to discuss the effect of the elastic impact of a sphere impacting a surface. The Hertz theory of elastic impact best defines this phenomenon. The force-time function of the impact resembles a half cycle-sine curve (see the following equations).

$$F = F_{\text{max}} \sin\left(\frac{\pi t}{t_c}\right) \quad ; \quad 0 \le t \le t_c \tag{3.14a}$$

$$F_{\text{max}} = \frac{\left(1.140(v_0)^2 m_s\right)}{\alpha_m} \tag{3.14b}$$

$$\alpha_{m} = \left[\left[(15\pi v_{0}^{2}) / (16R^{0.5}) \right] (\delta_{s} + \delta_{p}) m_{s} \right]^{0.4}$$
 (3.14c)

where F_{max} = maximum force exerted during the impact (N)

t_c = contact time of the impact (s)

 m_r = mass of the sphere (kg)

 v_a = velocity of the sphere at impact (m/s)

It has been determined by elastic theory, that the contact time of a steel sphere dropped on concrete is approximated by the following equation (for E = 36 x 109 N/m2, ν = 0.2, and C_p = 4000 m/s) [Sansalone, 1986]:

$$t_c = 0.00858R/(h)^{0.1} (3.15)$$

where

R - radius of the sphere (m)

h - drop height (m)

From this equation, the radius dimension is directly proportional to the contact time. Notice also the moderate effect of the drop height on the contact time. However, when the impact occurs on a concrete surface, the contact times may actually be longer than predicted by equation 3.15. The cause is attributed to local material crushing at the point of impact on the concrete. In this case, the material at the impact point has lost its elastic behavior and now behaves as an inelastic material.

3.2.2.3 Piezoelectric Transducers

Many types of instruments such as accelerometers, geophones, and piezoelectric transducers can capture waveforms on a surface. For the experiments discussed in this work, piezoelectric transducers help record the waveforms generated by spring loaded impact devices. This section offers a brief explanation of the piezoelectric effect of some materials and the generation of electrical potentials from material deformations. Discussed as well are details about the transducer assembly of the MSR Impact-Echo system.

The Piezoelectric Effect

Essentially, a piezoelectric material has the property of producing electric charges on its surface if the material deforms due to external forces. The brothers Curie discovered this effect in 1880 and by the year 1881, the reverse effect was observed. In other words, if the piezoelectric material is subjected to an electrical charge, the material changes shape. The first phenomenon mentioned in this paragraph is called the *direct piezoelectric effect* and the second phenomenon, the *inverse piezoelectric effect* [Krautkrämer and Krautkrämer, 1983].

The oldest piezoelectric material is the quartz. A number of materials exhibit the piezoelectric effect. The asymmetry of a crystal structure characterizes the piezoelectric effect in materials. The presence of one or more polar axes in the crystal structure causes the asymmetry. Due to the quartz's hexagonal crystal nature there are three polar axes. X_1 , X_2 , and X_3 refer to the polar axes of a quartz crystal as shown in Figure 3.12.

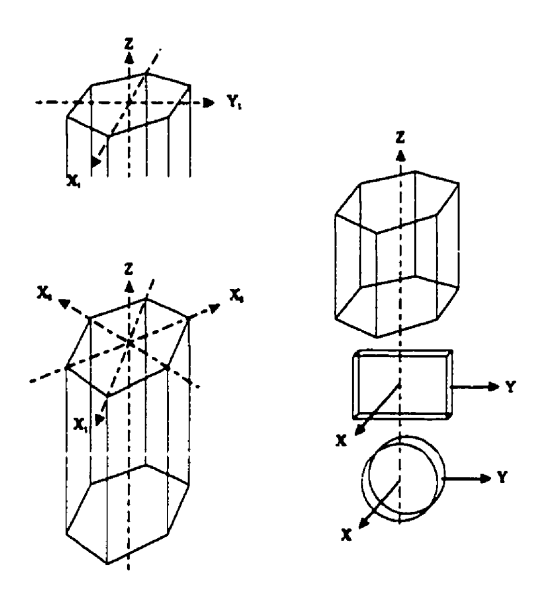


Figure 3.12 Polar axes X_1 , X_2 , and X_3 of a quartz crystal [after Krautkrämer and Krautkrämer, 1983].

In Figure 3.12 the Z-axis is parallel to the vertical axis of the prism. The Z-axis is referred to as the optical axis. The use of circular or rectangular plates cut at right angles from one of the X-axis serve to illustrate the piezoelectric effect. An applied compressive pressure on the right angle plate reduces its thickness due to the elasticity of the material. The applied pressure actually shifts electrically charged elements, such as in the case of quartz, silicon and oxygen ions (see Figure 3.13). The shift of these ions renders the plate polarized. This results in a free positive charge and a free negative charge on opposite sides of the plate. The charges on each side of the plate reverse their sign when there is crystal expansion (i.e., a thickness change). In other words, as the pressure on the plate changes from compression to tension, a likewise voltage sign change occurs on the plate surfaces.

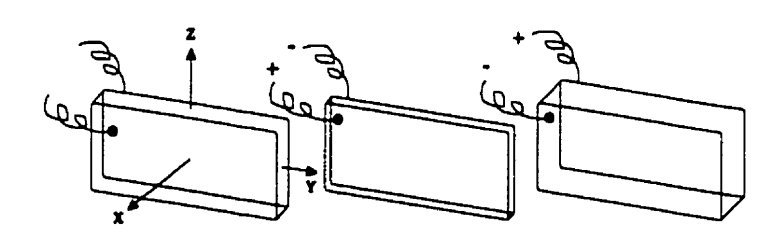


Figure 3. 13

Deformation (change of thickness) of an X-cut quartz plate [after Krautkrämer and Krautkrämer, 1983].

If, for instance, a seismic wave impacts a plate creating alternating compression and tension states, the plate produces an alternating voltage, which corresponds to the frequency of the wave. It is now common knowledge that the generated voltage is proportional to the applied pressure on the plate [Krautkrämer and Krautkrämer, 1983]. An oscilloscope can record the alternating voltages and display the resulting waveform in the time domain.

Piezoelectric Materials

For nondestructive testing, commonly used piezoelectric materials include lead zirconate-titanate (PZT), barium titanate (BaTiO₃), lead metaniobate (PbNb₂O₆), lithium sulphate (LiSO₄), quartz (SiO₂) and lithium niobate (LiNbO₃). The oldest piezoelectric material, quartz is clear and very hard. Only a limited number of substances can attack quartz on a chemical level. All other materials are less resistant to mechanical wear.

PZT piezoelectric materials equip the instruments used in the experiments presented in this thesis. The PZT material is often used as a sintered ceramic material. It is not possible to produce adequately sized crystals directly from a PZT element. The procedure involves grinding the raw material and adding the product to binders which help produce the crystals. Moldings help form the crystals into the required shape by applying pressure and sintering above a temperature of 1000 °C. The final shape of the PZT element is formed by grinding the coarse material with very precise instruments. PZT materials are white to yellowish in color and are more susceptible to wear than quartz. The PZT elements used in this work are of conical and pyramidal shapes.

Testing on Concrete

It is preferable to use broadband piezoelectric transducers for concrete testing. These transducers produce a low noise output signal over a wide frequency range. Ideally, to capture vertical and horizontal displacements on a surface, one must use a specific type of transducer designed for each purpose. This is the case for the MSR system although both transducers capture P- and S-waves.

The propagation and displacement vectors of the P-wave produce the vertical displacements on the surface. A special vertical displacement transducer responds to the sinusoidal surface oscillations. The S-wave vertical propagation vector generates vertical displacements at the surface. These are not the displacements of interest with respect to the S-waves. At the time the reflected vertical propagation vector produces displacements at the surface, it also generates horizontal surface displacements. A tangential displacement transducer captures the horizontal surface displacements. It is

important to note that this transducer also captures the radial expanding P-waves after reflection at the surface (see Figure 3.9). In other words, upon reflection at the surface P-waves produce horizontal surface displacements.

The MSR system uses two broadband displacement transducers: one tangential and one vertical (see Figure 3.8). Due to their small contact areas, they behave as point receivers [Sadri, 1996]. The vertical displacement transducer has a 1 mm diameter contact tip. The contact tip has the shape of a cone. In 1982, Proctor designed this transducer at the National Bureau of Standards[†] in the United States.

The transducer is now commercially available under the designation: IQI Model 501 Dynamic Surface Displacement Transducer. Proctor designed the transducer to produce a uniform response over a wide frequency range. Additionally, the transducer is extremely sensitive to normal (vertical) surface displacements and it generates a response directly proportional to the displacement. The transducer is commonly called the NBS conical transducer. It offers a very flat response in the range of 50 kHz to 1 MHz.

The transducer is 21 mm in diameter and 18.4 mm in thickness. The manufacturer adds a cylindrical brass backing, filled with a tin and tungsten powder epoxies up to the PZT conical tip. The brass backing causes the elimination of unwanted frequencies. It is essential to amplify the output signals from the transducer. Therefore, the IQI Model 501 transducer includes a matching preamplifier. The output impedance of the system is 50 ohms which allows for the use of coaxial cables up to 50 feet long. Only the intrinsic attenuation of the cable limits the performance of the transducer. This system requires the use of a 9V battery.

The addition of a metallic shield minimizes electrically induced interference. It is essential to ensure adequate coupling between the PZT tip and the surface. By placing a thin lead strip between the tip and the surface, one eliminates the need for viscous coupling agents. A copper plate serves as a coupler for the transducers of the MSR system.

The S-wave transducer is sensitive to a tangential displacements and was originally designed by Proctor in 1988. Permission was granted to McGill University by the designer to manufacture the proposed transducer for research purposes. The active element of this transducer is in the form of a truncated pyramid. The pyramid has a base area of 12 mm2 and height of 6 mm. The contact aperture is 0.5 mm by 2.0 mm. The shorter dimension is in the polarization direction which is the direction of maximum

^{† &}quot;The National Bureau of Standards" (NBS) is now called "The National Institute of Standards and Technology" (NIST).

tangential sensitivity [Sadri, 1996]. This transducer is also fitted with a brass backing having the following dimensions: 25 mm thick, 65 mm long, and 50 mm wide. The rear of the brass backing has a conical void which is filled with a molten tin metal. A low temperature tin-indium solder is was used to paste the active element to the brass backing. The transducer response is practically flat and constant over a 1.5 MHz bandwith.

The output voltage waveform is proportional to the dynamic tangential displacement on the surface of a material. Minimal vertical displacements are captured by the transducer. The transducer produces a null signal output when the polarization direction is at a right angle from the impact source [Sadri, 1996]. An amplifier is connected to the brass backing of the transducer and is powered by a standard 9V battery. The maximum output of the transducer is ± 2 volts, peak to peak.

The tangential displacement transducer must be placed near the impact source at a distance inferior to the S-wave wave length. This distance is a factor of the thickness of the test object and its material properties. The piezoelectric tip of the transducer is always in linear contact with the tested surface. It is important to position the active element at right angle to the impact point during the tests to avoid a null signal output.

3.3 DATA ACQUISITION AND DATA ANALYSIS USING THE FAST FOURIER TRANSOFRM (FFT)

A data acquisition system typically consists of the following elements:

- Sensors or PZT motion detection transducers.
- Signal Conditioning: This step converts the sensor output into signals readable by an oscilloscope or an analog to digital (A/D) converter board.
- Signal Recorders: An oscilloscope or A/D converter board which converts electrical signals into digital formats for signal processing.
- Signal Analysis: Specialized software for processing, analyzing, and storing data. Graphical display of the data is also essential for data analysis.

The previous sections discuss in detail the essential elements of the PZT transducers of the MSR system which serve as sensors. The following paragraphs describe the concepts of signal conditioning, and signal conversion or recording. Section 3.3.3 discusses in detail the signal analysis procedure of the MSR system.

3.3.1 Signal Conditioning

A signal conditioning device coupled to the transducer *amplifies* and *filters* the output sensor signal. The output from the amplifier alternates between positive and negative voltages that are easy to capture by an oscilloscope or an A/D converter board. Therefore, signal conditioning implies the alteration of the output from the transducer. Amplification of the output signal is essential for acquiring truly valid measurements. *Isolation*, overvoltage protection, and transducer excitation are of additional importance to signal conditioning.

Signal amplification is the transformation of the signal output from the transducer to a proper voltage level which an oscilloscope or A/D converter board can capture. Another term for amplification is *gain increase*. Typically, a signal undergoes a 40 to 60 dB increase according to equation 3.16 [Mindess, 1991]:

$$Gain = 20\log \frac{V}{V_i} \tag{3.16}$$

where

Gain = signal amplification in decibels (dB) V_l = input voltage (volt) V = output voltage (volt)

Filtering involves the elimination of unwanted signal frequencies. Isolation, as the word implies, isolates the output signal from electrical noise. Overvoltage protection prevents the possibility of picking up transient voltages in the electrical lines carrying the signals. Transient voltages can seriously damage and destroy electrical components and computers. Transducer excitation is essential for systems which require voltage or current excitation. For example, strain gauges need an excitation voltage, and LVDTs (Linear Variable Differential Transformer) need AC voltage since they function as electromagnets. For the MSR system, the transducers do not need excitation. The PZT elements are excited by surface displacements, not vice-versa. Therefore, the transducer excitation function is not present on the signal conditioning board.

3.3.2 Signal Recording

To record electrical output signals, A/D converter boards or oscilloscopes are required. The main functions of these instruments are to acquire and convert the conditioned signal into a digital format readable by a personal computer. Typically, the

output signal from the transducer is a continuous-time function. This type of signal is an analog output. To record this signal, the acquisition instruments transform the signal into a discrete-time sequence. This sequence is a digital signal specified at equally spaced time intervals. The conversion from analog to digital is essentially a ratio calculation. The output signal from the transducer is compared to a base reference and then converted into a fraction. The fraction results in an 8 bit binary code that is recognized by a computer.

One of the most important aspects of data acquisition is the sampling rate of the system. The sampling rate is an indication of the speed the oscilloscope or A/D converter board will scan the input channel. Each scan causes the acquisition instruments to associate the proper discrete value to the input signal with respect to the reference point. Aliasing occurs when the sampling rate is too slow. In this case, the recorded waveform is completely different with lower frequency components. The use of a benchmark frequency called the Nyquist Frequency prevents the possibility of aliasing the signal. A discussion of the Nyquist Sampling Theorem best describes this parameter:

"If a continuous bandwith-limited signal contains no frequency components higher than half the frequency at which it is sampled, then the original signal can be recorded without distortion. To avoid accidental low frequency aliasing while sampling a signal, one must take samples at 2 or more times the frequency of the signal being sampled [PC Handbook for Engineers and Scientists, 1996]."

In theory, a higher sampling frequency yields a higher level of measurement accuracy. However, it is important to assess the number of sampling points to use during the FFT process of the digitized signal. It is recommended that the number of data points in the time domain waveform be an integral number of periods of the signal. If this is not the case, errors will result in the calculation of the FFT spectrum. For the tests conducted and presented in this thesis, the MSR Impact-Echo system uses 2048 data points to calculate the FFT spectrum. The recorded number of points is called a record length. The frequency resolution in the frequency spectrum is a function of the number of sampling points and the time interval between each sample (see equation 3.17).

$$\Delta f = \frac{1}{n_r} \tag{3.17}$$

where

 Δf - frequency interval (Hz)

n - number of sampling points

r = time interval between samples (s)

The time interval (r) is used to calculate the sampling rate of the data acquisition system as shown in equation 3.18.

Sampling rate =
$$\frac{1}{r}$$
 (Hz) (3.18)

As previously discussed, if one takes 2048 samples (n) at a sampling time interval of 10 μ s (r), the resulting frequency interval is 48.8 Hz. The sampling rate for this test is therefore 100 kHz. In this case, the Nyquist frequency is 50 kHz, well above the 0-15 kHz range used for concrete testing by both the MSR and Impact-Echo methods. Therefore, aliasing is not a concern in this configuration.

By increasing the r and n values, the record length and resolution of the digitized signal increase. Note that the frequency interval has an inverse relationship with respect to the sampling rate. Consequently, reducing the sampling rate improves the frequency spectrum resolution. It is essential that the P- and S-waves reflect three times through the thickness of a concrete element. In other words, the record time of the signal must be at least three times the propagating wave travel time from the surface to the boundary and back. Therefore, the minimum required record time of the oscilloscope is:

$$R_c = 3 \left(\frac{2T}{C_p} \right) \tag{3.19}$$

where R_c = minimum record time (s)

T = thickness between surface and boundary (m)

C_p = P-wave velocity (or C_s for S-wave velocity) (m/s)

For example, if one tests a concrete element of 1.5 m thick with a P-wave velocity of 4000 m/s, the minimum required signal recording time is 0.00225 s. By using a record length of 2048 points at a sampling interval of 10 μ s, the recording time is 0.02048 s, almost 10 times the required time to obtain three reflections of the P-wave. For thin structures such as concrete slabs, reducing the sampling time r optimizes resolution. The following section is a brief discussion of the Fast Fourier Transform which is at the core of the data analysis procedure used by the MSR and Impact-Echo methods.

3.3.3 Data Analysis by the Fast Fourier Transform (FFT)

Multiple reflections from the boundaries or flaws of a concrete element create a displacement on the surface with a periodic property. As a result of these reflections, time domain waveforms exhibit complex behaviors that become difficult to analyze. Dominant peaks in the frequency spectrum represent the multiple reflections between the interfaces. The corresponding frequencies result from the arrival of wave reflections from the various boundaries. This method proves to be more efficient and simpler than time domain analysis [Sansalone and Carino, 1986].

The transformation of the digitized waveform from the time domain to the frequency domain is possible because of the well-documented concept that any periodic waveform is actually a sum of different sine waves. Each sine wave has a unique amplitude, frequency, and phase shift. The relative amplitudes and phases are functions of the frequency [Telford, 1990].

A frequency spectrum shows the frequency content of a captured signal. During the transformation from the time domain to the frequency domain the signal information remains intact. Therefore, it is possible to apply a *Fourier synthesis* which converts the signal from the frequency domain to the time domain.

The following discussion is a brief overview of the Fast Fourier Transform as it applies to the signal analysis procedure of the MSR system. Note that a more rigorous description of the FFT is easily found in the literature [see Strum and Kirk, 1988]. In order to adequately discuss FFTs, one must have a basic understanding of the *Discrete Fourier Transform* or DFT. Digital signal processing uses DFTs as a means to interpret the frequency content in digitized signals. Initially, a digitized signal is represented by a sum of complex exponentials or a sum of sine curves as shown in equation 3.20. This equation is called a periodic function g(t) with a period T, and a fundamental frequency f_n .

$$g(t) = \sum_{n=-\infty}^{\infty} \alpha_n e^{-j2\pi f_n t}$$
 (3.20)

where $f_n = n/T$ and

$$\alpha_n = \frac{1}{T} \int_{-T/2}^{+T/2} g(t) e^{-j2\pi f_n t} dt$$
 (3.21)

and in real form:

$$g(t) = \frac{a_0}{2} + \sum_{n=1}^{\infty} \left(a_n \cos 2\pi f_n t + b_n \sin 2\pi f_n t \right)$$
 (3.22)

or

$$g(t) = \sum_{n=0}^{\infty} c_n \cos(2\pi f_n t - \phi_n)$$
(3.23)

where

$$a_{o}/2$$
 = average of $g(t)$ in a cycle
$$c_{n} = \sqrt{a_{n}^{2} + b_{n}^{2}} = amplitude \text{ of the Fourier Series}$$

$$\phi_{n} = \arctan\left(\frac{b_{n}}{a_{n}}\right) = phase \text{ shift of the Fourier Series}$$

$$a_{n} = c_{n} \cos \phi_{n} \quad and \quad b_{n} = c_{n} \sin \phi_{n}$$

The periodic function g(t) represents an infinite number of complex exponentials. For practical purposes, it is necessary to use a finite number of terms in equation 3.20. In this event, it is important to assess the accuracy of the finite series that approximates the function g(t). Since the concern here is with respect to periodic waveforms, a series represents only a discrete set of values in each period. This is called the Discrete Fourier Series. The periodic exponential in equation 3.20 plays a key role in the series. From the literature, a finite sum of these exponentials exactly matches the results of a periodic sequence [Strum and Kirk, 1988]. Therefore, the problem associated with the accuracy of the method is of no concern here.

It is also possible to represent a *finite-duration* or *non-periodic* waveform as a finite sum of complex exponentials. The waveforms treated in this thesis are of the *finite-duration* type. A strict number of digitized points in the waveform are used to calculate the FFT. The number of points generally used is 2048. Note that this number is a power of 2, as needed for FFT calculations. From this perspective arises the use of DFTs.

A sum of a finite number of exponentials also represents a finite sinusoidal waveform. An important relationship is that if the finite sequence x(n) is a period of a periodic sequence $x_p(n)$, then:

$$x(n) = \begin{cases} x_p(n), & 0 \le n \le N - 1 \\ 0, & elsewhere \end{cases}$$
 (3.24)

The coefficients X(k) of the finite length sequence are found from:

$$X(k) = \sum_{n=0}^{N-1} x_p(n) e^{-j(2\pi/N)nk}, \quad \text{for } k = 0, 1, ..., N-1.$$
 (3.25)

and from the preceding relationship

$$X(k) = \sum_{n=0}^{N-1} x(n) e^{-j(2\pi/N)nk}, \quad \text{for } k = 0, 1, ..., N-1.$$
 (3.26)

Therefore, the DFT pair is shown as equations 3.26 and 3.27 [Strum and Kirk, 1988]:

$$x(n) = \frac{1}{N} \sum_{k=0}^{N-1} X(k) e^{i(2\pi/N)nk}, \quad \text{for } n = 0, 1, ..., N-1.$$
 (3.27)

Note that both X(k) and x(n) are zero outside the range of 0 to N-1. Solving equation 3.26 for every value of k helps determine the amplitude and phase of the various sinusoids in the waveform. Knowing the sampling rate of the system, one can determine the dominant frequency peaks in a frequency spectrum. Spectrum analysis includes the use of DFTs and is somewhat more complicated than the theoretical notions previously discussed. Solving the DFT of a finite signal is an extremely lengthy process, particularly when analyzing 2048 points (N). To solve equation 3.26, the total number of computations is over 4 million (equivalent to N^2). Obviously, computer programs handle these computations. At this point it is common to use Fast Fourier Transforms to simplify the computations.

Essentially, an FFT is a computer algorithm which significantly increases the computation efficiency of DFTs. The development stems from the work of Cooley and Tukey in 1965. The computation of an FFT requires that the number of sampled points in a DFT be an integer power of 2. The FFT computer algorithm that uses this criteria is called a radix-2 FFT. Generally, a divide-and-conquer strategy is at the basis of the FFT algorithm. In other words, the digitized waveform is divided into smaller sequences of waveforms which overlap one another. The amount of overlap depends on the requirements of the waveform analysis. On each smaller sequence, the FFT algorithm performs a DFT. This simplifies the calculations since there is a reduction in the number of digitized points in each sequence. From equation 3.26, one can see that the series length for the DFT is less, hence a reduction in the number of computations.

Using equation 3.26, each value of k requires N complex multiplies since the series is a summation. Therefore, the standard DFT requires $N \times N = N^2$ complex multiplies since there are N values of k. FFTs require $N/2 \log_2 N$ complex multiplies for an N-point DFT. For example, a 1024 point DFT requires 1 048 576 complex multiplies.

An FFT of this DFT requires only 5120 complex multiplies, thus reducing the computation time significantly [Strum and Kirk, 1988].

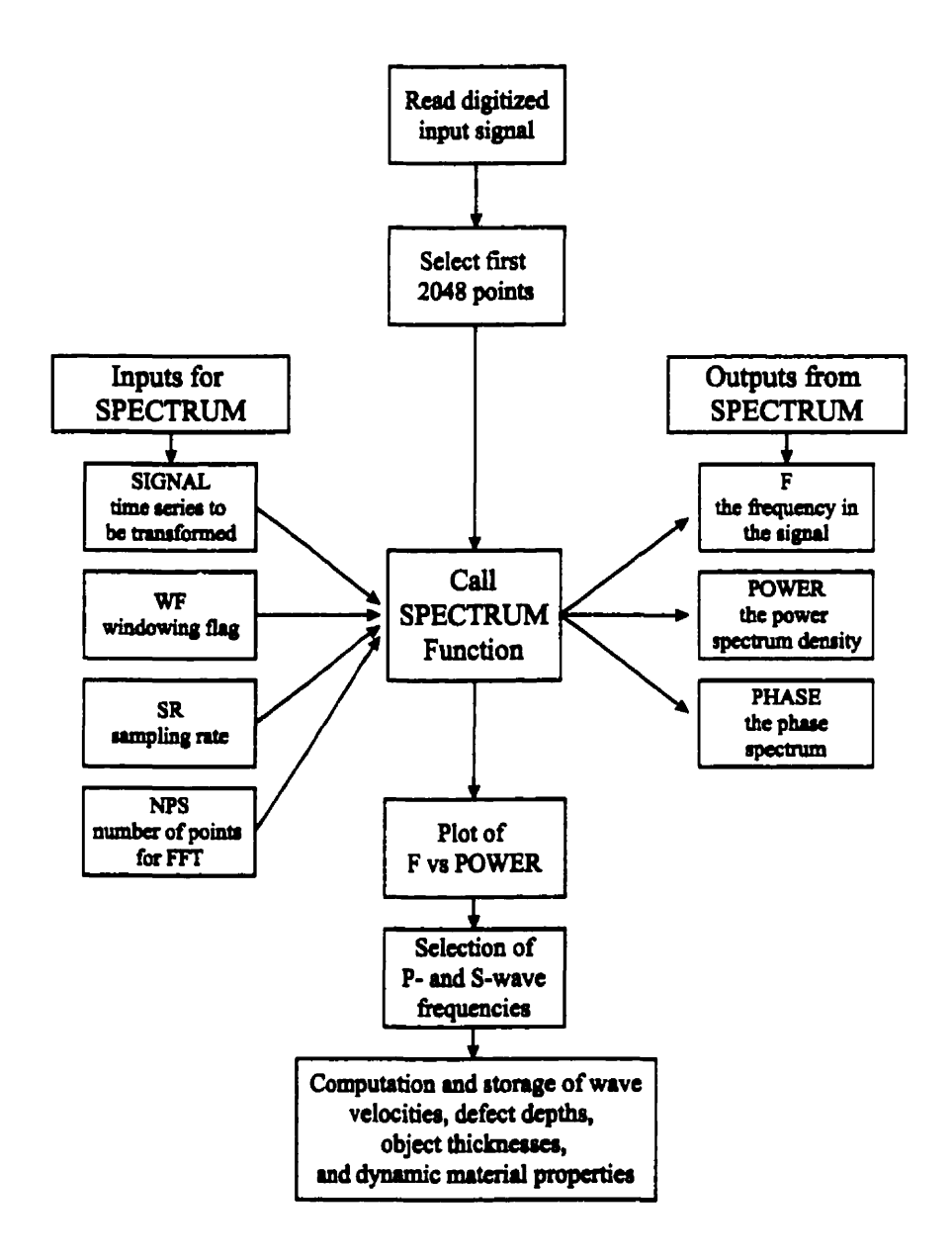
Many books in the literature offer a complete discussion of FFTs. Due to their complexity and wide range of various computer algorithms, the scope of the discussion of FFTs is limited to the previous paragraphs. The following sections briefly discuss the FFT computer algorithm used by the MSR system.

The frequency spectrum analysis program for the MSR system was developed on the GAUSS mathematical system. The GAUSS system is a matrix based language where one can create specific applications for their uses. A computer program developed on the GAUSS Time Series Analysis Package helps identify both the P- and SV-wave frequencies components of the waveforms.

Figure 3.14 is the flowchart of the FFT algorithm developed on the GAUSS system. A recent modification of the computer program effectively increases the data analysis time and storage efficiency. These changes are discussed in a further chapter of this thesis.

3.4 FINAL NOTES

The material presented in this chapter underlines the basic theoretical notions of the MSR and Impact-Echo methods. Section 3.1 gave a brief overview of elastic wave theory. The focus was on the propagation of miniature seismic waves in elastic solids. Section 3.2 described in detail the fundamentals behind the MSR Impact-Echo method followed by an overview of the instrumentation of the system. Section 3.3 discussed some important notions related to digital data acquisition and signal analysis.



Flowchart of the FFT algorithm developed on the GAUSS mathematical system for the MSR Impact-Echo method.

RESEARCH OBJECTIVES

The evaluation and quantitative determination of the structural integrity of a concrete dam is essential in order to establish its expected life span. Recent developments in nondestructive testing have generated promising results that may lead to the elaboration of a sound nondestructive testing procedure. The main objectives of nondestructive testing are inspection cost reduction, increased reliability, and increased confidence in the results. To attain these objectives it is essential to develop a sound and repetitive testing method. The MSR and Impact-Echo methods fall in this category of nondestructive testing methods. The following sections present the scope of work performed for this thesis along with an overview of the research needs and objectives. Section 4.3 presents three test beds built to assess the research needs related to expanding MSR Impact-Echo technology.

4.1 SCOPE OF WORK

The main focus on this research project is to help evolve MSR Impact-Echo technology from laboratory testing to actual in situ applications on concrete dams. Before turning this technique into a useful in situ application method for concrete dam assessment, it is essential to determine the capabilities and limitations of this system. This essential step is needed to move forward in the instrumentation development process. The MSR Impact-Echo instrumentation, assembled and developed by the Sub-Surface Sensing Laboratory of McGill University, has undergone extensive laboratory testing. The system has also been used to determine the thickness of concrete shaft liners in mines and concrete tunnel linings. These were all applications on thin concrete elements. For the system to be used on concrete dams, the penetration depth must be increased. Data analysis is performed in the lower P-wave frequencies because of the deep penetration depth in concrete dams.

The test beds discussed in the next sections serve as part of a continuous instrumentation development program. The tests were developed to assess some of Hydro-Québec's concerns with respect to the crack location capabilities of the system. The next sections describe in detail the goals and objectives of the tests conducted at IREQ.

4.2 RESEARCH NEEDS AND OBJECTIVES

Concrete dams suffer from many forms of deterioration caused by the simultaneous effects of a multitude of factors. Some forms of deterioration adversely affect the structural integrity of dams. A concrete structure is built to operate without incident during the course of a predetermined service life. For the past 80 years, structural engineers have noticed that major civil structures around the world are failing to reach their expected service lives. Many repair techniques and methodologies have been developed to address these problems. NDT is one solution available to the concrete industry. However, confidence in nondestructive testing has suffered in the past due to the heterogeneous nature of concrete and to technical limitations. In recent years, instrumentation technology has caught up to the theoretical applications of nondestructive testing of concrete. Practical applications of nondestructive testing are being reported more often in the literature. It seems that the concrete industry has regained confidence in the capabilities of nondestructive techniques.

Due to the continuous technological progress, the emergence of new nondestructive techniques is inevitable. Such is the case with the development of the Impact-Echo technique. For example the personal computer increased the efficiency and reliability of the data analysis procedure. The continuous development of this system has led the emergence of the MSR Impact-Echo method. The system combines defect location and thickness measurement capabilities with the appraisal of dynamic properties of the material under investigation.

4.2.1 Research Needs for the MSR Impact-Echo system

Presently, the penetration depth of the MSR Impact-Echo system is limited to approximately 0.5 meters. Many experimental and in situ tests have been conducted on concrete elements of this thickness (see Chapter 2). Tests have focused mainly on concrete slabs of uniform surface conditions. Concrete shaft and tunnel linings have also

been investigated. The thickness of these concrete elements generally falls in the above category.

Chapter 2 mentions case studies on the application of the Impact-Echo method on concrete dams. Only a few studies of this type were found in the literature. These studies focused on the location of cracks at depths. Hence, there is a lack of practical information related to the use of this miniature seismic technique on concrete dams and particularly on thick concrete structures.

To test thick concrete structures, various parameters need consideration, such as, the orientation of the crack, its depth, its thickness and its saturated or dry condition. In situ surface conditions and cold joint effects also need attention during tests. The work in this thesis addresses some of these factors by conducting systematic investigations on various test beds. Experimental work is needed to find the appropriate equipment and analysis methods required for testing concrete dams. This is the main focus of the work presented here. The reader will note that the test beds presented in the ensuing sections serve only as a preliminary investigation into the use of the MSR Impact-Echo system on concrete dams.

4.2.2 Research Objectives

The main goal of this research project is to extend the penetration depth of the MSR Impact-Echo system up to a depth of 7 to 10 m. To reach this goal, one must keep in mind that the miniature seismic waves generated inside a medium suffer an exponential energy loss with depth. This is a variable that must be taken into account during the analysis and development of the system.

It was deemed essential to determine if the system is capable of finding inclined cracks in concrete. Tests of this type have been performed before by other researchers, however only at depths up to 0.5 m [Sansalone and Carino, 1986]. A test was developed to determine if the instrumentation of the MSR Impact-Echo system was capable of determining the degree of inclination of a crack. Cracks in concrete dams are rarely uniform and straight. Most often they dip at various angles and have complex surface profiles. Hence, the necessity of determining the surface profile of inclined cracks. The precision of the system was also an important factor to determine.

Another area of interest is the minimum crack thickness detectable by the present instrumentation. A small scale test bed was built for the purpose of determining this parameter in dry and saturated crack conditions. This is the smallest of the three test beds presented in this thesis. This test gave an indication of the sensitivity of the system.

Cracks in concrete dams are sometimes very fine and difficult to observe by borehole and concrete core investigations. Internal cracks originating from the upstream face of the dam are usually filled with water. Internal parallel cracks may also be filled with water. Cracks originating from the downstream face of dams are usually dry.

The final test bed presented in this thesis is a section of a concrete gravity dam constructed for investigative purposes on the site of IREQ. The section serves as an evaluation of the limitations of the system and as a simulated field study for the newly developed MSR Impact-Echo system. The tests performed on this structure focus on evaluating the dynamic elastic properties of the concrete and the penetration depth of the system. The dimensions of the concrete gravity dam section are representative of an actual small gravity dam.

Another important objective of the research program was to enhance the data analysis procedure. When analyzing a massive structure such as a concrete dam, one must be aware of the incredible amount of information acquired. To analyze a large amount of data, a software program must be versatile enough to allow data file manipulation and storage of results. A computer program based on the GAUSS mathematical software package was modified to address these constraints. The program is partially based on the previous computer program but adds enhanced file manipulation and data recording capabilities. The analysis software was adapted to analyze both P- and S-wave frequency values and to give the dynamic properties of the tested material. The software development is discussed in detail in Chapter 6.

4.2.3 Summary of Research Needs and Objectives

To better understand the direction of this research project, a list describing the research needs and objectives is given in Table 4.1. The intent is to give the reader an overview of the work presented in this thesis. The research shown in the next chapters serves as a preliminary investigation into the use of the MSR Impact-Echo system as a method for investigating concrete dams.

Table 4.1Research Needs and Objectives

Needs	Objectives
Find a nondestructive method capable of locating cracks in large concrete dams. The needs are to reduce the present inspection costs, and increase reliability.	Determine if the MSR Impact-Echo system is capable of assessing the inclination of cracks, and to what precision?
 Determine the limitations of the present system for later modifications to reach main goal penetrating to 7-10 m in concrete 	2) What is the minimum dry or saturated crack thickness detectable by the system? What is the maximum penetration depth of the system?
 MSR Impact-Echo tests have never been conducted on a dam with the objective of determining dynamic material properties. 	3) Is the MSR Impact-Echo system capable of determining the material quality of concrete elements thicker than 0.5 m?
4) Increase the data analysis speed.	4) What software modifications are needed to increase the speed of the analysis.

4.3 TEST BED CONFIGURATIONS AND DESCRIPTIONS

This section is intended to allow the reader to understand the key points behind the research conducted in this thesis. Each of the three test beds are discussed in detail with respect to their key research objectives. The construction and setup of the tests are also discussed.

4.3.1 Inclined Crack Detection

Concrete dams suffer from many forms of deterioration such as alkali-aggregate reaction, surface delaminations, reinforcement corrosion and internal cracking. The development of cracks in these hydraulic structures remains an important preoccupation for their owners. Thermal, physical, and hydrostatic cycles contribute to the propagation of internal cracks that weaken dams to some extent. These internal cracks often have irregular profiles and inclinations. A test bed was developed to assess the potential of the MSR Impact-Echo system in order to determine the profile of various materials placed in concrete. For crack detection and location, the vertical displacement P-wave transducer was used.

4.3.1.1 Key Research Objectives

The first key objective of this test was to find artificial crack materials that simulate actual cracks in concrete. Since all materials possess a different acoustic impedance as discussed in Chapter 3, a judicious selection of materials was necessary. It was essential to select materials that best represent actual crack conditions. The second key objective was to determine if the MSR Impact-Echo system was capable of detecting inclined artificial cracks imbedded in concrete. Another question arose from this investigation. If it is not possible to detect the cracks, what changes to the test methodology are needed? Precision is an important factor that also needs consideration. The results from this investigation may lead to modifications of the equipment and methodology in order to reach a satisfactory level of precision.

4.3.1.2 Test Bed Construction

1) Materials selection

Three test materials were selected according to their ability to simulate actual crack conditions. It was difficult to determine the acoustic impedance of these materials due to their thickness. Table 4.2 describes each test material with respect to their thickness and expected simulation qualities.

Table 4.2
Artificial Crack Materials

Slab	Crack Material	Thickness Thickness	Simulation
1	Plastic Sheet	0.12 mm (0.005 in.)	Very fine crack
2	Plastic Carpet	0.53 to 0.80 mm (0.021 to 0.032 in.)	Fine to coarse crack
3	Plastic Bubble Wrap	0.13 to 1.9 mm (0.005 to 0.075 in.)	Rough concrete/air interface

The thickness of each material was measured with an electronic micrometer. Multiple readings were taken on each material. Due to the irregular pattern on the plastic carpet and plastic bubble wrap materials, readings were taken from the thinnest and thickest sections. The results were averaged and presented in Table 4.2. The first material is a thin uniform plastic sheet with the preceding even thickness. This material simulates a very fine crack, almost at the detectable thickness limit of the method.

The plastic carpet is the most rigid material of all three. Its rough surface was placed facing the test surface of the concrete slab. This ensured that the interface between the concrete and the artificial crack simulated the desired crack condition. The plastic bubble wrap was positioned in this way inside the concrete slab. This material created a concrete to air interface with an irregular pattern. The third material provided the best artificial crack simulation aside from fracturing the slab itself. It was the intention of the author to create an internal crack in the slab and not simply a thickness variation.

2) Concrete slab preparation

Three concrete test slabs were cast for the purpose of testing the three artificial crack materials. Each slab was 770 mm long by 730 mm wide and 300 mm thick as shown in Figure 4.1 (a) and (b). Inside each slab, an artificial crack was positioned at an angle of 30^0 degrees from the test surface. During placement of the concrete inside the formwork, an industrial electric vibrator was used to ensure the elimination of air voids. Careful attention was brought to the vibration time to prevent aggregate segregation. A long vibration period may lead to aggregate segregation in the formwork. As shown in Figure 4.1 (a), the crack material does not extend to the extremities of the slab. The distance between the edge of the slab and the crack material was 65 mm for all three slabs. To eliminate the chance of cracking the concrete, a 5 x 5 cm steel wire mesh was placed at each end of the artificial crack. Near the corner, the wire mesh contoured the crack material. The thickness of the wire mesh is small enough to not affect the results of the MSR Impact-Echo tests. Figure 4.2 (a) to (c) show the placement of the artificial crack materials in their respective wood forms.

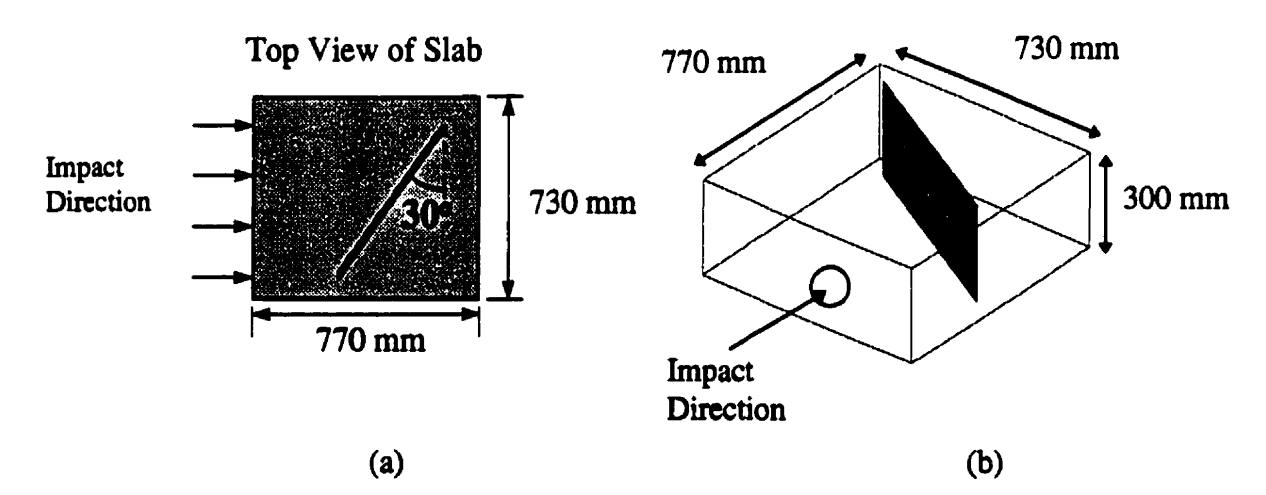


Figure 4.1

Placement of the artificial cracks in the concrete slabs with dimensions:

(a) top view of the slab, and (b) three dimensional view.

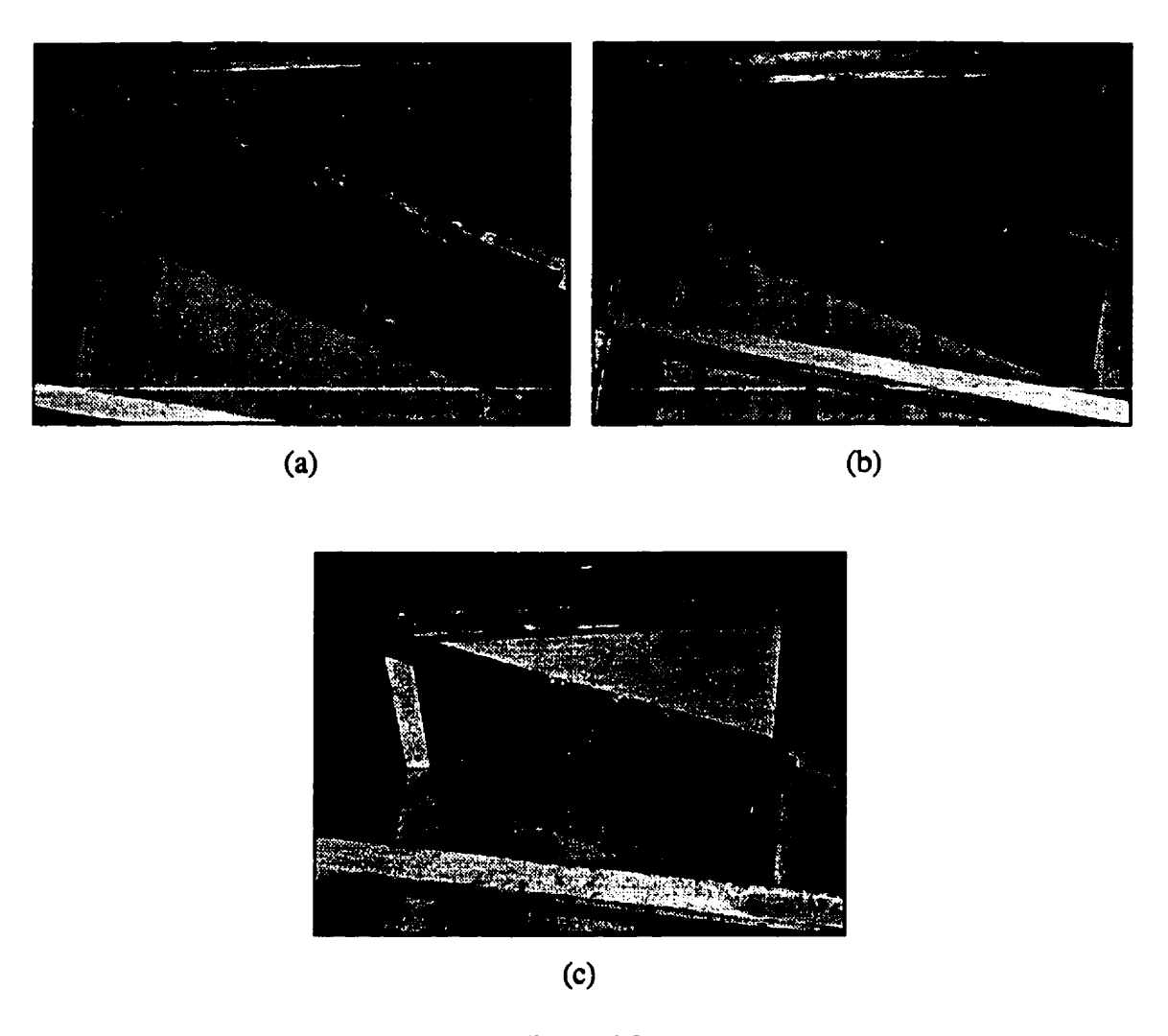


Figure 4.2

Placement of artificial crack materials in the formwork:

(a) plastic sheet, (b) plastic carpet, and (c) plastic bubble wrap.

As can be seen in Figure 4.2, the crack material in each slab was rigidly placed. Figure 4.3 is a picture of a finished concrete slab housing the plastic carpet material used during these tests. Note the angle of the artificial crack on the surface of the slab. In the top area of the slab, the dark line is only a surface defect caused by the supporting formwork shown at the bottom of Figures 4.2 (a) to (c). This was the same on all three slabs.

This concludes the test bed setup description for the first series of tests performed in this investigation. The test setup, configuration, and methodology are discussed in detail in Chapter 5.



Figure 4.3
Concrete slab showing the profile of the artificial crack at the bottom of the slab.

4.3.2 Crack Thickness Investigation

It is rare that cracks in concrete have a smooth and uniform surface area. Typical crack surfaces are rough and jagged due to fracturing of the cement paste around the aggregates. In some cases the aggregate resistance is inferior to the cement paste and fracturing occurs along the weak planes in the aggregate. For very fine cracks, this entails that the crack interface might be partially bonded in some areas. Therefore the crack interface is not an ideal seismic reflection surface.

Cracks in concrete dams are typically saturated with water for one reason or another (see Chapter 1). Water induces refraction of a stress wave at the interface between concrete and water. Refraction reduces the energy content of the reflected wave. This subsequently reduces the amplitude of the surface displacements at the test point. The refraction effect is discussed in detail in Chapter 3. The test is designed to verify if the MSR Impact-Echo system is capable of finding very fine cracks and if water creates undesirable effects.

4.3.2.1 Key Research Objectives

The research objectives of the investigation are quite straightforward. The tests are conducted for the sole purpose of evaluating the sensitivity of the system. The dimensions of the test bed show that it is a laboratory investigation and should be treated as such.

The key questions to answer are what is the minimum crack thickness detectable by the MSR Impact-Echo system and does water influence the readings in a tight saturated crack?

The next section describes the test bed setup used to evaluate the preceding research objectives.

4.3.2.2 Test Bed Construction

The test bed is the smallest of the three test beds presented in this thesis. Two 300 x 300 x 300 mm concrete blocks were poured with a plastic film between them. The main goal was to build two concrete blocks that would move one relative to another. By separating the blocks and measuring the crack thickness, one can evaluate the sensitivity of the system. A thin plastic sheet was rigidly placed in the formwork. The plastic sheet produced a negative and positive side on each concrete block. This ensures that the blocks can be completely joined when they are pressed together. Figure 4.4 schematically illustrates the test configuration of the crack thickness test.

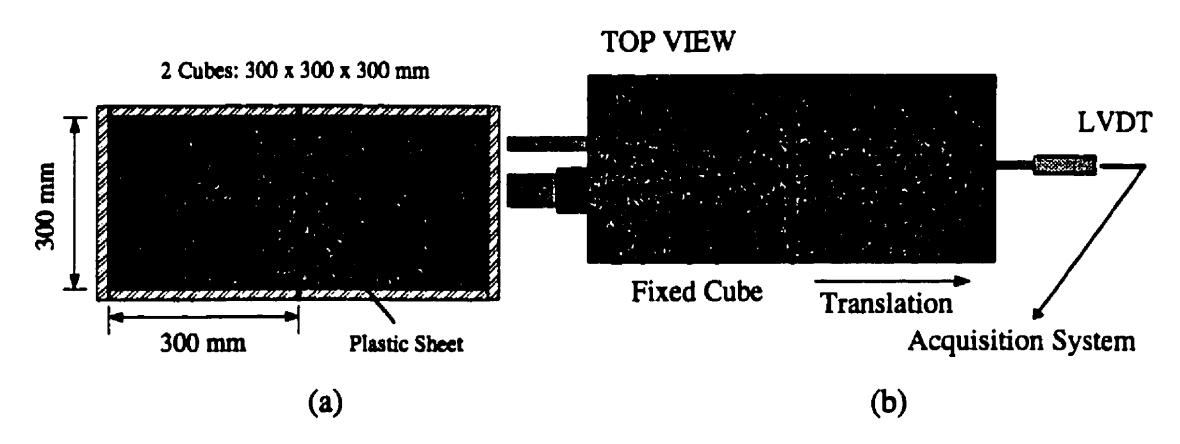


Figure 4.4

Schematic of the experimental setup used for the crack thickness investigation test:

(a) concrete blocks in formwork; (b) concept of tests to be conducted.

The forms were built to closely match the desired dimensions of the concrete blocks. Figure 4.5 (a) shows the position of the plastic sheet in the formwork. An epoxy bonding material was used to ensure watertight conditions in the box. Seepage of the cement paste at the edge of the plastic sheet was not desired. Figure 4.5 (a) and (b) shows the formwork used to build the two concrete blocks.

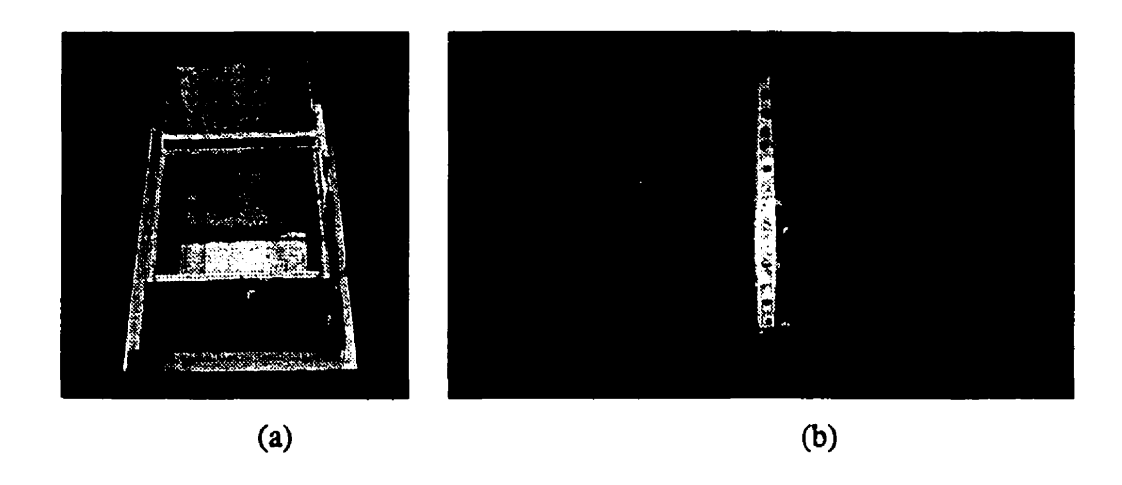


Figure 4.5
Formwork used to mold the concrete blocks.

Variable crack thickness is possible by the horizontal translation of one of the blocks. A rigid metallic base frame was built to help move one of the blocks. The metal frame consisted of four angles welded together at the corners. Each angle was of size 50 x 50 x 3 mm. The interior test frame dimensions were 790 mm long and 380 mm wide.

Holes were pierced into the long sides of the frame to allow the passage of metal rods. The metal rods were placed in the test frame to reduce the friction effect at the base of the translating block. Nine metal rods were inserted into the test frame. They were rigid enough to support the two concrete blocks. It was possible to move the translating block simply by adjusting assemblies anchored to the opposing sides of the concrete blocks. These assemblies are discussed later in the text. Figure 4.6 shows the rigid metallic frame during the construction stages with the metal rods used to support the concrete blocks.

To make sure that both blocks were properly aligned, another metal angle of type $50 \times 50 \times 3$ mm was added to one of the long sides of the frame. Holes were also drilled into this angle to allow the insertion of the metal rods. By using two 5/8 inch bolts, it was possible to align the concrete blocks by simply adjusting them. Figures 4.7 (a) and (b) illustrate this description. Notice the nine metal rods used to reduce the friction under the translating block.

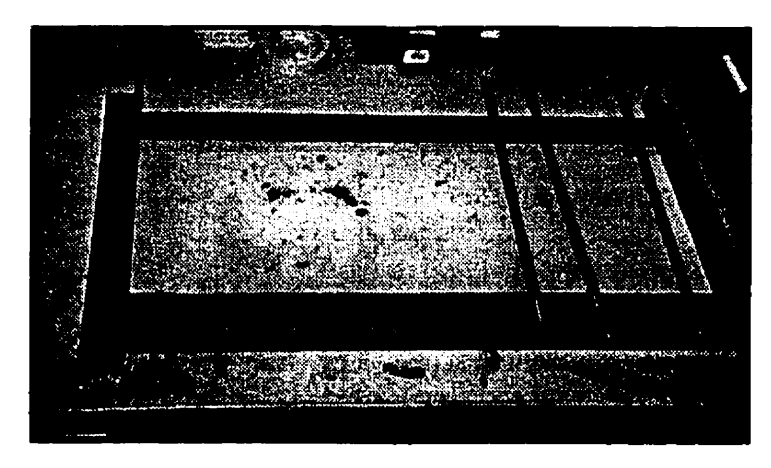


Figure 4.6

Rigid metal frame used to support the two concrete blocks.

Notice the rods used to reduce the friction under the translating block.

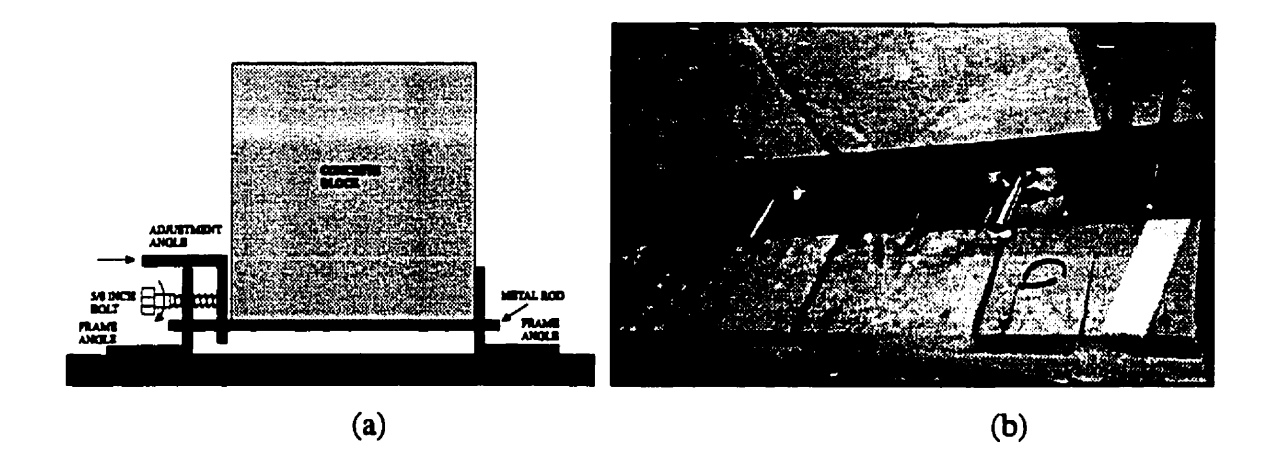
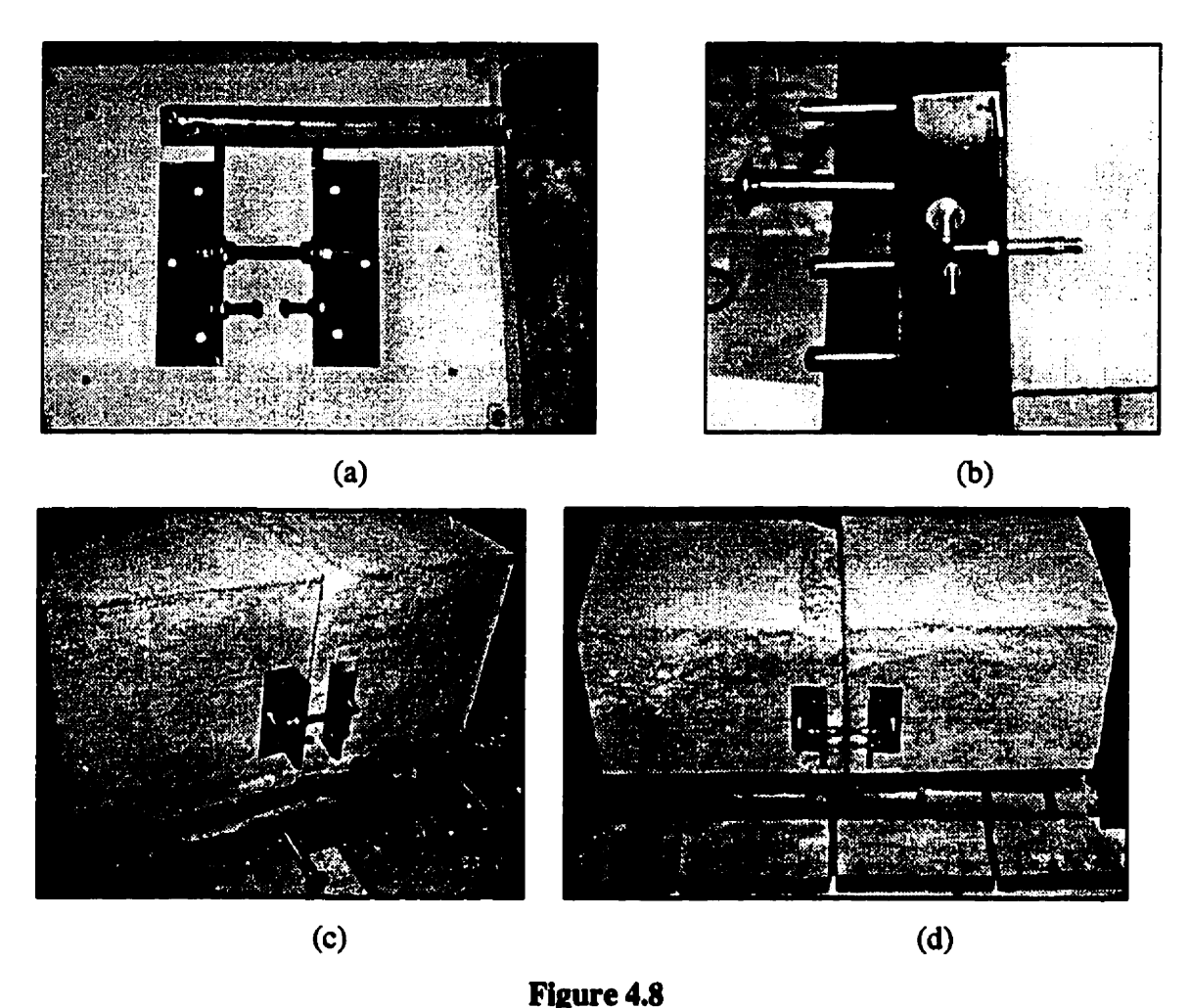


Figure 4.7
Adjustment assembly used to properly align both concrete blocks.

To ensure an initial zero crack width condition, a clamping mechanism was set up on two opposing sides of the concrete blocks. The clamping mechanism was part of assemblies anchored to the sides of the blocks. Each assembly consisted of two 40 x 40 x 3.5 mm steel angles anchored to the concrete with 6.4 x 57.2 mm concrete anchor bolts. The depth of the anchors in the concrete was such that they had no influence on the readings obtained during testing. The surface area of the imbedded part of the anchors was two small to detect. This is confirmed by the relation between flaw size and flaw depth. The ratio (D/T) of the anchor bolt's lateral surface area (D) to its depth from the test surface (T) is well below one. Previous work has confirmed that it is very difficult to detect these objects. Figures 4.8 (a) to (d) show the assembly assemblies as they were anchored to the concrete blocks. In Figure 4.8 (a), the bottom bolts were

added for the purpose of using an electronic displacement transducer. The transducers were intended to be connected to an MTS testing machine. The objective was to obtain digital readouts of the crack thickness when the blocks would be separated.

This concludes the test bed description for the crack thickness investigation tests. In Figure 4.8 (d), the top of the left concrete block shows an irregular surface. This was caused by the formwork support for the plastic sheet between the concrete blocks. Some additional information on the test methodology and equipment used to perform the tests can be found in Chapter 5.



Clamping and translation assembly anchored to each side of the concrete blocks:

(a) assembly with bolts and pre-drilled holes, (b) imbedded part of the anchors, (c) and (d) show assemblies anchored to opposing sides of the concrete blocks.

4.3.3 Investigation of a Section of a Concrete Gravity Dam

Hydro-Québec owns many concrete gravity dams. These are large mass concrete structures mainly used to retain water basins for the production of electricity. These structures often possess a complex geometry and suffer from many types of chemical and physical attack mechanisms. Often, they are victims of their size, mass, and asymmetrical geometry. Many of the concrete dams are reaching the limit of the service life and need to undergo serious rehabilitation procedures.

In order to use the MSR Impact-Echo system on such large concrete structures, a proper transition stage between laboratory testing and actual in situ testing is necessary. The test bed presented in this section serves as a way to bridge the gap between laboratory testing and in situ application. To bridge this gap, a section of a concrete gravity dam was built on site at IREQ. The test bed dimensions resemble those of an actual small scale concrete gravity dam.

The small dam served as an ideal testing environment to evaluate the equipment's capabilities and limitations with respect to the evaluation of large concrete structures. Since the concrete section was built with other tests in mind there were some anomalies added to the structure. An internal PVC pipe that crossed the thickness of the structure was added to eventually house a threaded steel bar. Internal reinforcement bars were also added to the structure during the construction phase. A foundation slab was built to support this large structure.

4.3.3.1 Key Research Objectives

The main focus of these tests is to evaluate the penetration depth capability of the MSR Impact-Echo system. It is the first time this system is used on such large concrete structures. Hence, it is extremely important to assess the limitations of the system by applying it to realistic in situ conditions.

The goal of the research project presented in this thesis is to increase the penetration depth of the system. The downstream face of hydraulic concrete dams is typically slanted. The upstream face is usually vertical. The distance between the two faces varies with respect to the slant of the downstream face. By applying the MSR Impact-Echo system to the vertical upstream face of the section, it is possible to investigate a concrete structure with a variable thickness and hence to assess the limitations of the system with respect to penetration depth.

The MSR Impact-Echo system is capable of locating anomalies in concrete structures and also determining the dynamic elastic properties of concrete. The preceding was proven during extensive laboratory tests of concrete cylinders [Sadri, 1996]. The small dam provides a great opportunity to determine if the MSR Impact-Echo system is capable of assessing the concrete quality of large structures.

4.3.3.2 Test Bed Construction

The test bed shown here is the largest presented in this work. The dimensions of the concrete section are given in Figure 4.9. The concrete foundation slab is 250 mm thick and is reinforced with two steel meshes. One steel mesh is positioned near the surface of the slab and the other at the bottom. A standard concrete cover thickness of 75 mm for exterior conditions was respected during the placement of the reinforcement. Steel anchor bars extend upwards from the concrete foundation. The anchors serve as continuity bars between the concrete foundation slab and the section of the gravity dam (see Figure 4.10 (a)).

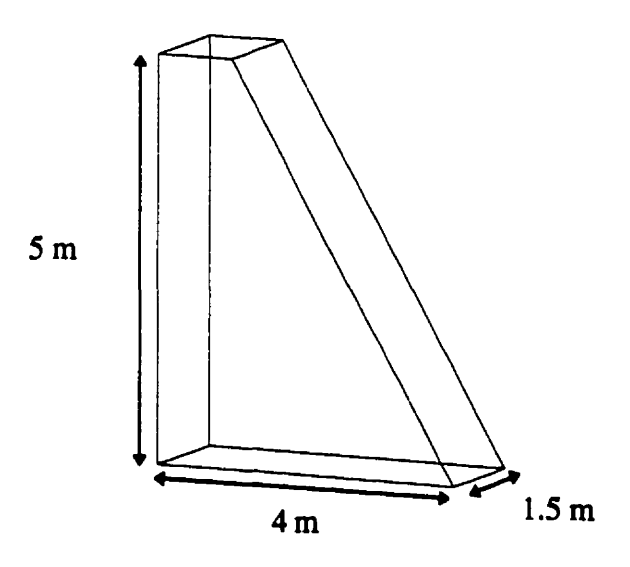


Figure 4.9

Dimensions of the concrete gravity dam section as built on the site of IREQ.

The concrete section was built in four stages. A period of time was needed to allow the concrete to properly cure after pouring each construction stage. The first stage consisted of building the concrete foundation slab that included assembling, placing, and leveling the formwork. The reinforcement was properly placed according to

[†] According to Canadian Standard CAN3-A23.3-M84.

specifications from a research engineer at IREQ. Two types of anomalies were incorporated into the concrete foundation slab for future testing (see Figure 4.10 (b)). Notice the protruding reinforcement bars that serve to anchor the section of the dam to the concrete foundation.

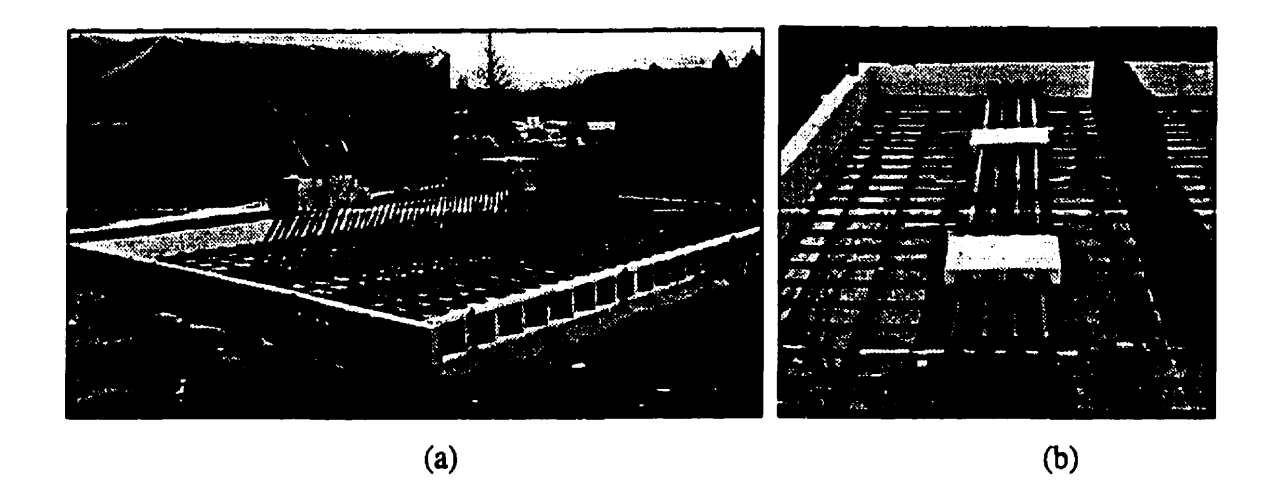


Figure 4.10

Construction of the concrete foundation slab:

(a) foundation formwork and embedded reinforcement,

(b) anomalies incorporated into the foundation slab for future work.

The second, third, and fourth stages dealt with the construction of the gravity dam. Formwork was built and put in place as designed and specified. The concrete was poured on three different occasions. This was necessary necessary the lateral forces created by the weight of the wet concrete. The concrete thickness poured at each stage was limited to about 1.5 m. This reduced the stress level applied to the formwork and avoided potential problems. A drop height of 1 to 2 meters ensured that aggregate segregation would not occur during concrete placement. Each stage was poured at 7 day intervals. This allowed the underlying concrete to reach an adequate resistance to support the next pouring stage. During the pouring process, an electric industrial vibrator was used to eliminate free air voids in the wet concrete. Figure 4.11 (a) to (c) show the formwork used to build the concrete gravity dam section. Notice the reinforcement extending out of the formwork. These reinforcement bars were eventually cut along with the protruding ends of the PVC pipe discussed previously.

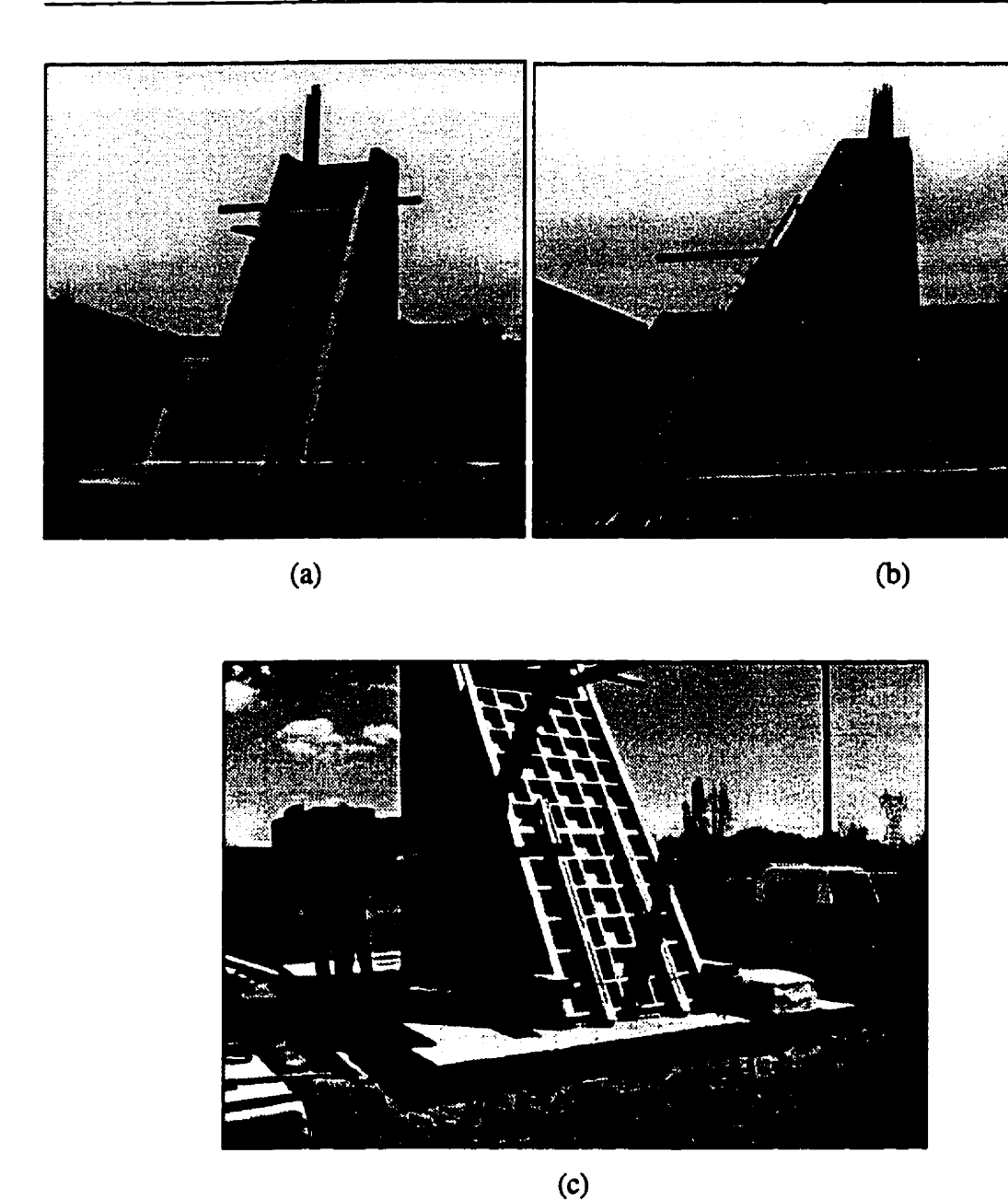


Figure 4.11
Formwork used to build the concrete gravity dam section.

Horizontal cold joints were created as a result of pouring the concrete in three separate stages. These joints also occur during the construction of large concrete dams. The dense reinforcement shown in Figures 4.11 (a) and (b) is not typical in a concrete gravity dam. This reinforcement was placed for future investigations to be conducted by IREQ.

TEST RESULTS AND DISCUSSION

Chapter 5 discusses the results obtained from tests performed on the test beds presented in the preceding pages. In this chapter, separate sections are dedicated to detailed discussions of each experiment. The following sections of the thesis present an overview of the experimental setup for each test..

Section 5.1 discusses results achieved from inclined crack detection tests. Two different test methodologies were necessary in order to improve the precision of the system. Tests performed on concrete cylinders yielded static and dynamic material properties. These results are also presented inside this section, however additional results can be found at the end of the thesis in Appendix A.

Section 5.2 presents the second experiment in the thesis. The test focuses on the crack thickness detection capability of the *MSR Impact-Echo* system. An overview of the results obtained during these tests along with the static and dynamic material property results are discussed. The tests were performed in dry and saturated crack conditions.

The third section of this chapter deals with extensive testing performed on a section of the gravity dam described in Chapter 4. Three main subsections constitute the framework of Section 5.3. Section 5.3.1 discusses the experimental setup used on the dam. Section 5.3.2 describes test results obtained from investigations on the east face of the concrete section. Section 5.3.3 presents results acquired from testing on the south face of the structure.

5.1 INCLINED CRACK DETECTION

The discussion will focus on the following aspects: the test methodologies used to investigate the three concrete slabs mentioned in Section 4.3.1.2, the static and dynamic results obtained from testing concrete cylinders, and the initial and final results of the MSR Impact-Echo tests.

NOTE TO USERS

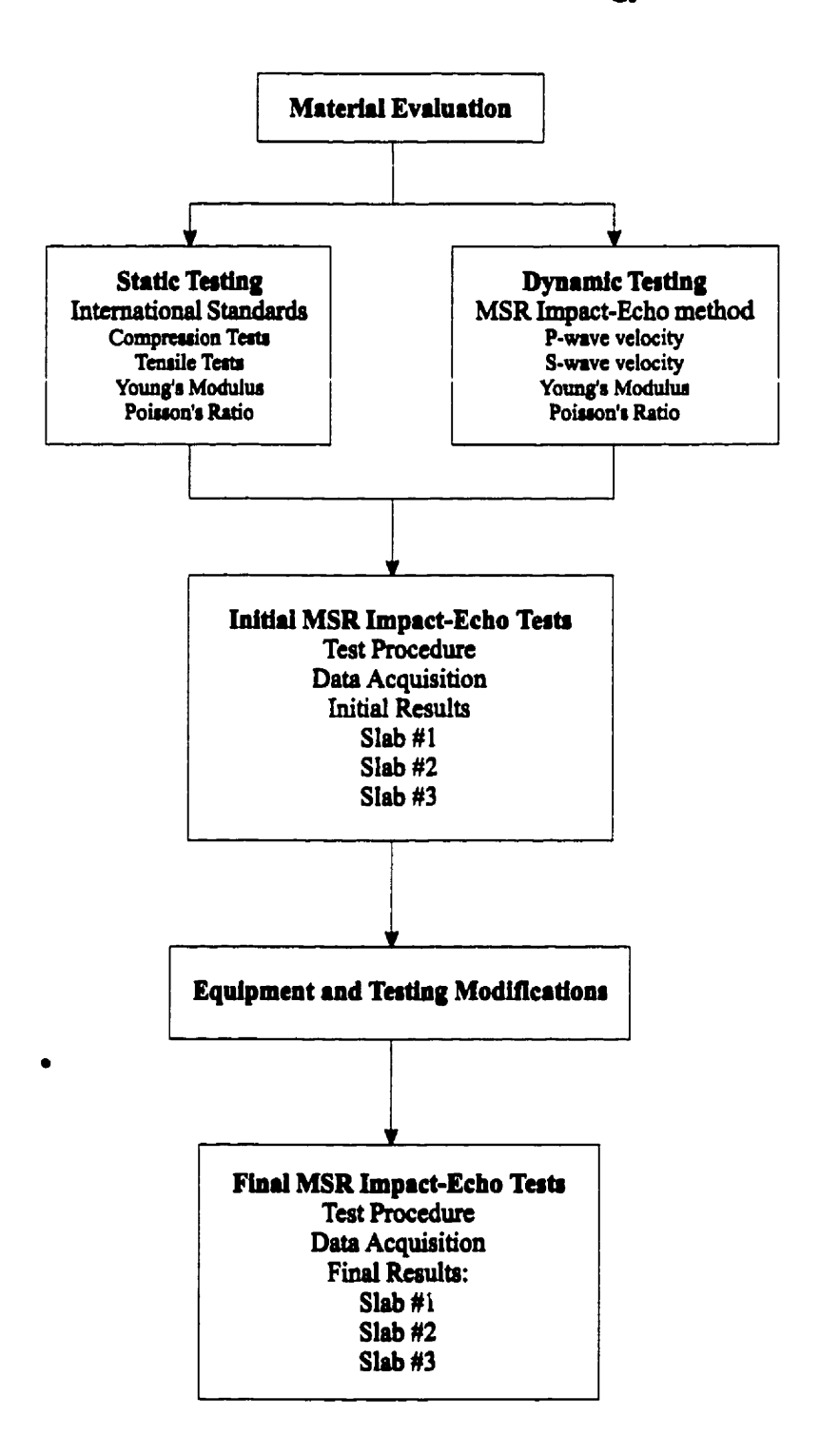
Page(s) not included in the original manuscript are unavailable from the author or university. The manuscript was microfilmed as received.

5-2

This reproduction is the best copy available.

UMI

Concrete Slabs Test Methodology



Flowchart of the experimental procedure used to perform the inclined crack detection tests.

After the dynamic tests were conducted, it was necessary to cap the concrete cylinders with a sulfur mortar for static tests in an MTS Rock Testing machine. The capping process ensures an even load distribution over the entire top and bottom surfaces of the concrete cylinder. The capping of each large concrete cylinder was performed according to standard ASTM C617-94². The compressive strength tests performed on these same concrete cylinders were conducted according to the standard ASTM C39-96³. The evaluation of the static modulus of elasticity and Poisson's ratio was accomplished in conformity to standard ASTM 469-94⁴.

As mentioned in the preceding paragraph, the three small concrete test cylinders were used to evaluate the splitting tensile resistance of concrete. These tests were performed according to the standard ASTM C496-96⁵.

The tests constitute common procedures used to evaluate the mechanical properties of concrete. All these tests were performed at the Concrete Laboratory of IREQ by the author with the supervision of a qualified research engineer. Table 5.1 is a summary of the standards used on the two different sets of concrete cylinders.

Table 5.1
List of ASTM Standards used for testing concrete test cylinders

	Concrete Test Cylinders									
ASTM Standards		152 mm Ø x 304 mm ↓						76 mm Ø x 152 mm ↓		
	1	2	3	4	5	6	1	2	3	
ASTM C192/192M-95 ¹	х	х	х	х	x	х	х	Х	x	
ASTM C617-94 ²	X	х	X	Х	х	х				
ASTM C39-96 ³	х	х	х	х	х	х				
ASTM C469-94 ⁴	X	х	X	х	x	х				
ASTM C496-96 ⁵							х	Х	х	

 \emptyset - diameter; \updownarrow - height

² ASTM C617-94, (1997). Capping Cylindrical Concrete Specimens. The American Society for Testing and Materials, 1997 Annual Book of ASTM Standards, Philadelphia.

³ ASTM C39-96, (1997). Compressive Strength of Cylindrical Concrete Specimens. The American Society for Testing and Materials, 1997 Annual Book of ASTM Standards, Philadelphia.

⁴ ASTM C469-94, (1997). Static Modulus of Elasticity and Poisson's Ratio of Concrete in Compression. The American Society for Testing and Materials, 1997 Annual Book of ASTM Standards, Philadelphia.

⁵ ASTM C496-96, (1997). Splitting Tensile Strength of Cylindrical Concrete Specimens. The American Society for Testing and Materials, 1997 Annual Book of ASTM Standards, Philadelphia.

Tables 5.2 and 5.3 show the physical properties of all cylinders presented in Table 5.1 with respect to their weight, volume, density, diameter, and height. The height of the cylinders with sulfur mortar caps was used as an input parameter for tests with the MTS machine. These tables show the actual height and diameters of the cylinders. The discrepancies are attributed to the dimensions of the plastic cylinder forms used to mold the concrete test samples. The test cylinders were moist-cured for 28 days in a wet room at 100% relative humidity. This delay allows the concrete to reach about 100% of its compression resistance [Mehta and Monteiro, 1993].

Table 5.2

Physical Dimensions of the concrete test cylinders
used for compression resistance tests and static material properties.

		Co	ncrete Te	st Cylinde	ers			
Physical Properties	152 mm Ø x 304 mm \$\(\) 1 2 3 4 5 6							
Weight (kg)	13.488	13.423	13.637	13.591	13.482	13.395		
Volume (m ³)	0.0056	0.0056	0.0057	0.0056	0.0056	0.0056		
Density (kg/m ³)	2408	2397	2392	2427	2407	2392		
Diameter (mm)	152.0	153.0	154.0	152.0	152.0	152.0		
Height (mm)	306.0	307.0	306.0	308.0	306.0	307.0		
Height with caps (mm)	311.0	311.0	315.0	314.0	312.0	311.0		

 \emptyset = diameter; \updownarrow = height

Table 5.3

Physical Dimensions of the concrete test cylinders used for tensile resistance tests

	Concrete Test Cylinders								
Physical Properties	76 :	76 mm Ø x 152 mm ‡							
	1	2	3						
Weight (kg)	1.677	1.655	1.672						
Volume (m ³)	0.0007	0.0007	0.0007						
Density (kg/m ³)	2430	2399	2432						
Diameter (mm)	75.6	75.9	76.0						
Height (mm)	153.0	152.4	152.7						

Ø - diameter; 1 - height

Table 5.4 presents the static compressive and tensile resistances of the concrete. The table also shows the static Young's Modulus and the Poisson's ratio obtained from testing three of the larger concrete cylinders described above. In order to obtain a representative value for the ultimate compressive resistance of the concrete, standard ASTM C39-96 suggests testing at least three samples cured in similar conditions. In this case, six cylinders were used to evaluate the compressive strength of the concrete. The average ultimate compressive resistance (f_c ') was 46.67 MPa with a standard deviation of 2.30 MPa. This is considered as a high strength concrete. Note however, that the supplied concrete was approximately 10 MPa above the requested compressive resistance. In the field, concrete producers typically supply higher strength concrete than the suggested by the designers in order to account for problems that may occur during the transportation and placement of the concrete. Fortunately, using higher strength concrete has no bearing on the test results presented in this section. Stress wave propagation velocities are not as yet directly linked to a material's compressive resistance.

The average tensile resistance of the concrete (f_t) was 4.88 MPa with a standard deviation of 0.47 MPa. This tensile resistance is typical of concrete. Three samples were tested as suggested by standard ASTM C496-96.

Table 5.4
Results of static testing on concrete cylinders

	Concrete Test Cylinders										
Material Property		152	mm Ø :	x 304 n	nm ‡		76 mm Ø x 152 mm ‡				-
	1	2	3	4	5	6	1	2	3	Average	Standard Deviation
$f_c'(MPa)$	45.20	51.24	46.40	45.20	46.40	45.60				46.67	2.30
$f_i'(MPa)$							5.26	5.02	4.35	4.88	0.47
E (GPa)				39.51	37.86	38.48				38.66	0.83
ν				0.26	0.22	0.25				0.24	0.021

 \emptyset - diameter; \updownarrow - height

The static mechanical properties of the concrete was evaluated by testing three of the concrete samples as indicated by standard ASTM C469-94. The static Young's Modulus was 38.66 GPa with a standard deviation of 0.83 GPa. The preceding standard mentions that it is best to conduct multiple tests on each concrete cylinder. Four tests were performed on each cylinder. The static Poisson's ratios given in Table 5.4 are

somewhat high for normal weight concrete (i.e.: $\rho = 2400 \text{ kg/m3}$). However, they were obtained according to the methodology described in ASTM C469-94. Typical static Poisson's ratios for normal weight concrete range from 0.15 to 0.2 [Mehta and Monteiro, 1993]. The average Poisson's ratio for the three concrete cylinders is 0.24 with a standard deviation of 0.021.

5.1.3 Dynamic Material Tests and Results

Static and dynamic material testing differ with respect to the strain rates produced in tested material. A strain rate is expressed as the amount of strain produced in a material over a specific amount of time. Static testing produces strain rates in the vicinity of 10^{+5} to 10^{-2} µe/s. Dynamic testing can produce strain rates up to 10^{-5} µe/s.

Three of the concrete cylinders described in Table 5.2 were tested with this system prior to the static tests and the capping of the cylinders. Cylinders 1, 3, and 5 were used for the tests. The results of the dynamic tests are presented in Table 5.5. Three series of tests were performed on each cylinder. The P- and S-wave frequencies and velocities are given for each cylinder along with the dynamic properties determined from those values. The stress wave velocities were calculated from equations 3.10a and 3.10b. The dynamic properties of the concrete were calculated with the equations in Table 3.2.

Table 5.5

Dynamic properties of the concrete cylinders

Cyl.	P-wave	S-wave	P-wave	S-wave	Dynamic	Dynamic	Dynamic	Dynamic
#	Frequency	Frequency	Velocity	Velocity	Young's	Shear	Bulk	Poisson's
	(Hz)	(Hz)	(m/s)	(m/s)	Modulus	Modulus	Modulus	ratio
					(GPa)	(GPa)	(GPa)	
1	6689.5	4071.5	4094.0	2491.8	35.85	14.95	20.43	0.21
3	6787.1	4130.9	4153.7	2528.1	36.66	15.29	20.89	0.21
5	6689.4	4071.5	4093.9	2491.7	35.84	14.94	20.42	0.21

5.1.4 Initial Crack Detection Results and Discussion

The initial tests performed with the MSR Impact-Echo system on the three concrete slabs are presented in this section. The principle objective was to evaluate the defect location capability of the system with respect to inclined cracks. The P-wave vertical displacement transducer was hence used to capture the surface displacements

caused by the reflecting P-waves between the surface and the internal crack. All three slabs were tested with the same equipment and in the same environmental conditions. The test procedure was also identical for each slab. The following sections point out the details of this investigation.

5.1.4.1 Initial Tests -- Experimental Setup

The test methodology presented in this section included important steps that need to be accomplished before proceeding with the data acquisition. At first, it is necessary to evaluate the P-wave velocity inside the concrete slabs. The P-wave velocity may significantly change depending upon the curing conditions of the concrete. Once the P-wave velocity is known, a test grid is drawn on the impact surface that faces the inclined crack. This is shown in Figures 4.1 and 5.2. The dimensions of the test grid are shown in Figure 5.2. Data acquisition was performed at each intersection on these grids. Data analysis was done afterwards and the results are presented in Section 5.1.4.3.

Figure 5.2 (a) shows the position of the impact device with respect to the P-wave transducer. This layout allowed the evaluation of 35 test points on each slab. The artificial cracks face the test grids. The grid extends from rows A to E, and from columns 1 to 7.

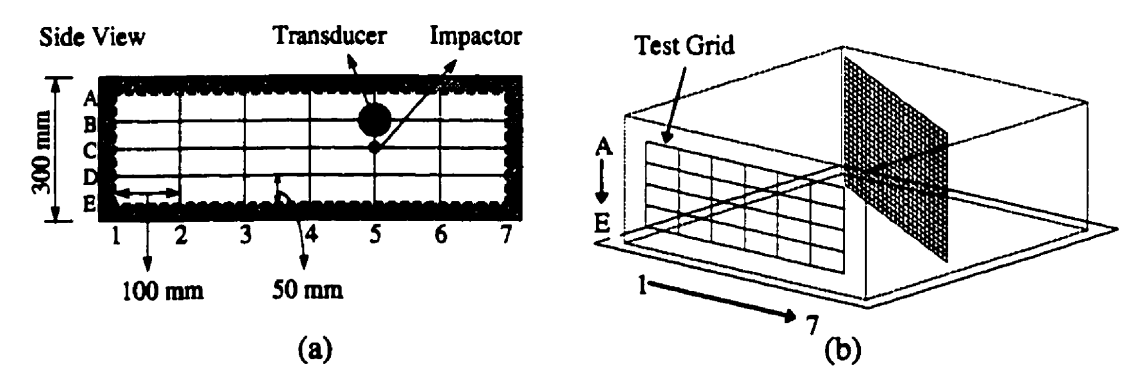


Figure 5.2
Test grid placed on the impact surface of all three slabs.

The concrete slabs were placed horizontally on wood pallets for easy manipulation inside IREQ's Concrete Laboratory. With the slabs in this position, the artificial cracks lie in a vertical plane. The initial tests were performed in the laboratory with the slabs placed in this position. The test grid surface was smooth with very few irregularities. Initial impact tests demonstrated that the contact times on this surface were

above normal at 120 µs for the lowest energy impactor. To remedy this problem, surface preparation was needed. A DremmelTM hand sander was used to slightly polish the impact positions. Careful attention was necessary to ensure that only a small layer of the surface concrete was removed. The sanding device allowed for a quick and efficient surface preparation on all three slabs. After this procedure the contact times were significantly reduced to the order of 60 to 90 µs. As mentioned in Chapter 3, the contact time defines the frequency content of a stress wave and hence its wavelength. The MSR Impact-Echo system includes a number of mechanical impact devices that generate stress waves with different frequency contents. Table 5.6 lists their mechanical properties and dimensions. At the time of the initial tests, there were only four of the five listed impact sources available.

Table 5.6
Specifications of the MSR Impact-Echo impact devices [after Sadri, 1996].

Impactor	Tip Diameter (mm)	Impact Body Mass (g)	Impact Energy (Nmm)
Custom Model #1	1.3	11.1	27.0
Custom Model #2	1.5	10.8	24.0
Custom Model #3	15	19.2	42.0
Equotip Model D	3.0	5.4	11.0
Equotip Model G	5.0	20.0	90.0

The Equotip models are manufactured in Switzerland by PROCEQ SA. The Equotip Model D impact device was chosen for the initial tests since the model G was not available at that time. The objective was to generate the lowest contact times and use the most reliable energy source. Data acquisition was performed at each point on every row of the test grid from columns 1 to 7. This procedure was applied to all three slabs.

The P-wave transducer was placed directly on the test point with the impact device always positioned 5 cm from the transducer. Previous analysis of tests performed on concrete specimens show that the optimal distance between the transducer and the impact source is 5 cm [Sadri, 1996]. The nomenclature chosen for the data file names included the position of the transducer on the test grid of each slab. The following two sections discuss the results of the P-wave velocity measurement tests and the initial results of the crack profiles in each slab.

5.1.4.2 P-wave Velocity Measurements on the Three Concrete Slabs

Before evaluating depths of defects in concrete, it was important to determine the average P-wave velocity in the material. Three tests were performed on each slab to evaluate their respective P-wave velocities. The evaluation of these velocities was performed across the 730 mm thickness of each concrete slab. The average P-wave velocity was determined from multiple tests. The sampling rate of the acquisition system was 5 µs or 200 kHz. The FFT analysis was performed on 2048 points taken from the time domain waveforms. A spectrum resolution of 97.6 Hz was obtained in the frequency domain. Table 5.7 gives the values of the P-wave velocities used to analyse the three concrete slabs. The frequencies associated to these velocities are also presented along with the actual travel distance of the waves.

Table 5.7
Initial P-wave Velocities for Each Concrete Slab

Concrete Slabs	Actual Thickness (m)	P-wave Frequency (f _p) (Hz)	P-wave Velocity (C _p) (m/s)
1 - Plastic Sheet	0.730	2890	4365
2 - Plastic Carpet	0.733	2832	4152
3 - Plastic Bubble Wrap	0.733	2832	4152

5.1.4.3 Discussion of Initial Results

In the first stages of the time domain signal analysis, it became clear that the concrete highly attenuated the stress waves. In other words, the energy content of the reflected signal is very low. Figure 5.3 (a) shows a typical sinusoidal waveform captured by the vertical displacement transducer during the initial tests. This waveform was taken from point C3 on slab 1 which has the plastic sheet as artificial crack material. The initial tests were performed with a non modified version of the test system. As shown in Figure 5.3 (a), the time domain waveforms are noisy. Figure 5.3 (b) shows the frequency spectrum associated with the previous waveform.

It was generally difficult to eliminate the noise in the signals. The noise was thought to be caused by improper grounding of the transducer. The power extension cable was replaced with a shielded cable to remedy this problem and possibly eliminate a cause of the excess noise. This type of cable is less susceptible to pick up electromagnetic fields which cause electrical currents in the wire. This change however only partially helped reduce the electrical noise in the signal. There were two other possible causes of the noise: human manipulation of the transducer or a defective piezoelectric tip in the vertical displacement transducer. These two possible causes of noise were eliminated in subsequent testing. The results of the tests conducted after the modifications to the system are presented in Section 5.1.4.4.

The horizontal position of the concrete slabs made it difficult to position the P-wave transducer in a stable position on the test grid. It was necessary to physically hunch over the slab and manipulate the transducer by hand. A grounding bracelet was also used to help eliminate the noise in the signal which was observed on the oscilloscope screen. Unfortunately, it was not possible to eliminate all the noise in the signal. Noise creates a very busy frequency spectrum that hinders the frequency selection process.

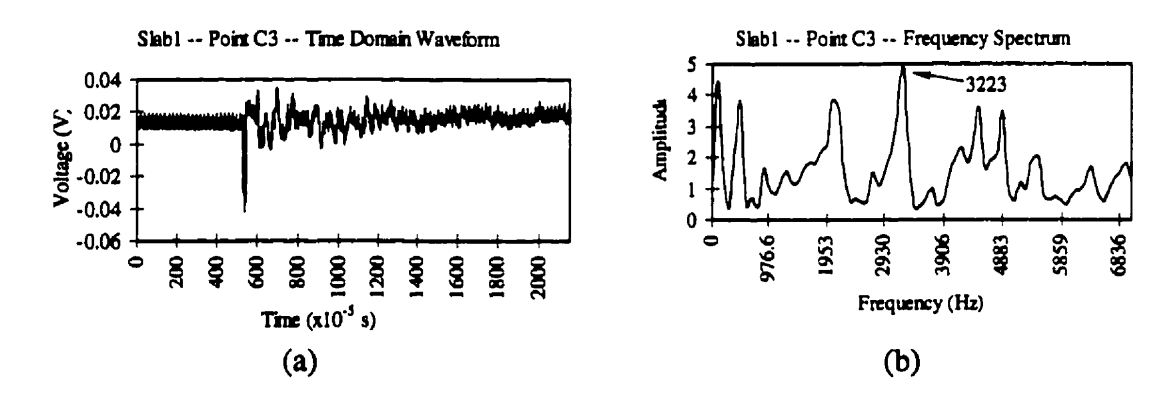


Figure 5.3

Results from initial test at point C3 on slab 1:

(a) time domain waveform; (b) frequency spectrum.

The straight portion at the beginning of the waveform shown in Figure 5.3 (a) illustrates the amount of noise in the signal. Noise was observed in all the captured waveforms, however the noise level varied. The time domain waveforms obtained from the initial tests on the three concrete blocks are shown in Appendix A. The associated frequency spectrums are also shown in the appendix and follow the time domain waveforms of each slab.

In general, frequencies associated with the depths of internal cracks were difficult to single out. This is attributed to the signal noise and the configuration of the slabs. The slab thickness of 300 mm is responsible for multiple internal reflections of the

P-waves. The noise in the frequency spectrum is easily observed by reviewing the spectrums given in Appendix A for the initial tests. Figure 5.3 (b) shows the frequency spectrum of point C3 on the first slab. Notice the complexity of the spectrum and its many frequency peaks. However, it is still possible to distinguish the frequency peak corresponding to the approximate position of the internal crack.

The three ensuing sections describe in detail the results obtained from the initial tests on the slabs. The depths are presented in tabular form in order to simplify the text and descriptions.

All results are compared to the actual crack position in the concrete slabs. Figure 5.4 schematically shows a top view of a slab with the actual depths of the crack with respect to the column positions 1 to 7 shown in Figure 5.2 (a).

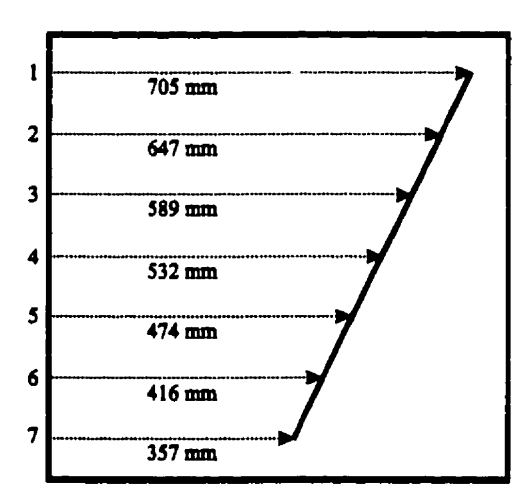


Figure 5.4

Top view of a concrete slab indicating the actual depths of the internal crack with respect to the lines on the test grid.

5.1.4.3.1 Concrete Slab 1 (Plastic Sheet): Initial Results

The results presented here pertain to tests performed on the first slab. That is, the concrete slab with the plastic sheet as artificial crack. At the end of Section 5.1.4, Table 5.8 presents the results of the crack depth in millimeters and the errors in percentage with respect to the depths given in Figure 5.4. For this slab and from tests performed with the non modified test equipment, the P-wave velocity was found to be 4365 m/s as given in Table 5.7.

The frequencies associated with the depths are given in Appendix A. In pages A4 and A5 the frequencies are individually signaled out in frequency spectrums corresponding to each test point. As the tests proceed from column 1 to column 7, the

frequencies corresponding to the depths of the internal crack increase from 3125 Hz to 6367 Hz. Using the selected frequencies and the P-wave velocity previously mentioned for this slab, one uses equation 3.11(a) to calculate the depths of the crack and determine the internal crack profile. At some test points, the errors are close to 20% with respect to the detected depths and the actual depths of the internal crack reach, while at other points the error is minimal. There is a certain subjectivity in the selection of the frequencies, however the author wishes to point out that adjacent frequency peaks in the spectrums generally provide higher errors than the ones shown in Appendix A. Note that the frequency selection was difficult to conduct due to the noise produced by the multiple reflections of the P-waves generated from impacting the boundaries of the slab. This is the case for all three slabs discussed in this section.

Figure 5.5 (a) shows a top view of slab 1. The rectangle represents the perimeter of the slab which is drawn to scale. The straight diagonal line represents the actual position of the internal crack while the mesh shows the profile of the results obtained from the tests. Figure 5.5 (b) shows a three dimensional perspective of the crack material (in gray), and the results from the initial tests. The blue hatched areas indicate calculated depths that are further than the actual depth of the crack which is shown in gray. The full blue areas indicate calculated depths that are closer to the impact surface than the actual depth of the crack material.

As shown in Figure 5.5, there are significant discrepancies with respect to the observed depths found with the MSR Impact-Echo system. At these short distances, it is common to observe accurate results with respect to depth. Therefore, it is essential to determine the causes of the error encountered.

It was difficult to detect the far end of the slab, near the edge of the crack which corresponds to points A1 to E1 on the test surface (see Fig. 5.2). The P-waves were expected to reflect back from the far edge of the slab after contouring the edge of the crack. Unfortunately, it was not possible to identify the peak frequency in the spectrums that corresponds to the 770 mm thickness of the slab. In Appendix A, the low amplitude frequencies shown in column 7 are generated from wave diffraction at the edge of the internal crack.

Overall, the results for slab 1 are acceptable to some degree. However, there are noticeable inconsistencies in the results. Modifications to the MSR Impact-Echo system should focus on resolving the previous problems. The objective should be to establish, at the least, an error level which is consistent at various depths. In this case, the results can be adjusted according to a pre-established error constant.

5.1.4.3.2 Concrete Slab 2 (Plastic Carpet): Initial Results

The results presented here originate from tests performed on the second concrete slab with has the plastic carpet material as artificial crack. The results of the tests are given in Table 5.8. For this slab and from tests with the non modified test equipment, the P-wave velocity was found to be 4152 m/s as given in Table 5.7.

The frequencies associated with the depths given in Table 5.8 are shown in Appendix A. Pages A8 and A9 show the frequencies that are individually singled out in the frequency spectrums. As the test methodology proceeded from column 1 to column 7, the frequencies corresponding to the depths of the internal crack increase from about 3125 Hz to 5945 Hz. As previously mentioned, equation 3.11(a) is used to calculate the depths of the crack and determine the crack profile.

The results from these tests were the most satisfactory of the initial tests performed on the three concrete slabs. From Table 5.8 it is clear that the errors encountered are more consistent for each column. However, the error still reaches above 10% in many cases. To illustrate the difficulty in selecting the appropriate frequency peak that corresponds to the depth of the slab (770 mm), the frequency spectrum for point E7 shows a frequency of 2696 Hz. Notice all the adjacent frequency peaks in the spectrum.

The plastic carpet is a more rigid and thicker material than the other two artificial crack materials. From these results one can deduce that the coefficient of reflection (difference in acoustic impedance of each material) is higher than the other at the crack interface in this slab. Figure 5.5 (c) shows the top view of slab 2 with the results of the tests shown in blue. Figure 5.5 (d) is the three dimensional view of the results given in Table 5.8.

5.1.4.3.3 Concrete Slab 3 (Plastic Bubble Wrap): Initial Results

The results presented here originate from tests performed on the third concrete slab with the plastic bubble wrap material as artificial crack. This material is used to simulate an irregular concrete to air interface. Table 5.8 presents the depths found from initial tests in millimeters and the errors in percentage with respect to the depths given in Figure 5.5. For this slab, the P-wave velocity was established at 4152 m/s as given in Table 5.7.

The frequency spectrums associated to each waveform captured on the test grid placed on the slab are given in appendix A (see pages A12 and A13). The time domain waveforms for these tests are given in pages A10 and A11. The captured signals clearly

show the presence of undesirable noise. The frequency spectrums of this slab are as complex as the previous two.

When reviewing the spectrums, one can see that the difficulty level has increased when selecting the correct frequency peaks. From Figures 5.5 (e) and (f) it is clear that the results for this slab are the most erratic of all three slabs. Test points E6 and E7 show very high discrepancies. Again, it was difficult to find the right frequencies that correspond to the depth of the slab.

In general, the results were not satisfactory for this slab. The difficulty level for selecting the correct frequency peak is much too high. Analysis in the frequency spectrum is supposed to eliminate much of the subjective interpretation in signal analysis. In this case, the analysis relies heavily on interpretation.

It becomes obvious that system modifications are required in order to enhance the accuracy of the results and ease the interpretation of the signals in the frequency domain. All slabs were tested according to the methodology described in the previous sections. The objective of the test was to establish the precision of the system with respect to the detection of inclined cracks at relatively short distances. These tests also determined the present status of the equipment. After the initial analysis, it was shown that the frequency selection was too difficult. The possible causes of discrepancies are the following:

- a) a damaged piezoelectric tip in the P-wave transducer.
- b) inadequate electrical grounding of the test equipment.
- c) difficult manipulation of the transducer due to its weight and the position of the slabs.
- d) the use of the low energy Equotip Model D impact device. This was the most reliable impact device available at the time of the initial tests.

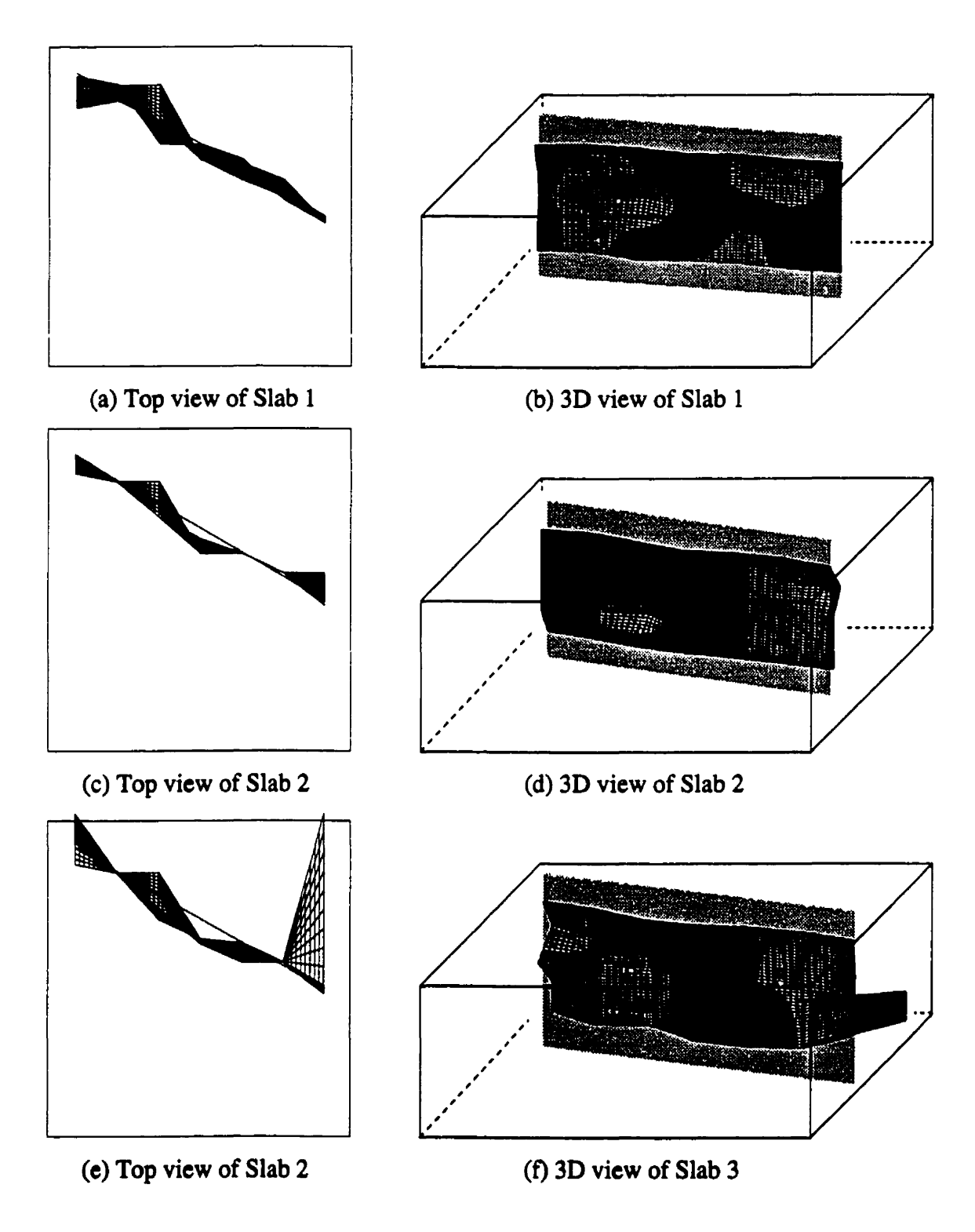


Figure 5.5
Results of initial MSR Impact-Echo tests on slabs 1,2, and 3.

Table 5.8Initial Test Results for slabs 1,2, and 3.

SLAB #1														
GRID	1 2		3		4		5		6		7			
	Depth	Error	Depth	Error	Depth	Error	Depth	Error	Depth	Error	Depth	Error	Depth	Еггог
Α	621	12%	639	1%	588	0%	497	7%	486	3%	406	2%	360	13%
В	677	4%	677	5%	588	0%	497	7%	486	3%	447	7%	344	17%
С	698	1%	675	4%	677	15%	497	7%	447	6%	407	2%	344	17%
D	677	4%	677	5%	588	0%	495	7%	486	3%	399	4%	344	17%
E	677	4%	677	5%	534	9%	532	0%	497	5%	399	4%	349	16%
SLAB #2														
GRID) 1		2		3		4		5		6		7	
	Depth	Error	Depth	Error	Depth	Error	Depth	Error	Depth	Error	Depth	Error	Depth	Error
A	664	6%	644	0%	559	5%	483	9%	471	1%	425	2%	349	16%
В	664	6%	644	0%	559	5%	483	9%	472	0%	425	2%	425	19%
С	664	6%	644	0%	559	5%	472	11%	472	0%	425	2%	373	10%
D	664	6%	644	0%	644	9%	472	11%	472	0%	425	2%	373	10%
E	709	1%	644	0%	559	5%	506	5%	472	0%	425	2%	770	85%
							SLAB #3	3						
GRID	1		2		3		4		5		6		7	
	Depth	Error	Depth	Error	Depth	Error	Depth	Error	Depth	Ептог	Depth	Error	Depth	Error
Α	708	0%	644	0%	531	10%	483	9%	472	0%	425	2%	348	16%
В	787	12%	644	0%	559	5%	472	11%	472	0%	425	2%	367	12%
С	664	6%	644	0%	644	9%	472	11%	472	0%	425	2%	367	12%
D	787	12%	644	0%	644	9%	472	11%	425	10%	425	2%	787	89%
E	787	12%	644	0%	644	9%	483	9%	425	10%	425	2%	787	89%
Depths	705		647		589		532		474		416		416	

5.1.5 Final Crack Detection Results and Discussion

After a series of modifications to the test equipment and the purchase of a high energy impact source, final tests were carried out on the three concrete slabs. The results presented in this section refer to tests conducted with the new Equotip Model G impact device. Due to modifications to the transducer, four impact devices were used during the final series of tests. The results obtained with these four devices were repetitive on all three slabs. In order to compare two similar impact devices, the discussion will focus on the final results obtained with the Equotip impact device previously mentioned. This also helps alleviate the text and reduce unnecessary repetition.

5.1.5.1 System and Test Bed Modifications

The first modifications to the system focused on reducing the electrical noise in the signal picked up by the piezoelectric transducer. To accomplish this task, three changes were proposed. The first modification involved the use of an independent ground electric socket to connect all the equipment. This was moderately successful, and proved to be unnecessary after further modifications were brought to the system itself. The second modification focused on the vertical displacement transducer. Since the piezoelectric tip had not been replaced in the last 6 years, it may have suffered some sort of damage in the past. Piezoelectric materials are very susceptible to crack when they are dropped or struck. The piezoelectric tip was replaced with a new and identical tip supplied by IQI Inc., the original manufacturer. The 9V battery was constantly replaced in order to ensure a minimum voltage level of 7.6V in the electrical circuit as suggested by the manufacturer.

The third modification involved eliminating the human intervention during the tests. The transducer's optimal test position is in a vertical direction and self supporting. All three concrete slabs were positioned upright as shown in Figure 4.3 to allow the transducer to stand on the test grid. The transducer could now be positioned in its optimal setting. Note that tests have been conducted in the past with the transducer positioned in various directions. The results of the tests were satisfactory [Sadri, 1996]. In this case, it was essential to eliminate all possible causes of problems, hence the reason to eliminate human intervention during the tests. Additionally, the sampling rate was reduced to 10 µs (100 kHz) from 5 µs (200 kHz).

5.1.5.2 P-wave Velocity Measurements on the Three Concrete Slabs

Due to the modifications performed on the transducer and to the use of a high energy impact device, the P-wave velocity was re-evaluated on all three slabs. Accordingly, the P-wave velocities were different and generally lower than the initial results. Multiple tests were performed on each slab to obtain a better representation of the velocities. It was found that for slabs 2 and 3 there were variations in the velocities. The P-wave velocities were obtained by testing the 300 mm thickness of the slabs. Before the slabs were rotated, tests were performed on the surface of the slabs at locations in line with columns 1 to 7 of the test grids. For simplification, the P-wave velocities are given in Table 5.9 along with the final test results.

5.1.5.3 Discussion of Final Results

At first glance, a review of the time domain waveforms captured during the final tests indicates a significant reduction in the electrical noise level. The waveforms are given in Appendix A on pages A14-15, A18-19, and A22-23. In almost all cases, the surface response captured by the transducer is typical of MSR Impact-Echo testing. One can note the clearly sinusoidal waveform pattern in these plots. The main reason for these good waveforms is the use of the high energy impact device. The reflected P-waves contain more energy and a lower frequency content. The reduced frequency content of the waves is of no concern since the frequencies of interest are in the range of 2000 to 7000 Hz.

The frequency spectrums were generally less noisy with the elimination of arbitrary frequency peaks. The selection of the appropriate frequencies was easier and more accurate than the initial tests. Apart from reducing the noise level by equipment modifications, it was impossible to reduce or eliminate the noise caused by the physical limitations of the test samples.

5.1.5.3.1 Concrete Slab 1 (Plastic Sheet): Final Results

Figures 5.6 (a) and (b) show the depths of the internal crack detected with the MSR Impact-Echo system after the system modifications were performed. Table 5.9 gives the depths and the errors encountered in the analysis. The results in this table correspond to the depths of the crack directly beneath the test points on the grid. The errors are related to the depths given in Figure 5.5.

The P-wave velocity in the slab was constant at 3984 m/s. The frequencies selected in the analysis are given in Appendix A, pages A16 and A17. The frequencies were generally easier to select due to dominant peaks in the spectrums. The was most difficult frequency selection was in columns 3 to 5 where the amplitudes were quite smaller than columns 1, 2, 6, and 7. In column 1, the peak frequency is 2588 Hz for all 5 test points. The frequency corresponds to the 770 mm depth of the slab. The large amplitude peaks indicate that the wave is reflecting off the far edge of the slab which is an ideal interface (concrete to air). The errors encountered were rarely above 5% with the exception of column 1 where the error was 9% due to the detection of the far end of the slab. The time domain waveforms of points C6 and C7 show only a portion of a usual waveform. This is due to a momentary setup error during the data acquisition stage. However, these waveforms illustrate the need for three complete sinusoidal periods in the waveform. Looking at spectrums C6 and C7, one notes the lack of accuracy in the spectrum compared to adjoining frequency spectrums.

In Figure 5.6 (a), the top view of the slab shows the detected profile of the crack. The results agree well with the actual crack profile. Notice the edge of the crack that was detected along column 1 on the left side of the figure. In column 7 it was possible to detect the near edge of the internal crack by judicious investigation of the frequency spectrum. The frequencies corresponding to the far end of the slab were also detected in the previous spectrums.

5.1.5.3.2 Concrete Slab 2 (Plastic Carpet): Final Results

The results obtained in the analysis of the second slab were quite similar to slab 1. However the P-wave velocity was found to slightly vary in this slab. The P-wave velocity was 3984 m/s for columns 1, 4, 5, 6, and 7 while columns 2 and 3 had velocities of 3896 m/s. The time domain waveforms presented in pages A18 and A19 are generally good with definitive sinusoidal patterns. In the frequency spectrums, the far end of the slab was once again easily detected in column 1. The peak frequency corresponding to the edge of the slab was 2588 Hz. Columns 3 and 4 were the most difficult to analyze due to the low amplitude frequencies that correspond to the depth of the internal crack. The errors related to the depths were generally below 5% except at column 1 where the error reached 9%. Figures 5.6 (c) and (d) show the profile of the results superimposed on the actual profile of the crack. As a reminder, the gray area in the three dimensional view is the actual crack. The results are shown in the blue solid and mesh areas. These visual representations show that the results agree well with the actual crack profile. However the results are more scattered than the results from slab 1.

5.1.5.3.3 Concrete Slab 3 (Plastic Bubble Wrap): Final Results

For the two previous slabs, the results from column 2 are significantly closer to the test surface. The results from the third slab show the same phenomenon. This is probably due to wave reflections from the left side of the slabs or from the material twisting towards the test surface during concrete placement in the forms. The most significant variations in P-wave velocity appears in this slab. Table 5.9 shows the velocities varying from 3896 m/s to 4420 m/s. The errors encountered were in the range of 2% to 5% with occasional high error levels.

Figures 5.6 (e) and (f) show the results of the test superimposed on the actual crack profile. Note that the far end of the slab was detected in column 1. Appendix A shows the results from the frequency spectrum analysis. It was generally easier to single out the frequency peaks in all the spectrums and specifically in columns 3 to 5 where the selected amplitude peaks were quite small for the first two slabs. The analysis tends to point out that the plastic bubble wrap used to simulate a concrete to air interface was the better material for use as an artificial crack. Generally, the result profiles in Figures 5.6 (a) and (e) are very similar. However the frequencies are easier to select in the slab 3.

5.1.6 Conclusions of the Inclined Crack Detection Tests

Two series of tests were needed in order to obtain the desired results. The experiments confirm that it is possible to determine the inclination of cracks in concrete at short distances with relatively good accuracy. The 300 mm thickness of the slabs induced many reflections of the propagating stress waves that resulted in complicated frequency spectrums. However, after a judicious frequency selection it was possible to determine the profile of the internal cracks. The modifications to the system included the replacement of the piezoelectric tip on the vertical displacement transducer, the use of a high energy impact device to counter balance the highly attenuation effect of the concrete, and the rotation of the slab in the upright position that eliminated the need to support the transducer by hand. After the final analysis of the three slabs it is safe to conclude that the plastic bubble wrap material served best as the artificial crack material due to the constant high amplitude frequency peaks throughout the final test spectrums in Appendix A.

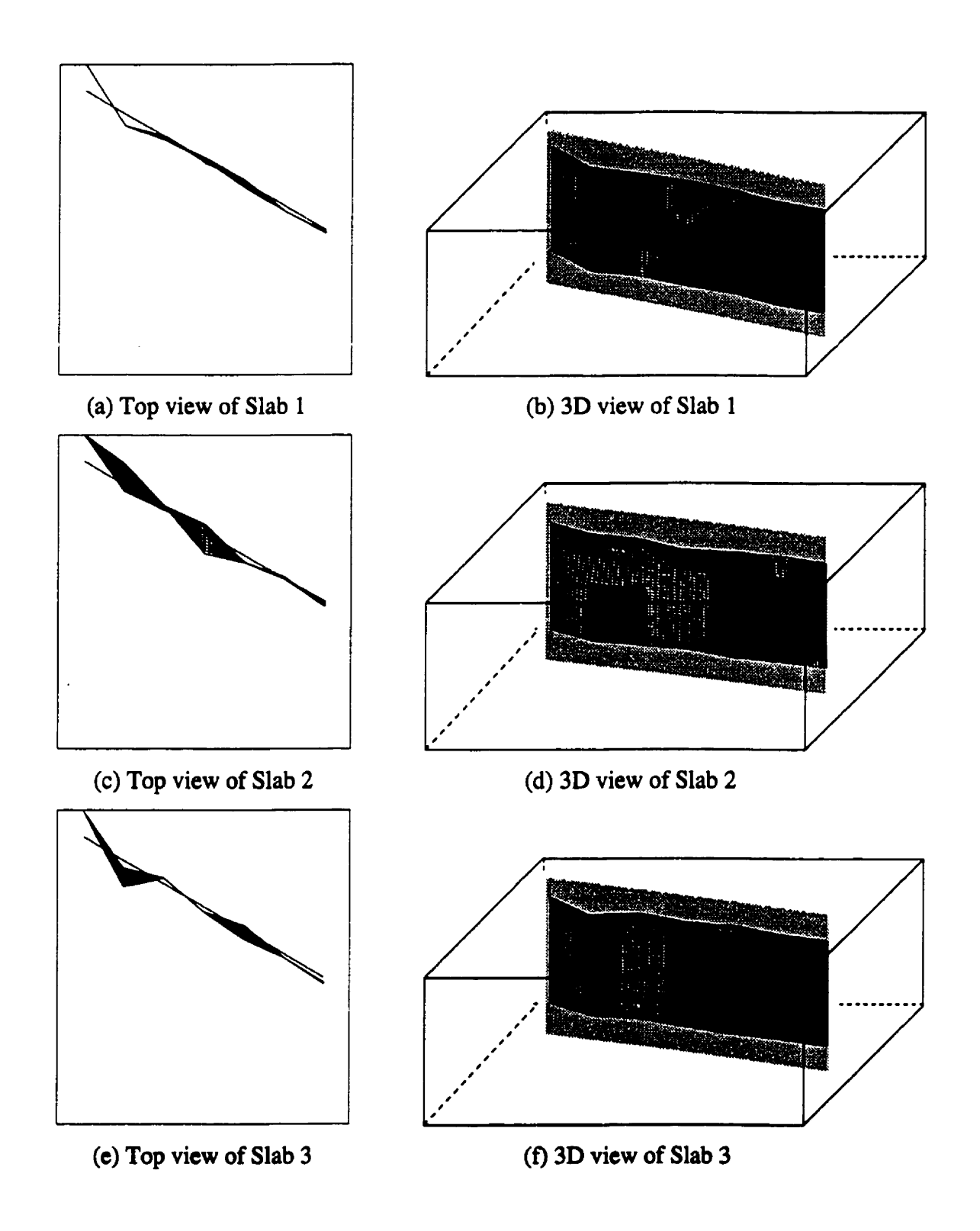


Figure 5.6
Results of final MSR Impact-Echo testing on slabs 1,2, and 3.

Table 5.9 Final Test Results for slabs 1,2, and 3.

SLAB #1														
GRID	1		2		3		4		5		6		7	
Cp:	3984 m/s		3984 m/s		3984 m/s		3984 m/s		3984 m/s		3984 m/s		3984 m/s	
	Depth	Error	Depth	Error	Depth	Ептог	Depth	Error	Depth	Error	Depth	Error	Depth	Error
A	770	9%	618	4%	583	1%	537	1%	448	5%	404	3%	355	1%
В	770	9%	618	4%	583	1%	537	1%	469	1%	404	3%	355	1%
С	770	9%	618	4%	583	1%	531	0%	463	2%	404	3%	355	1%
D	770	9%	618	4%	591	0%	531	0%	443	7%	404	3%	352	1%
E	770	9%	618	4%	591	0%	510	4%	480	1%	404	3%	355	1%
SLAB #2														
Cp:	: 3984 m/s		3896 m/s		3896 m/s		3984 m/s		3984 m/s		3984 m/s		3984 m/s	
	Depth	Error	Depth	Ептог	Depth	Error	Depth	Ептог	Depth	Егтог	Depth	Error	Depth	Error
Α	770	9%	644	0%	587	0%	480	10%	458	3%	421	1%	349	2%
В	770	9%	700	8%	587	0%	551	4%	458	3%	416	0%	349	2%
С	770	9%	644	0%	587	0%	551	4%	458	3%	416	0%	349	2%
D	770	9%	633	2%	587	0%	551	4%	458	3%	416	0%	349	2%
E	770	9%	633	2%	587	0%	551	4%	458	3%	416	0%	361	1%
							SLAB #:	3		•	-			
Cp:	:3896 m/s		3984	3984 m/s 4420 m/s		4420 m/s		3984.5 m/s		3984.5 m/s		3896 m/s		
	Depth	Error	Depth	Error	Depth	Error	Depth	Ептог	Depth	Error	Depth	Error	Depth	Error
Α	767	9%	583	10%	603	2%	520	2%	486	3%	408	2%	347	3%
В	767	9%	628	3%	603	2%	520	2%	453	4%	408	2%	347	3%
C	767	9%	628	3%	603	2%	520	2%	453	4%	408	2%	344	4%
D	767	9%	628	3%	603	2%	520	2%	453	4%	408	2%	344	4%
Е	767	9%	628	3%	603	2%	520	2%	448	5%	408	2%	344	4%
Depths	705 64		7	589		532		474		416		416		

5.2 CRACK THICKNESS INVESTIGATION

This section reports on work performed to evaluate the minimum crack thickness detectable with the MSR Impact-Echo system. The ensuing sections focus on the following subjects: the test methodology, the static and dynamic values of the concrete, and the results obtained from testing in dry and saturated crack conditions.

5.2.1 Test Methodology

The two concrete blocks described in Section 4.3.2.2 were first tested with both P- and S-wave transducers. The initial tests served to evaluate the dynamic material properties of the concrete. Static testing was not necessary because these concrete blocks were cast at the same time and with the same type of concrete as the three concrete slabs discussed in Section 5.1. The dynamic tests were performed on 3 sides of each concrete block. Block A is the translating block that is used to create a crack opening. Block B is fixed to the rigid metallic test frame.

The first tests consisted of evaluating the minimum crack thickness detectable by the system in dry conditions. The second tests involved saturating the crack with a constant flow of water and evaluating the minimum crack thickness detectable in this condition. The Equotip Model D and G impact devices were used during the tests (see Figure 5.7). The Model D impact device is on the right and the tall Model G impact device is on the left. It is shown in the analysis that the system is extremely sensitive to concrete and air interfaces.

5.2.2 Static Material Tests and Results

In the previous section, it was mentioned that the static material properties of the concrete blocks under investigation are the same as those of the concrete slabs discussed in Section 5.1. The static test results can be found in Section 5.1.2 and will not be repeated.

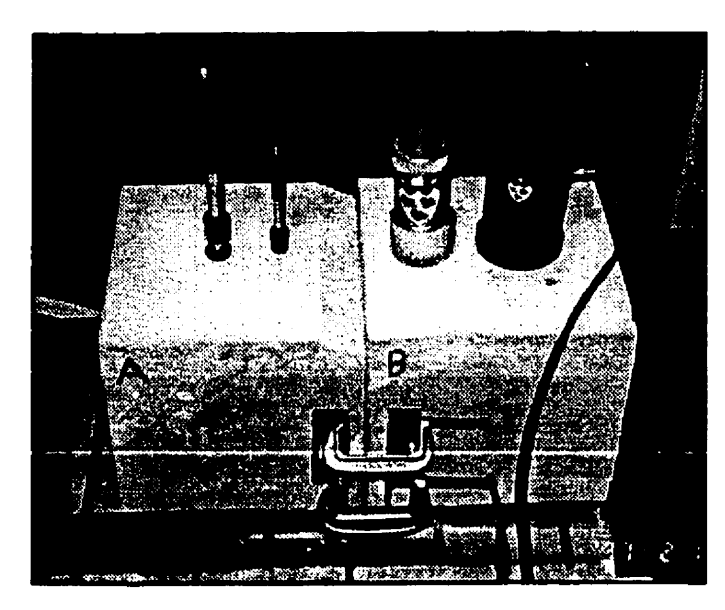


Figure 5.7
MSR Impact-Echo test equipment used

5.2.3 Dynamic Material Tests and Results

Dynamic material tests were performed on each slab. The tests were conducted with the Equotip Model D impact device on the three axes of each block. This allows for a true representation of the material's dynamic properties. The results of the tests are given in Table 5.10. The P- and S-wave velocities were calculated with equations 3.10a and 3.10b. A thickness of 0.3 m corresponding to the thickness of the blocks was used in the calculations along with a density of 2400 kg/m³. The dynamic properties of the concrete were calculated with the equations given in Table 3.2.

Table 5.10

Dynamic properties of the concrete blocks

Bl. #1	P-wave Frequency (Hz)	S-wave Frequency (Hz)	P-wave Velocity (m/s)	S-wave Velocity (m/s)	Dynamic Young's Modulus (GPa)	Dynamic Shear Modulus (GPa)	Bulk	Dynamic Poisson's ratio
Тор	6250	3857	3750	2314	30.66	12.85	16.62	0.192
Side1	6396	3906	3838	2344	31.71	13.19	17.77	0.203
Side2	6250	3515	3750	2109	27.09	10.67	19.52	0.269
Bl. #2								
Top	6152	3662	3691	2197	28.40	11.58	17.25	0.226
Side1	6152	3955	3691	2373	31.03	13.51	14.68	0.148
Side2	6298	3710	3779	2226	29.37	11.89	18.42	0.234

5.2.4 Dry Crack Test Results and Discussion

The tests were performed under laboratory conditions and at constant temperature. The first tests involved the detection of a crack thickness of approximately 0 mm in a dry crack condition. To ensure that both blocks were completely in contact with one another at the interface, two metal clamps were attached to assemblies anchored on each block. Figure 5.7 shows two of the clamps on one side of the blocks. Block A is the translating block.

After the clamps were tightened, it was possible to observe the full contact between both blocks by looking at the exterior profile of the crack. Since a plastic sheet was used to create the interface between the two blocks, the contact area was smooth enough to ensure good contact.

Three impact devices were used during these tests to ensure repeatability of the results. Namely, the Equotip Model D and G impact devices and the custom built 15 mm tip impact device (see Table 5.6). The distance separating the impact devices and the transducer was maintained at 5 cm in all cases. The tests were performed on the immovable block (block B) with the modified P-wave transducer. Figure 5.8 shows the time domain waveform and the frequency spectrum plots generated with the Equotip Model D impact device. In the frequency spectrum, it is easy to single out the dominant frequency peak of 6152 Hz corresponding to the frequency of the P-wave propagating between the crack interface and the test surface. The frequency spectrum shown in Figure 5.8 was typical for all tests performed in the dry crack condition.

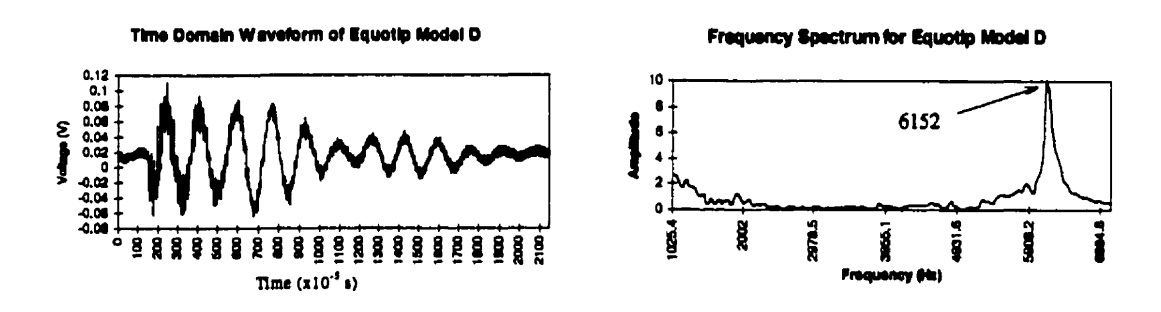


Figure 5.8

Dry crack condition time domain waveform and frequency spectrum for Equotip Model D impact device.

Figure 5.8 shows that the MSR Impact-Echo system is capable of detecting very fine cracks without difficulty. Note however that these tests were performed in ideal

laboratory conditions. The analysis shows that the other two impact devices yielded the same results. The detected P-wave frequency was also 6152 Hz.

5.2.5 Saturated Crack Test Results and Discussion

This section discusses the results obtained after saturating the crack interface between the two concrete blocks. The saturation condition was ensured by first separating both blocks with the translating assembly and then saturating the crack surface with water. The blocks were subsequently clamped together to regain the inital test condition. Special attention was brought to the alignment of both objects to ensure surface contact at the interface.

The interface was constantly saturated with water as the tests proceeded (see Figure 5.9). Notice the dark areas indicating the presence of water and the clamps used to ensure contact between the two blocks. Special attention was given to the instruments in order to avoid possible damage by the flowing water. The tests were conducted on the right side of the right block (block B). As in Section 5.2.4, the tests were conducted with the same three impact devices. All three tests revealed a dominant P-wave frequency of 6201 Hz in the frequency spectrums. Figure 5.10 shows the time domain wavefrom and the frequency spectrum as a result of testing with the Equotip Model D impact device. Notice the high amplitude P-wave frequency peak in the spectrum. It can be concluded that water saturation of the crack does not affect the resolution in the frequency spectrum.

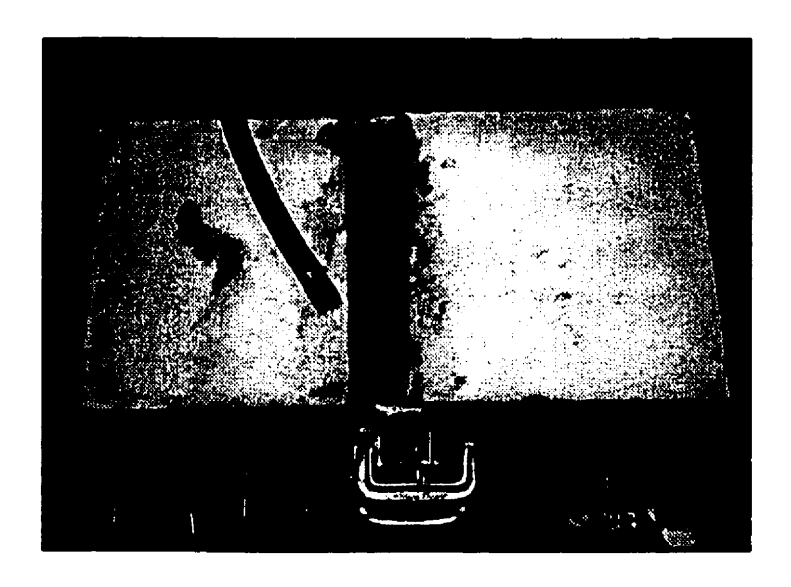
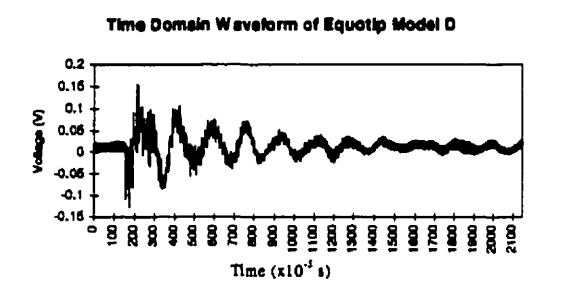


Figure 5.9

Top view of the blocs showing saturation of the crack interface.



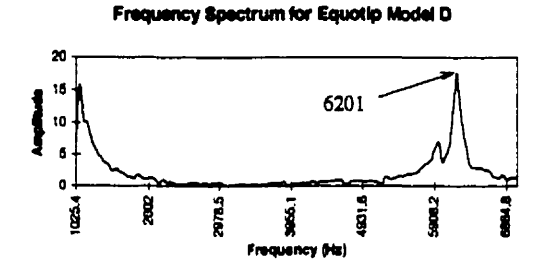


Figure 5.10
Saturated crack condition time domain waveform and frequency spectrum for Equotip Model D impact device.

5.2.6 Conclusions of the Crack Thickness Investigation Tests

It was shown that the MSR Impact-Echo system is capable of detecting cracks that are approximately 0.08 to 0.1 mm in thickness or less in dry or saturated conditions. It is important to note however that the tests were performed on small scale samples and the results should be interpreted as such. The detectable crack thickness in large concrete structures is still not known. However, ongoing research at McGill and IREQ is being performed to determine this parameter.

The results for both the saturated and dry crack conditions were the same regardless of the impact device used. The cause for this consistency lies in the length of the waveform generated by each impactor. The wavelengths were all inferior to the 0.3 m thickness of the blocks and allows the waveforms to complete a total wavelength. The importance of this factor was discussed in Chapter 3.

Initially, the intent was to perform tests on thicker cracks. As shown in the discussion, the minimum detectable crack thickness was determined in the early stages of the experiment. Therefore, it was not necessary to increase the thickness of the crack and perform tests.

5.3 INVESTIGATION OF A SECTION OF A CONCRETE GRAVITY DAM

A section of a concrete gravity dam was investigated with the MSR Impact-Echo system. The concrete section was built on site at IREQ with the help of the author as previously mentioned in Chapter 4. The construction steps of the concrete section are shown in Figures 4.11 (a) to (c.). The test bed serves as a benchmark for the evaluation of the system with respect to extending its capabilities to greater depths.

Figure 4.9 shows the dimensions of the gravity dam. Tests were performed on two faces of the structure, namely the east and south faces. P- and S-wave velocities were determined in both cases. From these two velocities it is possible to determine the dynamic material properties of the concrete at each test point from the equations in Table 3.2. The following sections discuss the test methodology applied to the concrete section and also the results obtained after the analysis of the time domain waveforms. Due to restrictions associated to the length of this manuscript, close to 2000 time domain waveforms and frequency spectrums are not shown. However, the results are consolidated in figures shown in the following sections.

5.3.1 Test Methodology

The first step taken before the investigation of the structure was to establish the layout of the test grids. On each side, a grid mesh of 20 x 20 cm was drawn. The mesh size allowed for fast and efficient scanning of the structure. Figure 5.11 (a) shows the layout the test grid placed on the south vertical face of the dam. This south side faces the slant of the dam. The grid was placed 10 cm from the left side and 20 cm from the right side. The top and bottom spacing was 20 cm. Figure 5.11 (b) shows the grid placed on the east face of the dam. The grid on the east face of the dam yielded 324 test points and the grid on the south face yielded 168 tests points.

Two types of impact devices were used during the investigation: the Equotip Model G and a hammer with a spherical tip. During initial tests it was noted that the concrete structure highly attenuated the stress waves as they propagated through the material. The attenuation was manly due to high concentrations of reinforcement bars parallel to the east and west faces of the dam (see Figure 4.11 (a)). Two dense reinforcement meshes were in the travel path of each reflected stress wave. Note that the reinforcement mesh placed in this structure is not typical of large gravity dams where the reinforcement to concrete ratio is usually very low.

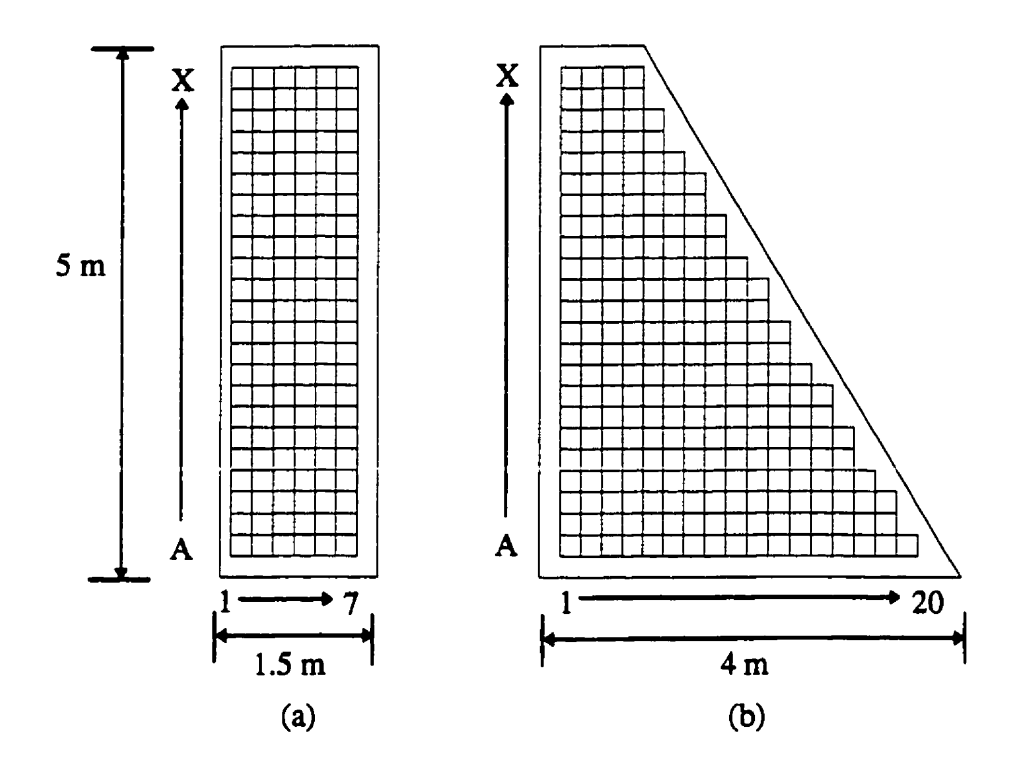


Figure 5.11
Test grids placed on the concrete gravity dam section:
(a) the south face; (b) the east face.

The Equotip Model G impact device did not fair very well in these conditions. It was difficult to detect the waves and trigger the transducer. Since this mechanical impact device generates the highest energy at impact of all the mechanical impact sources available, another solution was sought. The solution was to use a hand held hammer with a spherical tip at one end of the impact head. Figure 5.12 shows the equipment used for testing the concrete section. Notice the spherical tip on the right side of the hammer head.



Figure 5.12

MSR Impact-Echo test equipment used to evaluate a section of a concrete gravity dam.

Data acquisition proceeded from the base of the structure to the top. Both the P-and S-wave transducers were used at each test point on the grids. The hammer was mainly used as the impact source during the data acquisition period. The sampling rate was constantly maintained at 10 µs (100 kHz). The number of points analysed from each time domain waveform was 2048. The frequency resolution in the spectrum was 48.8 Hz.

A scaffold was placed on the east and south sides of the dam when access to the top sections was required. At the top section of the dam, a PVC pipe was imbedded in the dam in the east to west direction. The pipe made some test points inaccessible. Figures shown in the following sections have a black patch in the top section due to those unavailable test points. Figures 5.13 (a) and (b) shows the scaffolding used during the tests and a view of the south and east sides of the dam. In both cases the scaffolding is placed on the east face.

Sections 5.3.2 and 5.3.3 discuss in detail the results obtained from testing on the east and south faces. It is important to mention that the travel distance from the south face to the slanted north face increases from 1 m to 4 m towards the base of the structure. Therefore tests on the south side of the dam help establish the penetration depth of the system.



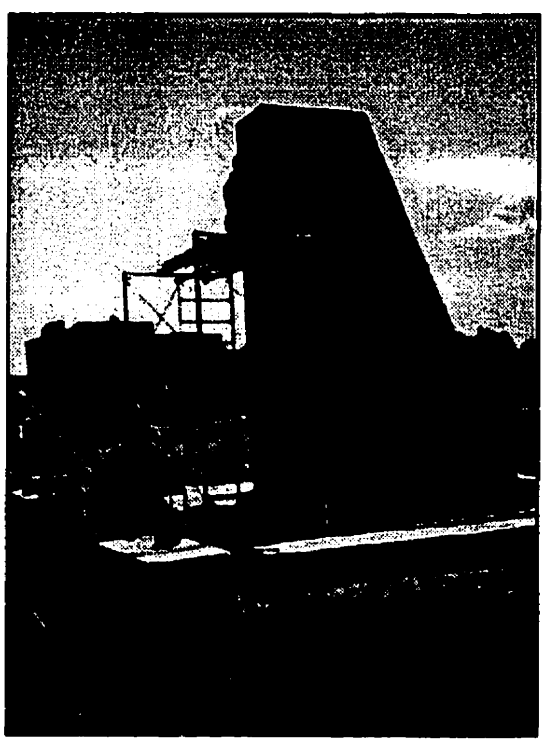


Figure 5.13
Scaffolding used to access the higher section of the dam:
(a) view of the south face; (b) view of the east and north faces.

5.3.2 East Face Results and Discussion

The following discussion focuses on results obtained from the analysis of time domain waveforms captured on the east face of the dam. To illustrate the vast amount of data accumulated, interpolated contour plots of the results are shown. The P- and S-wave velocities are presented in the first subsection. The subsequent section discusses the dynamic properties of the concrete derived from the evaluation of the stress wave velocities.

5.3.2.1 P- and S-wave Velocity Profiles

Figure 5.14 shows the P-wave velocities obtained after analysing the time domain waveforms. The velocities range from 3000 m/s to 5000 m/s. A high concentration of velocities in the 4000 m/s range appears in the middle of the structure. The bottom section of the dam shows areas with P-wave velocities close to 5000 m/s. Incidentally, the area up to a height of 1.5 m corresponds to the first poured layer of concrete. The major concentrations of high velocities are found near the joint between the foundation slab and the structure of the dam. The lower P-wave velocities are found around the perimeter and in the top section of the dam. Generally, the P-wave velocities indicate that the concrete is of good quality and density.

Figure 5.14 shows the S-wave velocities that fall mostly in the 2300 m/s range. High velocity S-waves are also concentrated in the lower section of the dam. The frequency spectrum analysis was somewhat difficult since the S-wave frequencies were close to the resonance frequency of the transducer. However it was still possible to single out the correct frequencies. Rarely did the S-wave velocities fall below 2000 m/s. The jagged profiles in both figures indicate the test points and approximate the actual inclination on the north face of the dam.

5.3.2.2 Dynamic Material Properties

After obtaining the stress wave velocities of interest it is possible to calculate the dynamic material properties of the concrete dam. Figure 5.15 shows the dynamic Young's Modulus, Poisson's ratio, Shear Modulus, and Bulk Modulus. In each graph the black spot at the top of the structure indicates the position of the PVC pipe and its bearing plate. The dynamic modulus of elasticity tends to decrease towards the top of the dam. As a reminder, the dam was built in three successive stages. The higher results are in the

lower section of the dam. There is significant variation in the results throughout the structure. In some cases, the variation is approximately 20 GPa. The dynamic Poisson's ratio was found to be somewhat uniform. The top right hand figure in Figure 5.15 shows that most results lie in the vicinity of 0.22 to 0.25. Typically, concrete has a static Poisson's ratio of 0.15 to 0.20 [Mehta and Monteiro, 1993]. It has been shown in the past that the dynamic Poisson's ratio is typically higher in concrete [Sadri, 1996]. The Shear modulus was found to be uniform throughout the structure with occasional increases to 20 GPa. The results ranged from approximately 10 to 20 GPa. Figure 5.15 also shows the dynamic Bulk modulus. Generally, there is a high variation in the results. High levels of the Bulk modulus are found in the middle and bottom sections of the structure. The results range from 10 to 30 GPa. It is important to note that the results shown in Figures 5.14 and 5.15 represent average values of the stress wave velocities and the dynamic material properties. The P- and S-wave velocities are considered average velocities since the stress waves travel through the structure. Internally, some areas may possess different dynamic properties and different densities. Hence the velocity of the stress wave is a factor of all the internal anomalies in its path. Since the dynamic material properties are derived from those average stress wave velocities, it is clear that the results in Figure 5.15 are average values taken at each test point on the test grid.

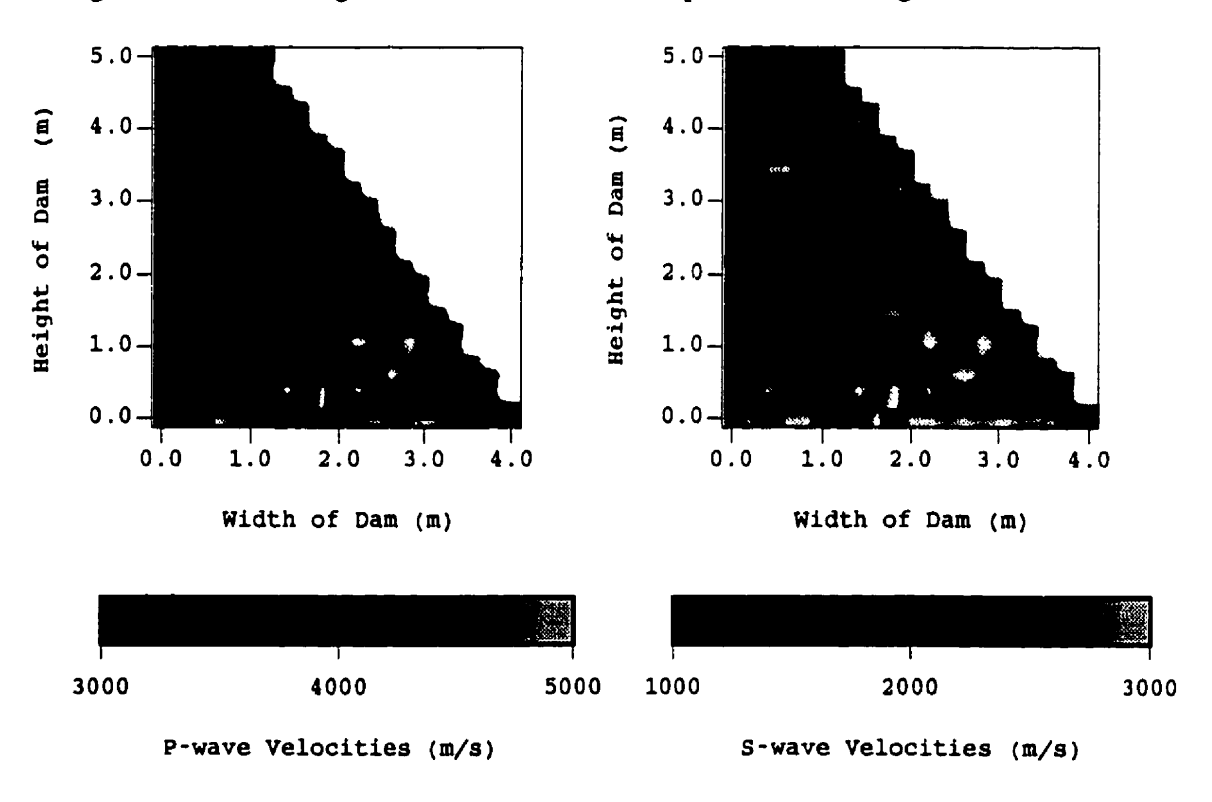


Figure 5.14
P- and S-wave velocities obtained on the east face of the dam.

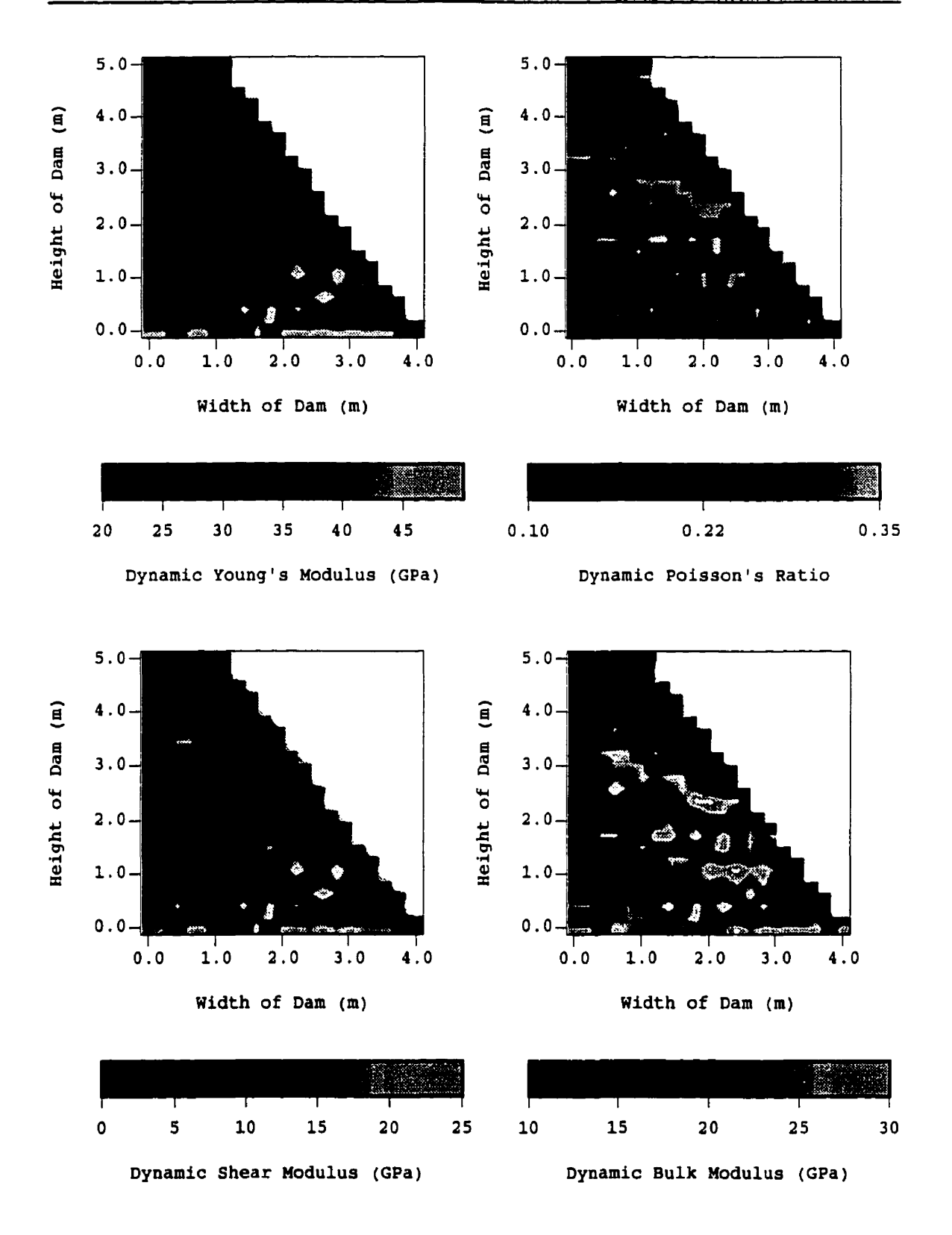


Figure 5.15

Dynamic material properties determined on the east face of the dam.

5.3.3 South Face Testing Results and Discussion

This section focuses on the results obtained from the analysis of time domain waveforms captured on the south face of the dam. As in Section 5.3.2, the results are presented in interpolated contour plots. Section 5.3.3.1 discusses the results of the P- and S-wave velocities determined with an increasing depth. From these stress wave velocities it was possible to evaluate the dynamic material properties.

5.3.3.1 P- and S-wave Velocity Profiles

Figure 5.16 shows the P- and S-wave velocities determined after analysing the time domain waveforms obtained from the south face of the dam. The P-wave velocities range from 3663 m/s to 5400 m/s. Uniform P-wave velocities are found on the top section of the dam. In this area, it was possible to determine the peak frequencies in the spectrums. The P-wave velocities in that area are close to 4250 m/s. Note the high variation in the P-wave velocities in the lower section of the dam below the 3 m level. The discrepancies are due to difficult frequency selection in the frequency spectrums. As the travel distance of the P-wave increases, the frequency of the wave reflections decreases and hence the P-wave frequency becomes confused with the resonance frequency of the transducer. The resonance frequency is the frequency vibration of the transducer assembly. It usually dominates the low frequency spectrum.

The S-wave velocities shown in Figure 5.16 are also uniform on the top area of the dam. The velocities are generally close to 2500 m/s. Below the 3 m mark, the variation in the velocities is higher. The discrepancies are due to the same problem previously mentioned. The S-wave velocities in the lower part of the dam vary from 1500 m/s to 3500 m/s.

It is interesting to note that the stress wave travel distance at a height of 3 m is approximately 2.20 m. Therefore it is possible to deduce that the MSR Impact-Echo system's penetration depth is limited to that distance. Longer travel paths mean detecting frequencies in the lower section of the frequency spectrum which is dominated by the resonance frequency of the transducer.

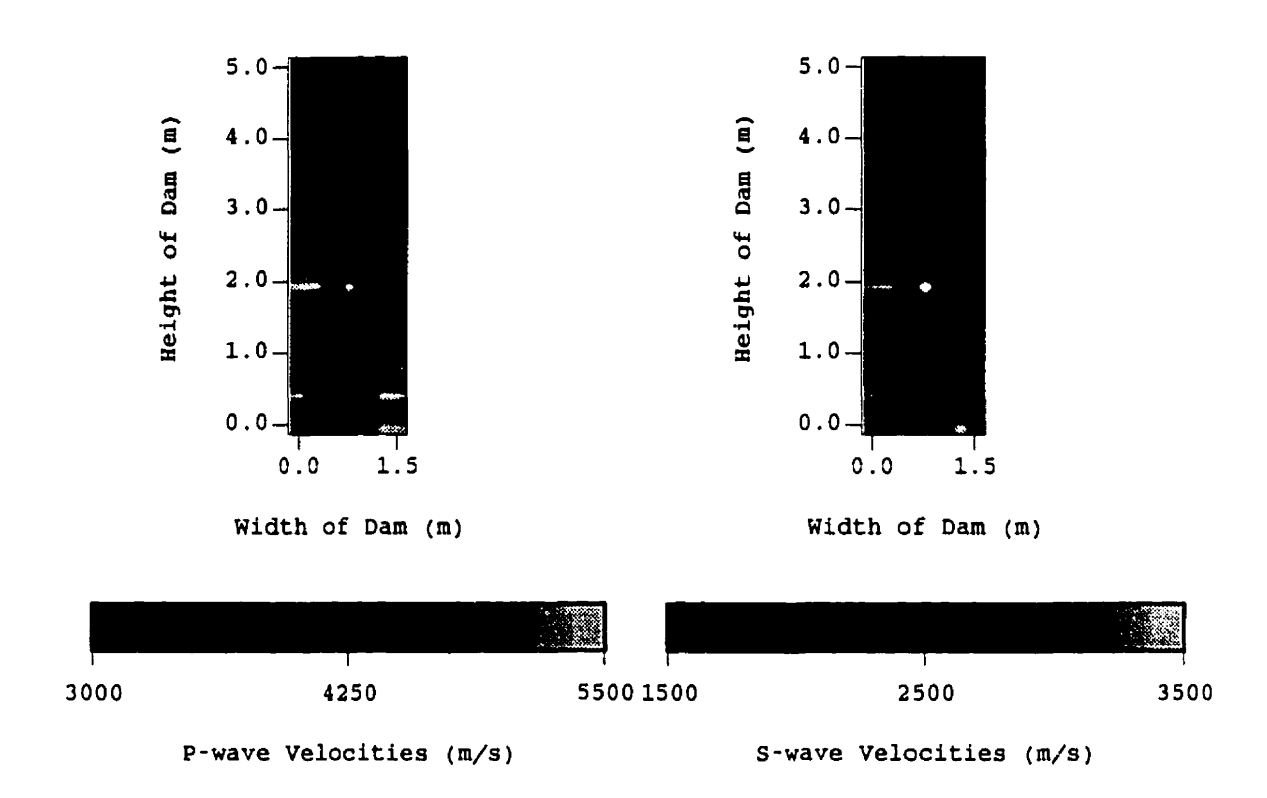


Figure 5.16
P- and S-wave velocities obtained on the south face of the dam.

5.3.3.2 Dynamic Material Properties

The preceding stress wave velocities were used to determine the dynamic material properties from the south face of the dam. In Figure 5.17, it is shown that the results below the 3 m mark are inconclusive. The lack of uniformity in the results is caused by the explanation given in the previous section. The dynamic Young's modulus shows the highest variation in that portion of the graph. The results range from 20 to 50 GPa. With short distances between each test point, it is highly unlikely that actual results vary so significantly. The dynamic Poisson's ratio is centred around 0.25 on the top portion of the figure with occasional increases above that value. The lower portion shows a wide variation of values, specifically the centre vertical line. The dynamic Shear modulus was found to be quite uniform in the top portion of the dam with a higher variation in the lower section. The same can be said of the dynamic Bulk modulus.

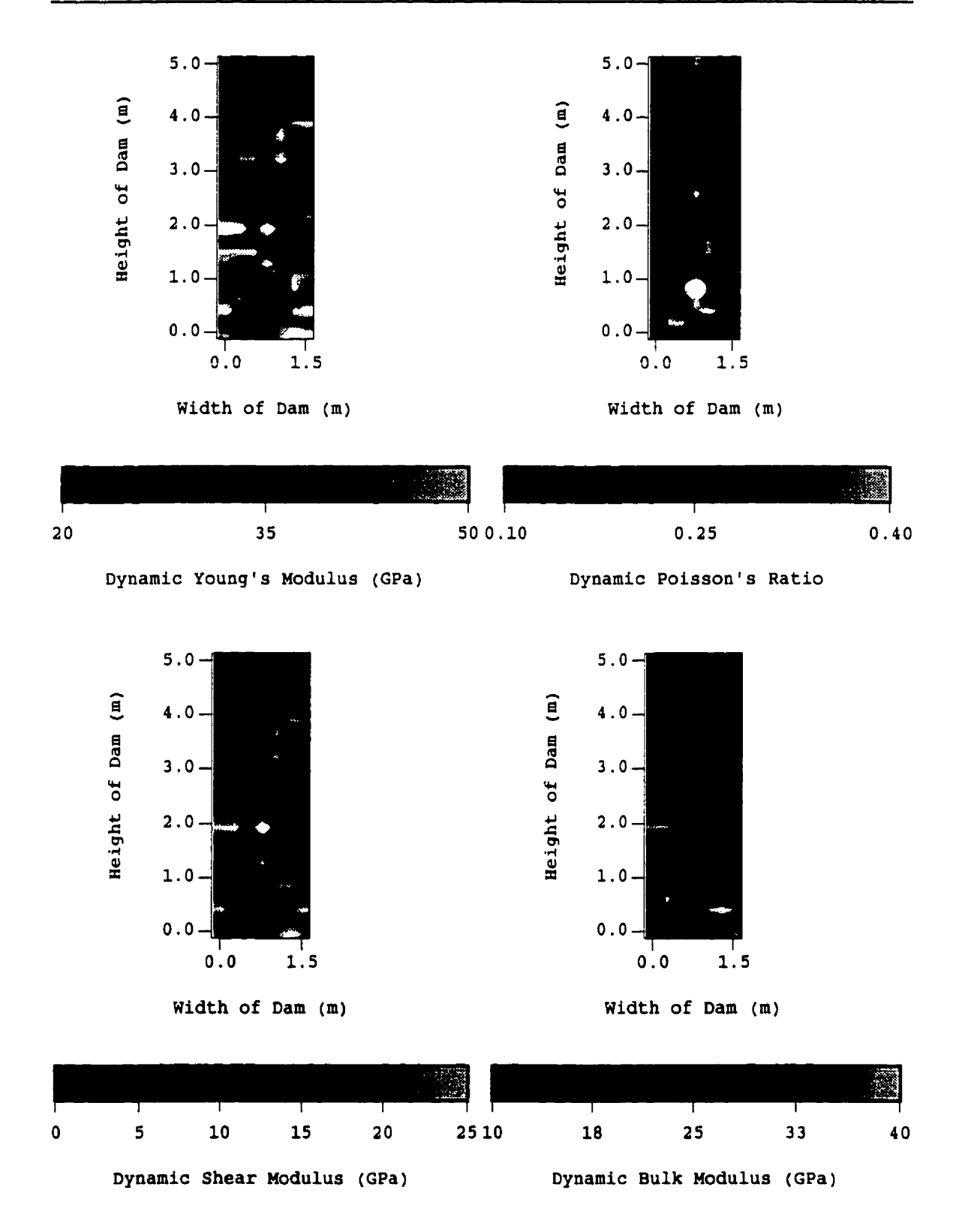


Figure 5. 17
Dynamic material properties on the south face of the dam.

5.4 FINAL NOTES

The tests presented in this chapter serve as the basis for further work on extending the capabilities of the MSR Impact-Echo system. The first objective was to establish the limitations of the system with respect to inclined crack detection and penetration depth. Three test beds served to assess those limitations.

The first test bed concentrated on determining the precision of the instrumentation with respect to inclined crack detection. The initial results yielded errors inconsistant with expected results. Modifications to the experimental setup and to the equipment helped reach the precision expected from this system. The third concrete slab with the plastic bubble wrap as artificial crack material yielded the best results based on the ability to detect the peak frequencies in the spectrums. This was mainly due to the simulated concrete-air interface provided by the plastic bubble wrap material.

The second test bed focused on determining the sensitivity of the system with respect to thin crack detection. It was clearly shown that the system is capable of detecting cracks of thickness 0.08 to 0.1 mm at short distances. The tests were performed in dry and saturated crack conditions.

The third test bed was best suited to determine the penetration depth of the system. The test bed dimensions were representative of an actual small concrete gravity dam. It was shown that it is possible to determine the dynamic properties of such a structure. However, it was also noted that the penetration depth of the MSR Impact-Echo system is presently limited to approximately 2.20 m. On the south face and in the lower section of the dam the frequency analysis was conducted in a region mostly dominated by the frequency response of the transducer assembly. It is recommended to try to eliminate the frequency response of the transducer and also amplify the signal.

SOFTWARE DEVELOPMENT

The analysis of the MSR Impact-Echo's time domain waveforms was always performed as a point by point method. A computer program written with the GAUSS mathematical system is at the basis of the analysis procedure. The Time Series Analysis package is used to perform the FFT on the time domain waveforms. The program was initially written for use in the laboratory. The number of data files to dissect was usually small and required only a simple program to determine the peak P-wave frequencies in the frequency spectrums. Once the frequency was selected, the user would have to manually input the results in a spreadsheet software package. The spreadsheet was then programmed to determine the depths of anomalies or a material's thickness. A major inconvenience of this process occurs when the results are not satisfactory. The user must return to the GAUSS software and re-examine the data files and then re-input the results into the spreadsheet. Additionally, the user must continuously edit the core program code in order to change the data filename. The procedure makes for a very tedious process when the number of data files increases. However, when a limited number of data files are to be analyzed, the program is sufficient.

When the S-wave transducer was initially added to the MSR Impact-Echo system, the same program was used to determine the frequency of the S-waves. The addition of a transducer meant the analysis of both the P- and S-wave data files to determine the dynamic properties of materials. The data analysis becomes immediately tedious and complex. At this point, there are seven parameters to determine: the P- and S-wave frequencies, the dynamic modulus of elasticity, Poisson's ratio, Shear modulus and Bulk modulus, and the depth of anomalies. After the selection of the peak frequencies for each data file, viewing the results in a spreadsheet is a long process. No method was available to immediately return to the software program to correct discrepancies in the results. Laboratory investigations were once again limited to a low number of files to examine. The data analysis of the small concrete gravity dam discussed in Section 5.3 would have been extremely complex and difficult. The number of files to scrutinize was close to 2000 and this is a relatively small concrete structure.

The author proceeded to modify the computer program in order to accelerate the analysis of this number of files. The following sections describe the objectives reached to increase the efficiency of the program and to adapt it to field analysis.

6.1 SOFTWARE MODIFICATIONS

The objectives of the software modifications can be summarized in three main categories:

- 1) easier data file manipulation and easier insertion of input parameters
- 2) increased efficiency during the analysis process
- 3) easy recall of the stored results

It was determined that two programs were needed to examine the time domain signals and increase the versatility of the MSR Impact-Echo system. The first program focused on defect location. That is, the use of only waveforms captured with the P-wave vertical displacement transducer. The second program focused on the evaluation of the dynamic material properties of materials. This meant analyzing the waveforms captured with both the P- and S-wave transducers. Both programs are quite similar. The first program looks at only one waveform and gives the results. The second program analyses the P- and S-wave waveforms, and subsequently yields the dynamic material properties. Figures 6.1 and 6.2 show the flowcharts of each program. The following computer program description applies to both programs.

6.2 COMPUTER PROGRAM DESCRIPTION

The first stage of the development focused on eliminating the need to access the program code in order to analyze a specific data file. Previously, the user had to manually input the file name and directory along with the sampling rate used for each test point. Any mistake would halt the program. With the new programs, the user can set the directory where the files are stored and input the parameters needed for the analysis.

The user is not permitted to access the source code of the program, thus eliminating possible problems caused by inadvertently modifying the core code. The user can then specify which file to examine by simply imputing the file name. Once the input parameters are set, the program asks the user if any modifications are needed. If none are

required, the program sorts the data files for easy access. It is important to ensure that the P- and S-wave files correspond with one another when they are requested for analysis.

The user can now proceed to view the time domain waveforms and the associated frequency spectrums of the data files. The name of the current data file is shown above the frequency spectrum. After selecting the peak frequency or frequencies, the user is shown a table of results. The results are a function of the input parameters initially set in each program. The user is then asked a series of questions. The options are shown in the following figures.

The results are appended into a specified text file while imputing the initial parameters. The user can recall the text file at a later date and append additional results into the file without deleting the initial results.

Two additional computer programs were written. The programs allow the user to create data files that can reproduce the time domain waveforms and frequency spectrums. The output files are in text format and are importable to spreadsheet programs. The figures shown in Appendix A were generated from these files. The programs run independently after initial input parameters are given.

6.3 FINAL NOTES

The new modified programs significantly improved the speed of the data analysis. The output files were easy to read since the output data is formatted into a table structure. Table headers are appended to the output file at the beginning of the analysis.

The new dynamic property measurement program was very useful during the examination of the small gravity dam. It was mentioned in Chapter 5 that close to 1000 data files were generated. By immediately viewing the results, it was possible to quickly assess the validity of the results and re-analyze data files as required. The programs are more robust and simpler to use than the older program. Eventually, all four programs should be integrated into one data analysis package.

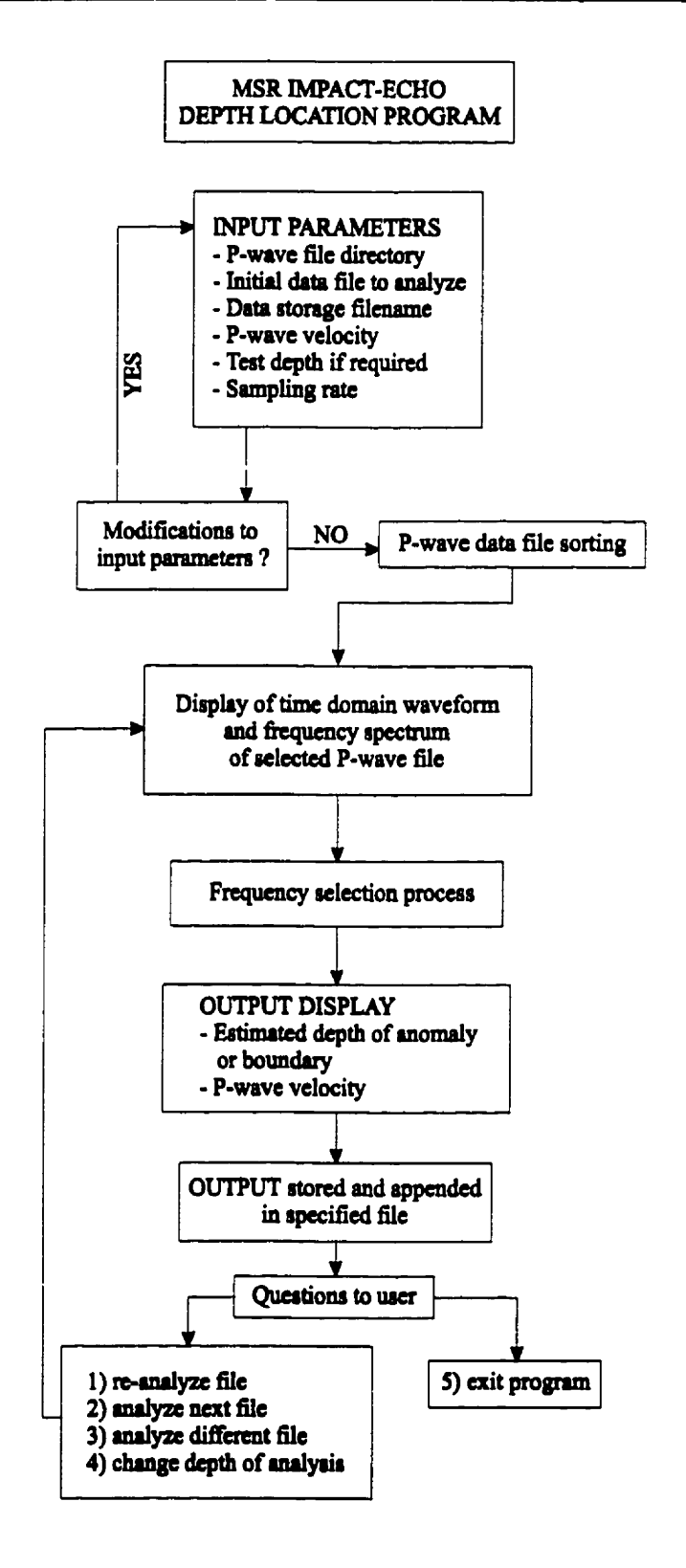


Figure 6.1
Flowchart of new program for defect depth location and thickness measurement.

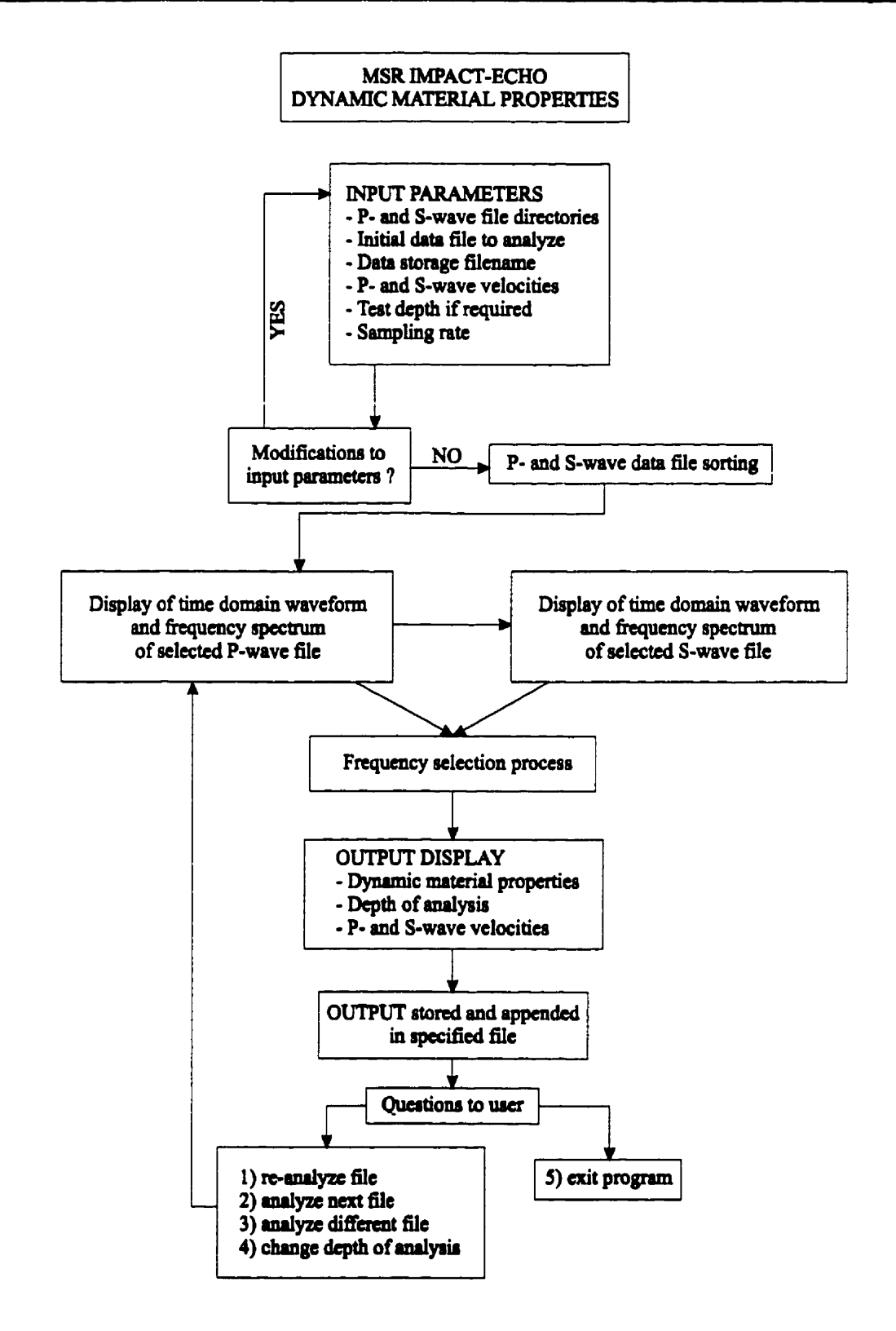


Figure 6.2
Flowchart of new program for determining the dynamic material properties.

CONCLUSIONS

7.1 SUMMARY OF THE RESEARCH

The work presented in this thesis focused on evaluating the MSR Impact-Echo system with the intent of using the technique for crack detection in concrete dams. The study was conducted as part of a three year research program between McGill University and Hydro-Québec. The crown corporation's interest in the use of seismic methods is in reducing the utility's high inspection costs. At this time, and with the use of destructive techniques, it is difficult to determine the precise location of cracks in concrete dams. Therefore, developing a low cost and accurate nondestructive technique is of great interest. Presently, the MSR Impact-Echo is best suited for this type of development. The technology and theory behind the system is developed. The system was initially developed to determine the thickness and material properties of concrete linings in mine shafts and tunnels. Hence, the focus of the research is extending the system's penetration depth into large scale structures such as concrete dams. The first step in extending the capabilities of the system involves the evaluation of the present qualities of the system.

The MSR Impact-Echo system is based on the propagation of miniature seismic waves in an elastic medium. The waves reflect off boundaries, internal anomalies, and crack interfaces. Surface displacements are generated at the impact point due to the multiple reflections of both the P- and S-waves. Waveforms are captured on the surface with the help of vertical and tangential displacement transducers. The analysis of the waveforms yields the frequency content of the wave. Subsequently, the P- and S-wave peak frequencies are determined and used in equations that determine the depth of defects and a material's dynamic elastic properties. The miniature seismic waves are introduced into a medium with the help of spherically tipped impact devices.

The work discussed in the thesis included both laboratory and field work. Three test configurations were studied. The first test setup focused on evaluating the precision of the system with respect to the detection of inclined cracks. The second test involved investigating the minimum crack thickness detectable in dry and saturated conditions.

Finally, the third test served to determine the penetration depth of the system and to determine the dynamic material properties of a large scale concrete structure. The work presented in the preceding chapters served to establish the groundwork for future development of the MSR Impact-Echo system for crack detection in concrete dams. Section 7.2 presents the conclusions and Section 7.3 recommends some future work.

7.2 CONCLUSIONS

The conclusions are subdivided in sections with respect to the three experiments presented in the thesis.

7.2.1 Inclined crack detection tests

Two series of tests were required in order to increase the precision level of the findings to an acceptable level. The experiments confirm that it is possible to detect the inclination of cracks. The tests were performed on three concrete slabs where an artificial crack was inserted at 30 degrees from the test surface. The P-wave velocities were determined for each slab and for each test sequence. Dynamic and static material properties were presented. The main conclusions of the tests are the following:

- The 300 mm thickness of the slabs induced many reflections of the propagating stress waves. Initial results were not satisfactory. The amplitude of the P-wave frequencies was generally low and difficult to signal out in the spectrums. There was presence of excess electrical noise in the time domain signal. The concrete slabs highly attenuated the waves.
- After the analysis of the first tests on each slab, it was determined that
 modifications to the instruments were required. First, the piezoelectric tip
 was replaced to reduce the electrical noise in the time domain signal.
 Second, the impact initial device was changed to an Equotip Model G high
 energy impact source. The change was necessary in order to counter the
 effect of the high attenuation of concrete.

- The concrete slabs were positioned upright in order to eliminate all possible interference caused by manipulation of the transducer. The noise in the signal was clearly eliminated after all the modifications.
- The second series of tests yielded satisfactory results. The inclined cracks were detected without difficulty. For all three slabs, the error between the actual crack depth and the detected crack depth varied from 0 to 5% in the middle of the slabs. Occasional errors above 5% occurred in other regions of the test grids.
- Of the three materials used, the best results were obtained with the plastic bubble wrap material based on the ease of frequency selection in the associated spectrums. This material was intentionally used to simulate a concrete-air interface.

7.2.2 Crack Thickness Investigation

An experiment was setup to evaluate the system's limitations with respect to the minimum crack thickness detectable with the MSR Impact-Echo system. The following conclusion were drawn:

- The system is capable of detecting cracks of at least 0.08 to 0.1 mm in thickness.
- The tests were performed in dry and saturated conditions. In both cases the results were the same. The cracks were clearly detected as shown in the frequency spectrums presented in the thesis.
- Both the Equotip Models D and G were used with identical results.

7.2.3 Investigation of a Section of a Concrete Gravity Dam

A section of a concrete gravity dam was investigated with the MSR Impact-Echo system. The concrete structure was built at IREQ with the help of the author. The gravity dam section measured 5 m high by 4 m long at the base. Tests were conducted on two faces of the dam. On the East face, the dynamic material properties were determined.

The South face investigation also yielded the dynamic properties, as well as the penetration depth of the system. Close to 2000 time domain signals were analyzed with a new software developed to improved the speed of the data analysis. The new software allows the user to store results, immediately find a defect's depth, and also determine a material's dynamic elastic properties. The following conclusions were obtained:

- The concrete gravity dam consists of mainly uniform concrete of good quality as observed with the P- and S- wave velocity profiles shown in the thesis. High stress wave velocities were found in the lower portions of the dam.
- The penetration depth of the current MSR Impact-Echo system has been established at 2.20 m. This was determined from tests conducted on the south face of the dam. The distance to the opposite face varied from 1 m at the top to 4 m at the base of the dam.
- On the south face and in the lower section of the dam the frequency analysis was conducted in a region dominated by the frequency response of the transducer assembly. Hence, the difficulty to observe the correct Pand S- wave frequencies at depths greater than 2.20 m.

7.3 FUTURE WORK

On concrete dams, it may occur that high volumes of data are recorded. At this time, the *MSR Impact-Echo* system is a point by point test method that scans the intersections of a test grid. An automated version of the equipment can increase the data acquisition speed and the frequency analysis process.

Most dams are located in remote areas with limited access. Therefore, a more rugged system needs to be designed with a backup system.

Further modifications to the system are necessary in order to reach the goal of a 7 to 10 m penetration depth of in concrete dams.

REFERENCES:

- ASTM C215-91, (1991). Standard Test Method for Fundamental Transverse, Longitudinal, and Torsional Frequencies of Concrete Specimens. ASTM Standards, Annual Book 1991, Section 4, Philadelphia, pp. 124-129.
- Bieniawaki, Z.T., (1978). *The "Petite Sismique" Technique A Review of Current Developments*. Proc. 2nd Conference on Acoustic Emission / Microseismic Activity in Geologic Structures and Materials, Pennsylvania State University, November 13-15, pp. 307-318.
- Bolt, B.A., (1976). Nuclear Explosions and Earthquakes. W.H. Freeman and Company.
- Bracs, G., Balint, E., Orchard, D.F., (1970). <u>Use of Electrical Resistance Probes in Tracing Moisture</u>
 <u>Permeation Through Concrete</u>. Proceedings of the ACI Journal, Vol. 67, No. 8, August, pp. 642-646.
- Carino, N.J., (1992). Recent Developments in Nondestructive Testing of Concrete. In Advances in Concrete Technology, V.M. Malhotra, editor, CANMET, pp. 281-328.
- Carino, N.J., and Sansalone, M., (1984). <u>Pulse-Echo Method for Flaw Detection in Concrete</u>. Technical Note 1199, National Bureau of Standards, Gaithersberg, Maryland, USA, 35 pp.
- Carino, N.J., Sanalone, M., and Hsu, N.N., (1986). <u>A Point Source-Point Receiver, Pulse-Echo Technique</u> for Flaw Detection in Concrete. Journal of the American Concrete Institute, Vol. 83, No.2, April, pp. 199-208.
- Carino, N.J., and Sansalone, M., (1990). Flaw Detection in Concrete Using the Impact-Echo Method. In Proceedings on the NATO Conference on Bridge Evaluation, Repair, and Rehabilitation, A.S. Nowak, editor, Kluwer Academic Publishers, Netherlands, pp. 101-118.
- Carino, N.J., and Sansalone, M., (1992). <u>Detection of Voids in Grouted Ducts Using The Impact-Echo</u>
 <u>Method</u>. ACI Materials Journal, Vol. 89, No.3, May-June, pp. 296-303.
- CEB, (1993). <u>Durable Concrete Structures: Design Guide</u>. Comité Euro-International du Béton, Thomas Telford Publishers, London, England, 42 p.
- Claytor, T., and Elligson, W.A., (1983). <u>Development of Ultrasonic Methods for the Nondestructive</u>
 <u>Inspection of Concrete</u>. Ultrasonics Symposium Proceedings, Halifax, Nova Scotia, July, 1983.
- Clemeña, G.G., (1991). Short Pulse Radar Methods. In Handbook on Nondestructive Testing of Concrete, V.M. Malhotra and N.J. Carino editors, CRC Press Inc., Boca Raton, Florida, USA, pp. 253-274.
- Davis, A., and Dunn, C., (1974). From Theory to Field Experience with the Nondestructive Vibration of Piles. In the Proceedings of the Institute of Civil Engineers, Vol. 57, Part 2, December, p. 571.
- Evans, R.H., and Robinson, G.W., (1955). <u>Stress in Prestressed Concrete from X-ray Photographs</u>. Proc. Institution of Civil Engineers, London, England, V. 4, No. 2, Part 1, March, pp. 212-235.
- Foster, B., (1968). Attenuation of X-rays and Gamma Rays in Concrete. Materials Research and Standards, V. 8, No. 3, Mar. 1968, pp. 19-24.

- Ghorbanpoor, A., Virmani, Y.P., and Fatemi, G.R., (1992). Evaluation of Concrete Bridges by Impact-Echo. In Nondestructive Testing of Concrete Elements and Structures, ASCE, F. Ansari and S. Sture Editors, pp. 82-93.
- Goldsmith, W., (1965). *Impact: The Theory and Physical Behavior of Colliding Solids*. Edward Arnold Press Ltd., pp. 24-50.
- Green, A.T., (1970). Stress Wave Emission and Fracture of Concrete Reactor Vessel Materials. In Proceedings of the Inter-American Conference on Materials Technology, ASME, Vol. 1, p. 635.
- Hassani, F.P., Momayez, M., Guevremont, P., Saleh, K, Tremblay, S., (1996a). Revue de la littérature:

 Méthodes d'inspections non destructives pour la détection de fissures dans les ouvrages en

 béton. Institut de Recherche d'Hydro-Québec (IREQ), November 1996, repport # IREQ-96-111,
 201 pp.
- Hassani, F.P., Sadri, A., and Momayez, M., (1996b). Application of MSR for the Evaluation of Excavated Tunnel and Shaft Concrete Linings. In Proceedings from the 2nd North American Rock Mechanics Symposium, NARMS '96, Rock Mechanics Tools and Techniques, A.A. Balkeema Publishers, Rotterdam, M. Aubertin, F.P. Hassani, and H. Mitri Editors, Montreal, Canada, June 19-21, pp. 875-882.
- Hassani, F.P., Momayez, M., and Wang, E., (1989). Concrete Shaft Lining: Thickness Measurement and Quality Control. McGill University, Department of Mining and Metallurgical Engineering, Montreal, March, pp. 356.
- Henrickson, C., (1995). Impact-Echo Testing. Concrete International, May 1995, pp. 55-58.
- Higgs, J., (1979). Integrity Testing of Piles by the Shock Method. Concrete, October, p. 31.
- Kharrat, Y., Côté, and Ballivy G. (1993), <u>Essai de mesures tomographiques sur le barrage de Sorin</u> (*France*). University of Sherbrooke, Canada, report no. GR 93-01-02.
- Krautkrämer, J., and Krautkrämer, H., (1983). <u>Ultrasonic Testing of Materials</u>. Springer-Verlag, New York, 3rd Edition, pp. 119-124.
- Lauer, K.R., (1991). Magnetic and Electrical Methods. In Handbook on Nondestructive Testing of Concrete, V.M. Malhotra and N.J. Carino editors, CRC Press Inc., Boca Raton, Florida, USA, pp. 203-225.
- Leeb, D., (1979). <u>Dynamic Hardness Testing of Metallic Materials</u>. NDT International, December, 1979, pp. 274-278.
- Leslie, J.R., and Cheesman, W.J. (1950). An Ultrasonic Method of Studying Deterioration and Cracking in Concrete Structures. Journal of the American Concrete Institute, Michigan, USA, Vol. 21, No. 1, September, pp. 17-36.
- Lim, M.K., and Koo, T.K., (1989). Acoustic Emission from Reinforced Concrete Beams. Magazine of Concrete Research, Vol. 41, No. 149, December, pp. 229-234.
- Lin, J.-M., and Sansalone, M., (1994). <u>Impact-Echo Response of Hollow Cylindrical Concrete Structures</u>
 <u>Surrounded by Soil and Rock: Part II Experimental Studies</u>. Geotechnical Testing Journal,
 GTJODJ, Vol. 17, No. 2, June, pp. 220-226.
- Lin, Y., Sansalone, M., Carino, N.J., (1990). Finite Element Studies of the Impact-Echo Response of Plates

 <u>Containing thin Layers and Voids</u>. Journal of Nondestructive Evaluation, Plenum Publ. Corp.,
 Vol. 9, No. 1, pp. 27-47.

- Malhotra, V.M., and Carino, N.J.,, editors (1991). <u>CRC Handbook on Nondestructive Testing of Concrete</u>. CRC Press Inc., Boca Raton, Florida, USA, 343 pp.
- Malhotra, V.M., and Sivasundaram, V., (1991). <u>Resonance Frequency Methods</u>. In CRC Handbook on Nondestructive Testing of Concrete, V.M. Malhotra and N.J. Carino editors, CRC Press Inc., Boca Raton, Florida, USA, pp. 147-168.
- McCabe, W.M., Koerner, R.M., and Lord, A.M. Jr., (1976). <u>Acoustic Emission Behaviour of Concrete Laboratory Specimens</u>. ACI Journal, July-August, 73, p. 367.
- McHenry, D., Oleson, C.C., (1967). <u>Pulse Velocity Measurements on Concrete Dams</u>. In Transcripts of the 9th International Congress on Large Dams, Istanbul, Turkey, Q. 34, R. 5, pp. 73-89.
- Mehta, P.K., and Monteiro, P. J.M., (1993). *Concrete: Structure, Properties, and Materials*. 2nd Edition Prentice-Hall Inc., Englewood Cliffs, New Jersey, pp. 56-57.
- Mindess, S., (1991). <u>Acoustic Emission Methods</u>. In Handbook on Nondestructive Testing of Concrete, V.M. Malhotra and N.J. Carino editors, CRC Press Inc., Boca Raton, Florida, USA, pp. 317-333.
- Momayez, M., Sadri, A., and Hassani, F.P., (1995). Impact-Echo: A Technique for Determining the Mechanical Properties of Rocks. In Proceedings for the 35th U.S. Rock Mechanics Symposium, University of Nevada, A.A. Balkema, Rotterdam, pp. 843-848.
- Mullins, L., Pearson, H.M., (1949). <u>The X-Ray Examination of Concrete</u>. Civil Engineering and Public Works Review, London, England, V.44, No. 515, May, pp. 256-258.
- Muenow, R., (1963). A Sonic Method to Determine Pavement Thickness. Journal of the PCA Research and Development Laboratories, Vol. 5, No. 3, September, pp. 8-21.
- Naik, T.R., (1979). <u>The Ultrasonic Testing of Concrete</u>. In Experimental Methods in Concrete Structures for Practitioners. ACI Publication, G.M. Sabnis and N. Fitzimons editors, October 1979.
- Naik, T.R, and Malhotra, V.M., (1991). <u>The Ultrasonic Pulse Velocity Method</u>. In Handbook on Nondestructive Testing of Concrete, V.M. Malhotra and N.J. Carino editors, CRC Press Inc., Boca Raton, Florida, USA, pp. 169-188.
- Nikkanin, P., (1962). On the Electrical Properties of Concrete and Their Applications. Sarja III, Rakennus 60, French version.
- Olson, L.D., (1991). <u>Developments in Nondestructive Testing Offer Powerful Methods for Analyzing</u>
 <u>Concrete</u>. The Construction Specifier, December, pp. 91-101.
- Olson, L.D., (1992). Sonic NDE of Structural Concrete. In Nondestructive Testing of Concrete Elements and Structures, ASCE, F. Ansari and S. Sture Editors, pp. 70-81.
- Olson, L.D., and Sack, D.A., (1991). Nondestructive Evaluation of Concrete Dams and Other Structures. In Proceedings from SPIE Conference on Nondestructive evaluation of Aging Structures and Dams, June 7th and 8th, Oakland, California, pp. 113-124.
- Olson, L.D., and Wright, C.C, (1990). *Nondestructive Testing for Repair and Rehabilitation*. Concrete International, March 1990, pp. 58-64.
- PC Handbook for Engineers and Scientists, (1996). <u>PC-Based Data Acquisition and Instrumentation</u>. CyberResearch Inc., Connecticut, USA, pp. T1-T10.

- Robertshaw, J., and Brown, P.D., (1955). <u>Geophysical Methods of Exploration and Their Application to Civil Engineering Problems</u>. Proceedings of The Institution of Civil Engineers, London, U.K., V. 4, No. 5, Part. 1, Sept., pp. 645-690.
- Robinson, G.S., (1968). Methods of Detecting the Formation and Propagation of Microcracks in Concrete. In Proceedings of the Inter. Symp. on the Structure of Concrete, A.E. Brooks and K. Newman editors, Cement and Concrete Assoc., London, England, pp. 161.
- Rothig, H., (1974). <u>Influence of the Radiation Pattern on Ultrasonic Attenuation Measurements of Concrete</u>. Materials Evaluation, April, pp. 69-74.
- Rüsh, H., (1959). Physical Problems in Testing of Concrete. Zement-Kalk-Gips, 12,1.
- Sack, D.A., Olson, L.D., and Aoud, M., (1995). <u>Impact Echo Scanning of Concrete and Wood</u>. In Nondestructive Evaluation of Aging Structures and Dams, S. Nazarian and L.D. Olson Editors, SPIE Proceeding Series, Vol. 2457, pp. 137-147.
- Sadri, A., (1996). <u>Development of the Miniature Seismic Reflection (MSR) System for Nondestructive</u>
 <u>Evaluation of Concrete Shaft and Tunnel Linings</u>. Ph.D. Thesis, McGill University, Montreal,
 Canada, December 1996.
- Sadri, A., Momayez, M., Hassani, F.P., Ibrahim, R., and Megharieff, J., (1995). Nondestructive Evaluation of Grouted Ducts on the Champlain Bridge. In Proceedings of the International Conference on Composite Materials and Energy, Enercomp '95, Montreal, Canada, May 8-10, pp. 699-705.
- Saleh, K., Hassani, F.P., Guevremont, P., Sadri, A., Lapointe, R., Ballivy, G., Rhazi, J., and Kharrat, Y., (1997). *Three Seismic Nondestructive Methods Used to Monitor Concrete Slab Injection Tests*. Accepted for publication in the *Journal of Pure and Applied Geophysics*, special publication, 1997.
- Saleh, K., Tremblay, S., and Mnif, K. (1995). <u>Injection de la dalle de béton no 30 par le coulis de ciment Portland type 10</u>. Institut de Recherche en Électricité d'Hydro-Québec, Varennes, Québec, Canada, Report # IREQ-95-209, 37 pages.
- Sansalone, M., (1986). <u>Flaw Detection in Concrete Using Transient Stress Waves</u>. Ph.D. Thesis, Cornell University, Ithaca, New York, 220 pp.
- Sansalone, M., and Carino, N.J. (1986). Impact-Echo: A Method for Flaw Detection in Concrete Using

 Transient Stress Waves. National Bureau of Standards, Gaithersberg, Maryland, report #

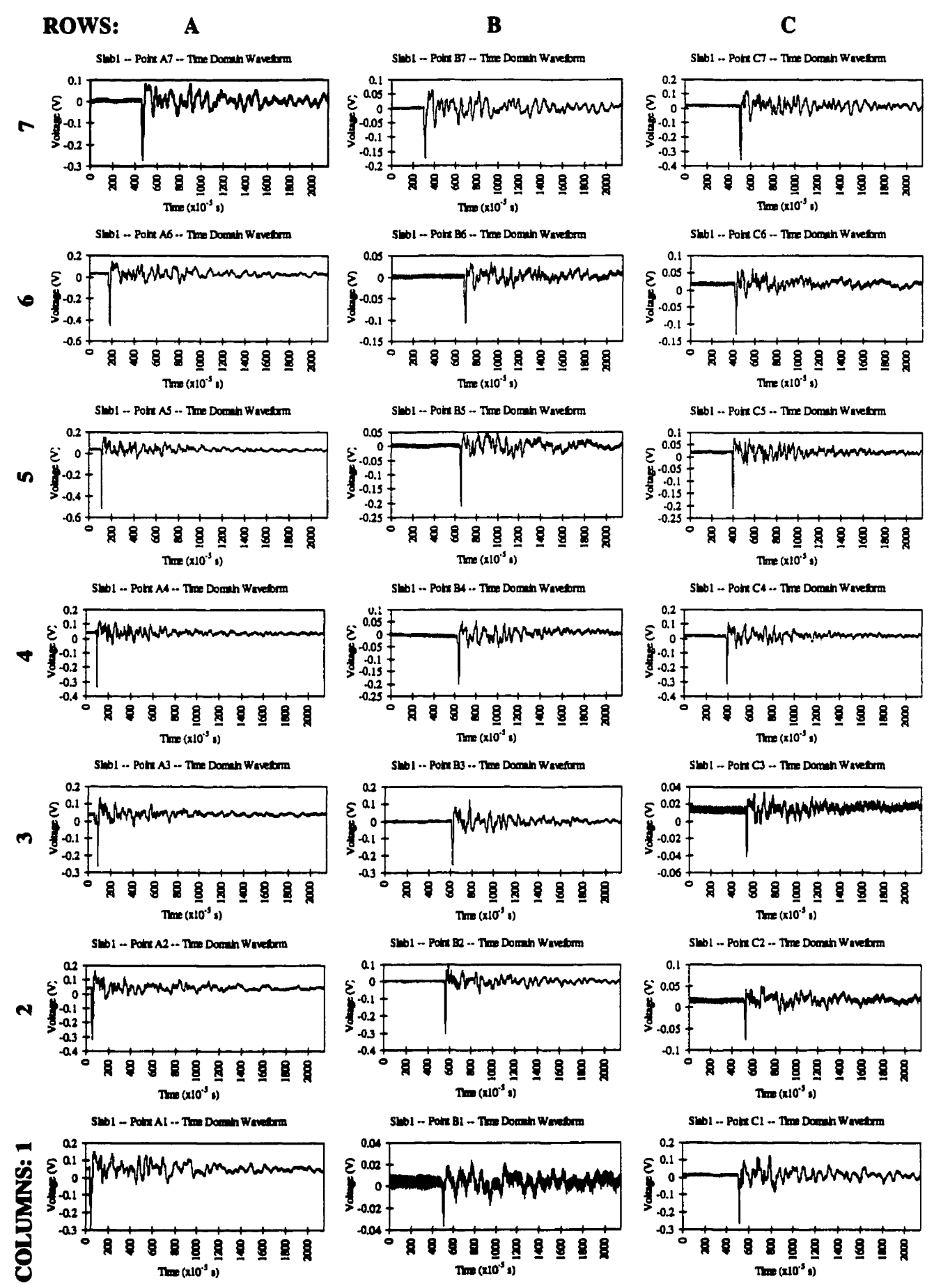
 NBSIR 86-3452, 222 pp.
- Sansalone, M., and Carino, N.J., (1987). *Transient Impact Response of Thick Circular Plates*. Journal of Research of the National Bureau of Standards, Vol. 92, 6, November-December, pp.355-368.
- Sansalone, M., and Carino, N.J., (1988). <u>Impact-Echo: Detecting Honeycombing, the depth of Surface-opening Cracks, and Ungrouted Ducts</u>. In Nondestructive Testing of Concrete, ACI publication SP-112, pp. 1-20.
- Sansalone, M. and Carino, N.J., (1989). <u>Laboratory and Field Studies of the Impact-Echo Method for Flaw Detection in Concrete</u>. In Nondestructive Testing, H.S. Lew editor, American Concrete Institute, SP-112-1, March, pp. 1-20.
- Sansalone, M., and Carino, N.J., (1991). <u>Stress Wave Propagation Methods</u>. In Handbook on Nondestructive Testing of Concrete, V.M. Malhotra and N.J. Carino editors, CRC Press Inc., Boca Raton, Florida, USA, pp. 275-304.

- Sansalone, M., Lin, Y., Pratt, D., and Cheng, C.C., (1991). <u>Advancements and New Applications in Impact-Echo Testing</u>. In Proceedings of the International Conference on Evaluation and Rehabilitation of Concrete Structures and Innovations in Design, Hong Kong, December 1991, ACI SP-128, pp. 135-150.
- Strum, R.D., and Kirk, D.E., (1988). First Principles of Discrete Systems and Digital Signal Processing.

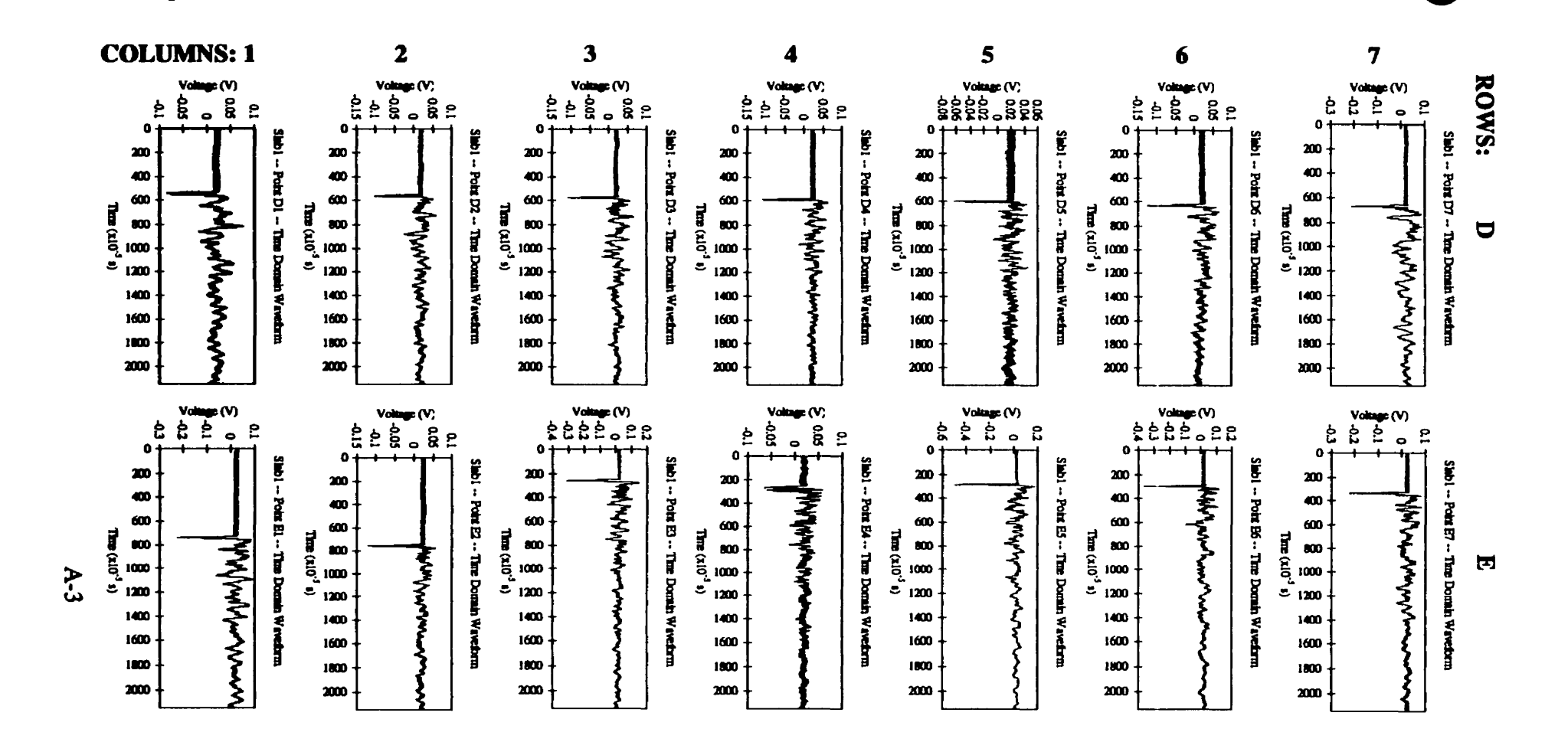
 Addison-Wesley Publishing Co. Inc., New York, New York, pp. 363-528.
- Sutherland, H.J., and Kent, L.A., (1977). <u>Erosion Rate Measurement Using an Acoustic Technique</u>. Review of Scientific Instrumentation, Vol. 48, No. 8, August, pp. 1010-1016.
- Telford, W.M., Geldart, L.P., and Sheriff, R.E., (1990). <u>Applied Geophysics</u>. Cambridge University Press, 2nd edition, pp. 136-273.
- Timoshenko, S.P., and Goodier, J.N., (1970). <u>Theory of Elasticity</u>. McGraw-Hill, New York, 3rd edition, 567 pp.
- Weil, G.J., (1991). <u>Infrared Thermographic Techniques</u>. In Handbook on Nondestructive Testing of Concrete, V.M. Malhotra and N.J. Carino editors, CRC Press Inc., Boca Raton, Florida, USA, pp. 305-316.
- Wells, D., (1970). An Acoustic Apparatus to Record Emissions from Concrete Under Strain. In Nuclear Engineering and Design, Vol. 12, pp.80.

APPENDIX A

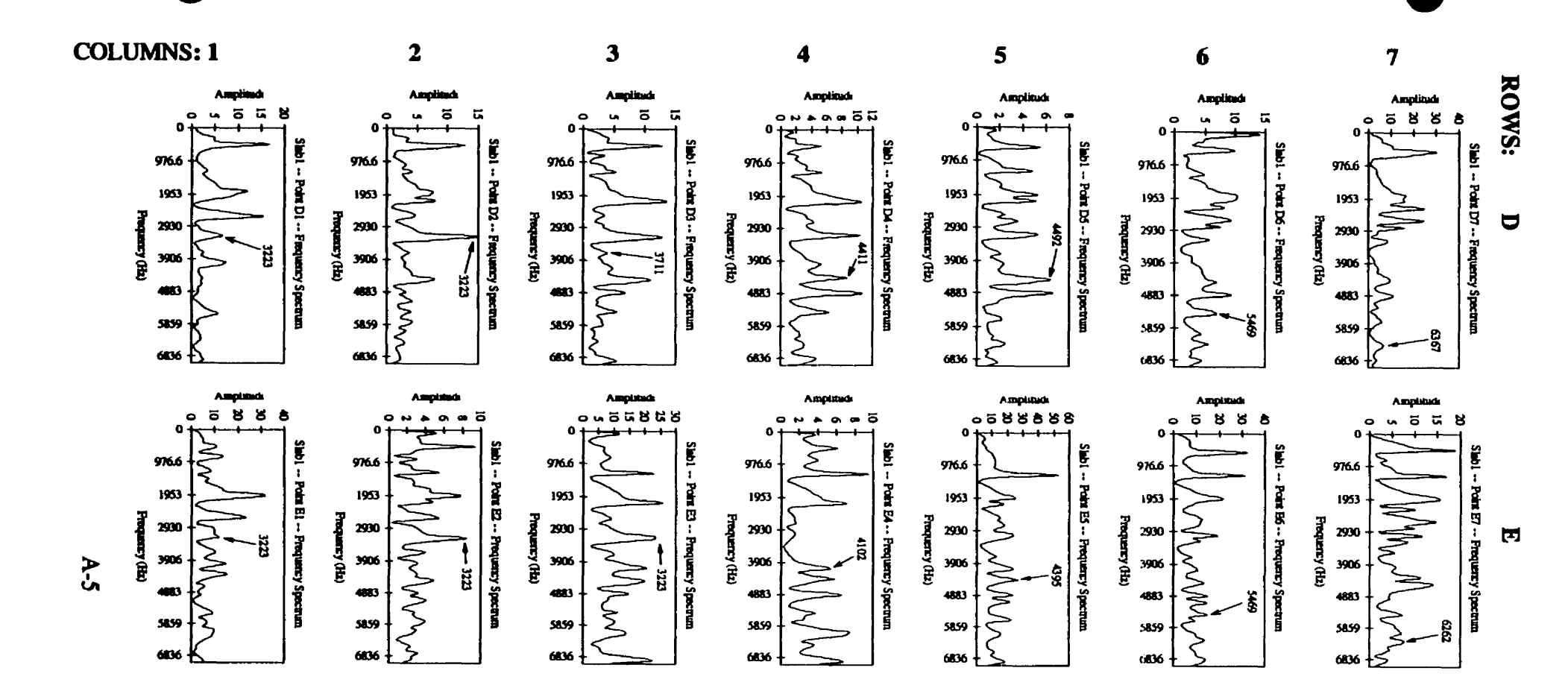
Time Domain Waveforms
and
Frequency Spectrums
for the
Inclined Crack Detection Tests

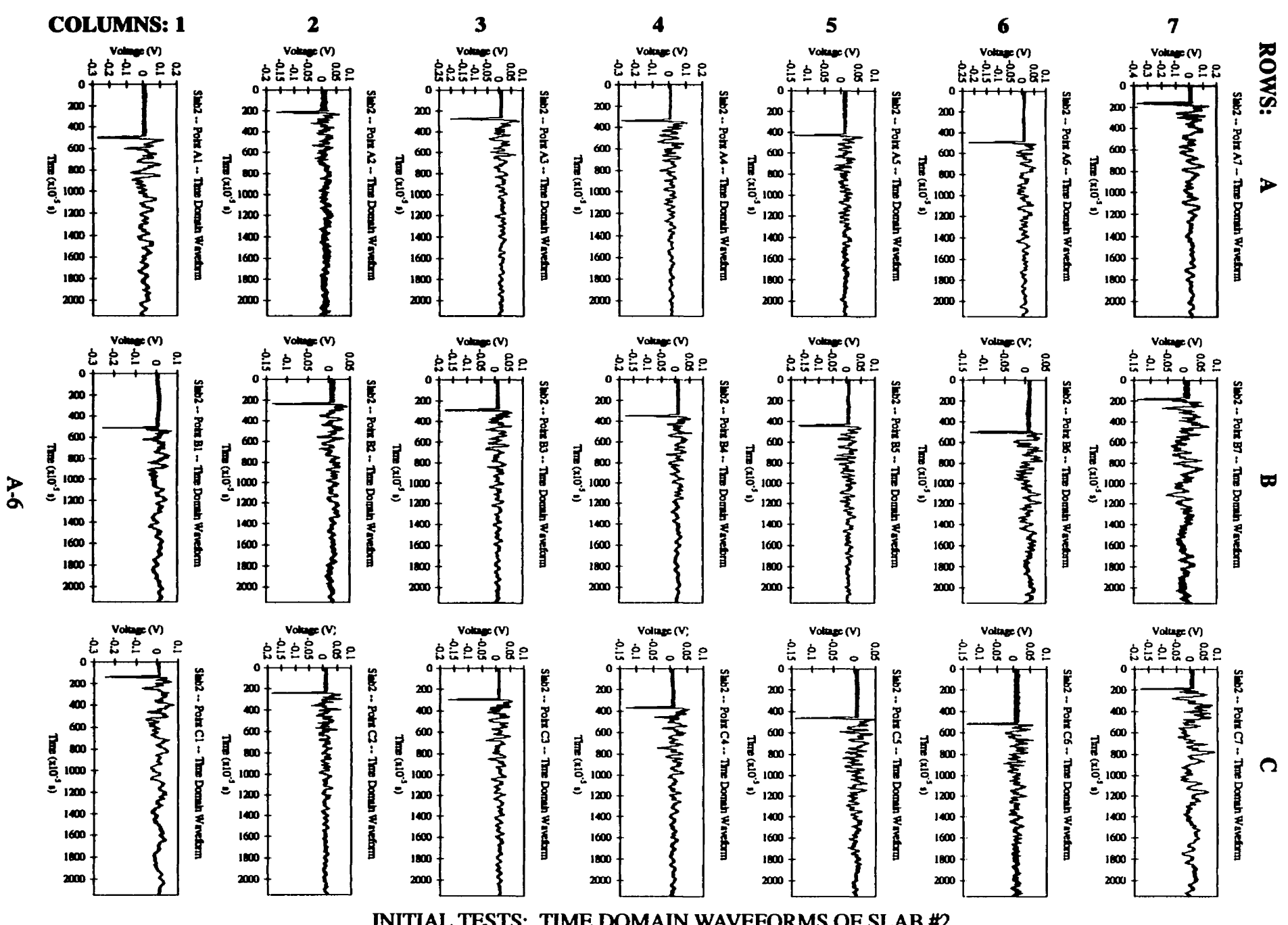


A-2

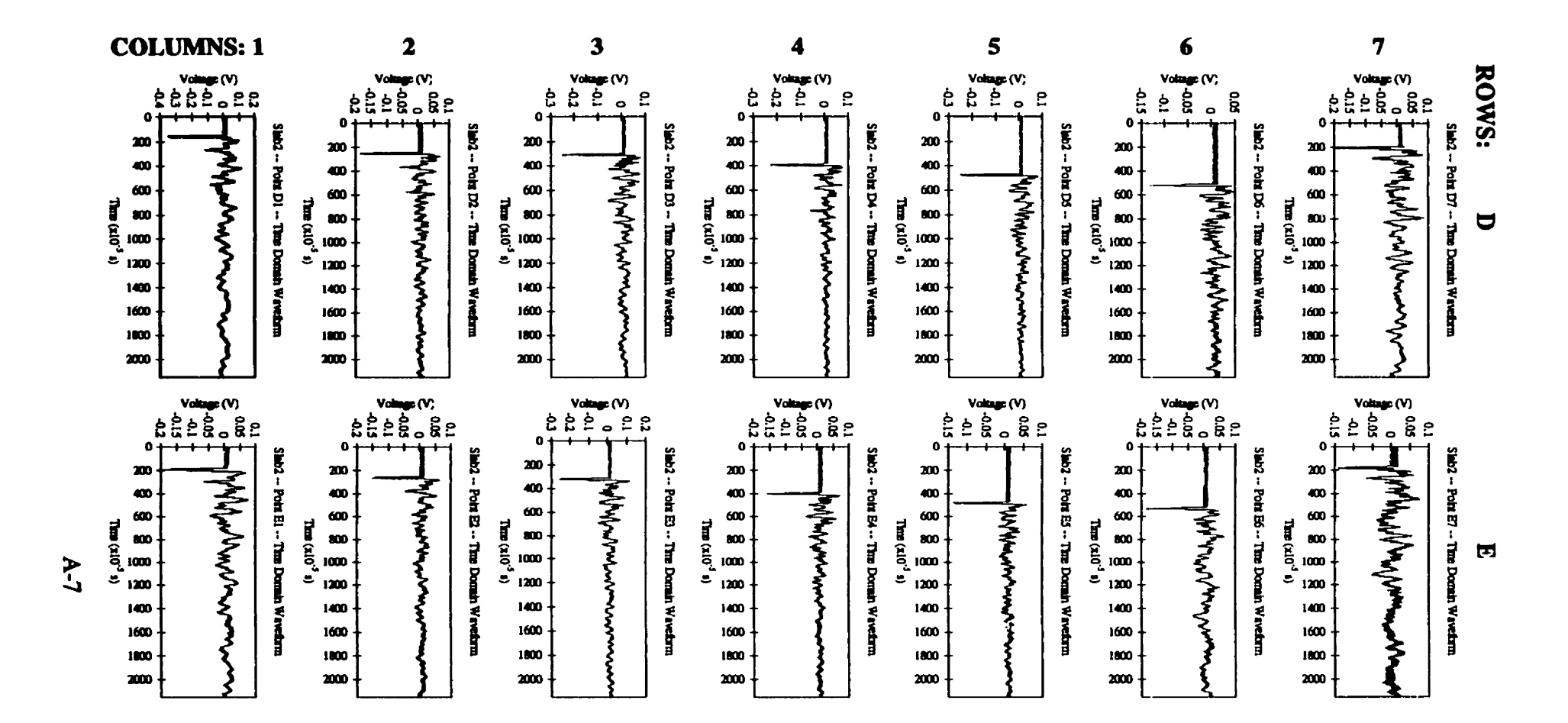


INITIAL TESTS: FREQUENCY SPECTRUMS OF SLAB#1 30 DEGREES PLASTIC SHEET: ROWS A TO C





INITIAL TESTS: TIME DOMAIN WAVEFORMS OF SLAB #2 30 DEGREES PLASTIC CARPET ROWS A TO C



INITIAL TESTS: FREQUENCY SPECTRUMS OF SLAB #2 30 DEGREES PLASTIC CARPET: ROWS A TO C

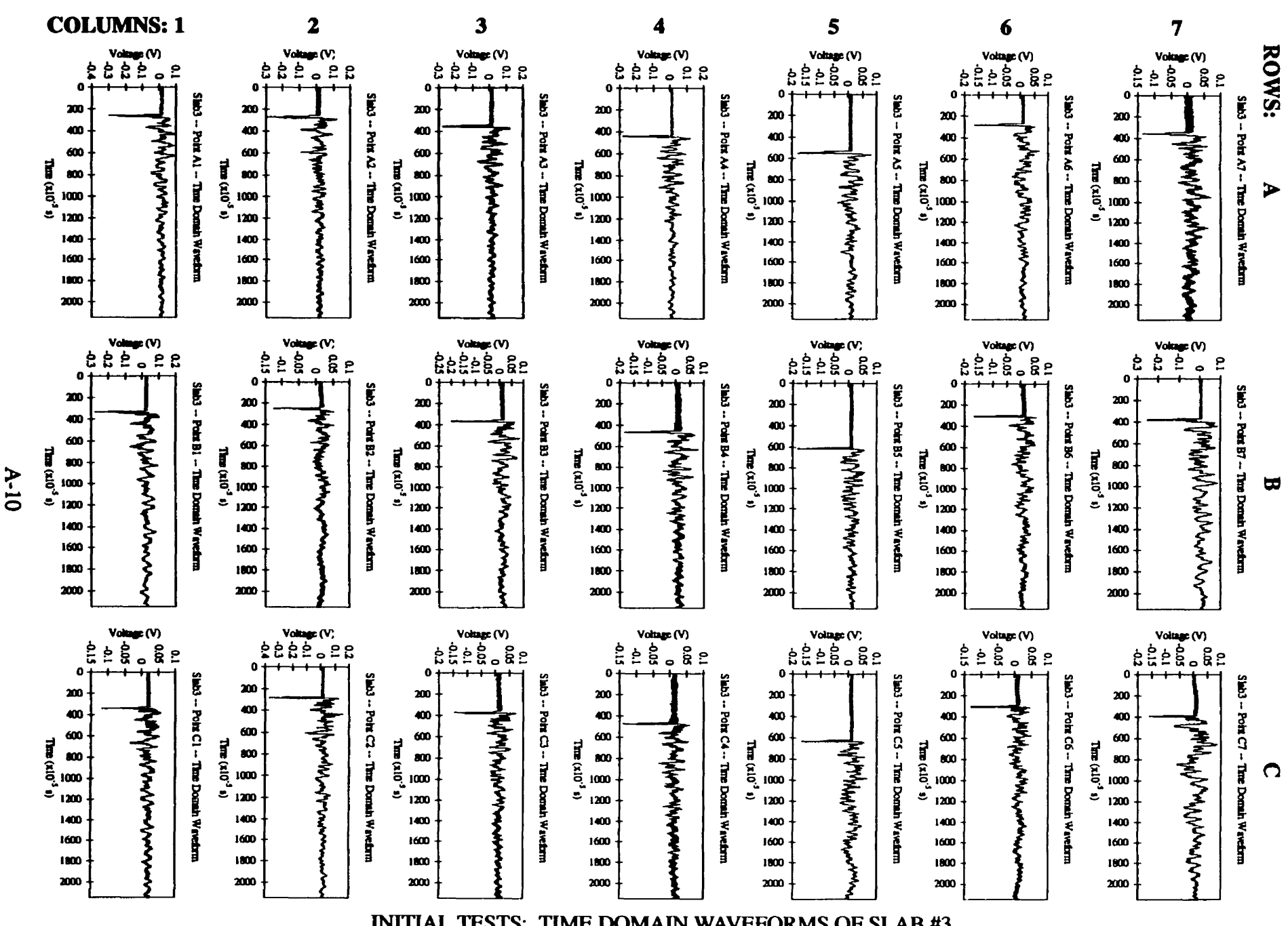
95

<u>5</u> 8

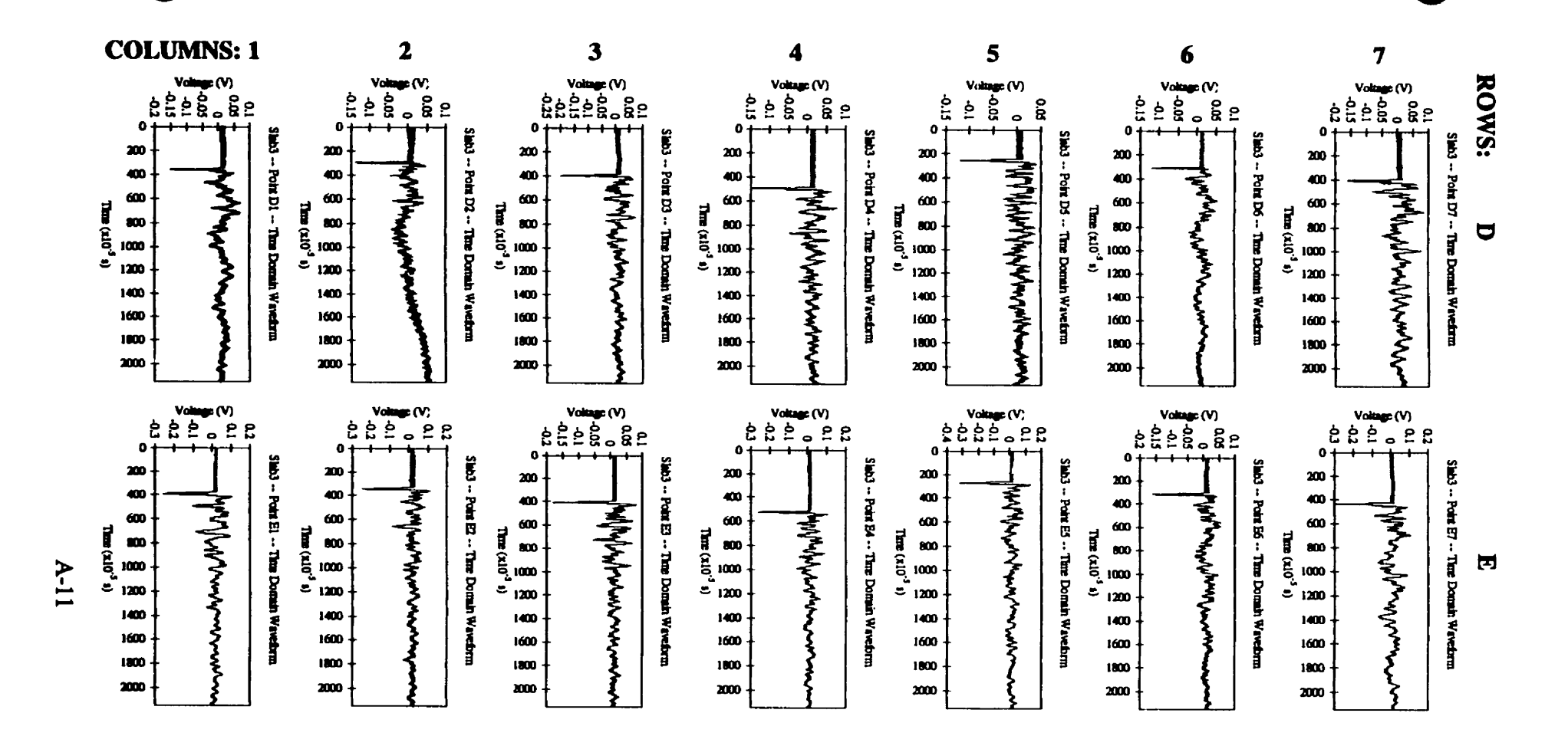
Proquency (Hz)

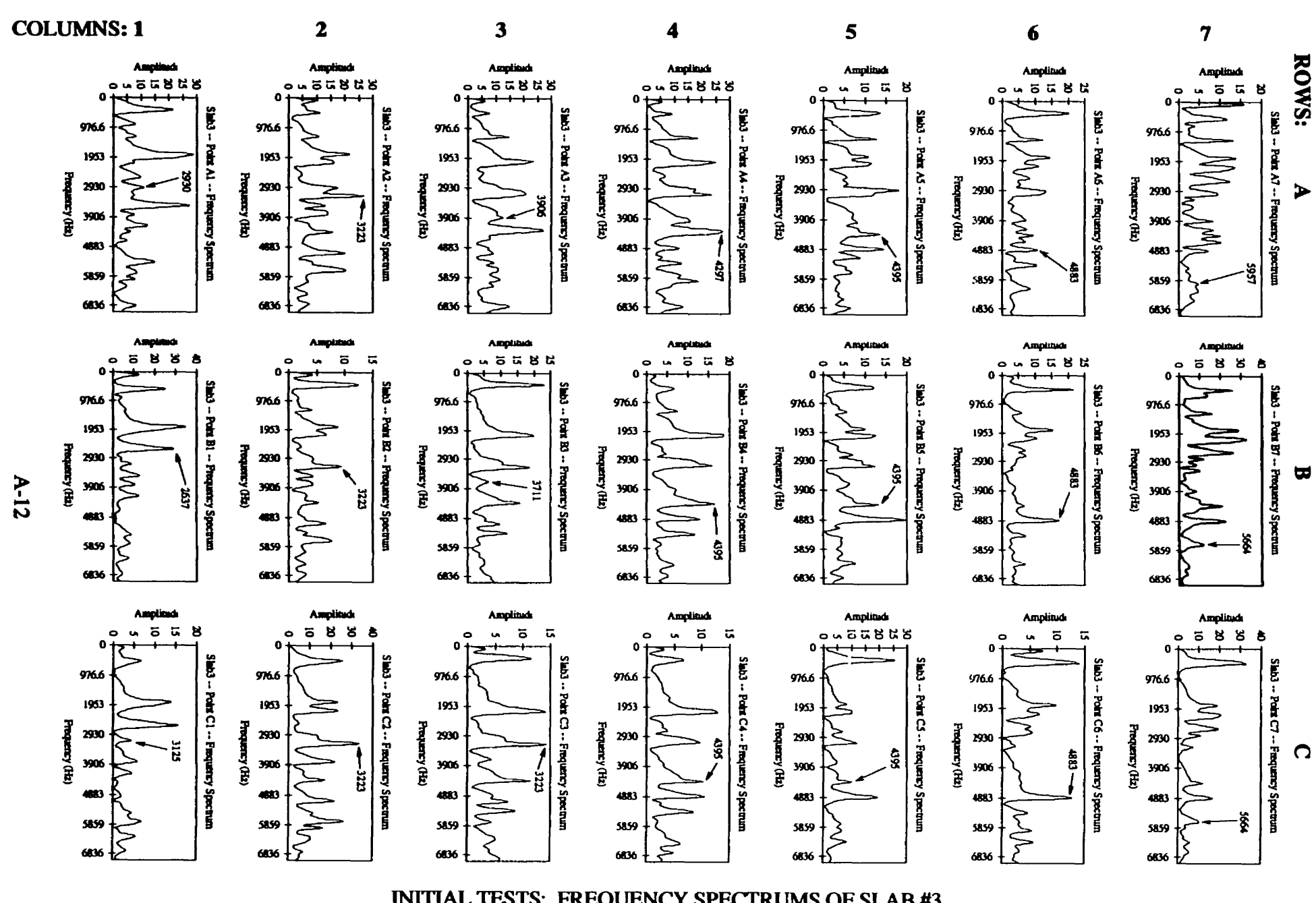
Prequency (Hz)

8 8

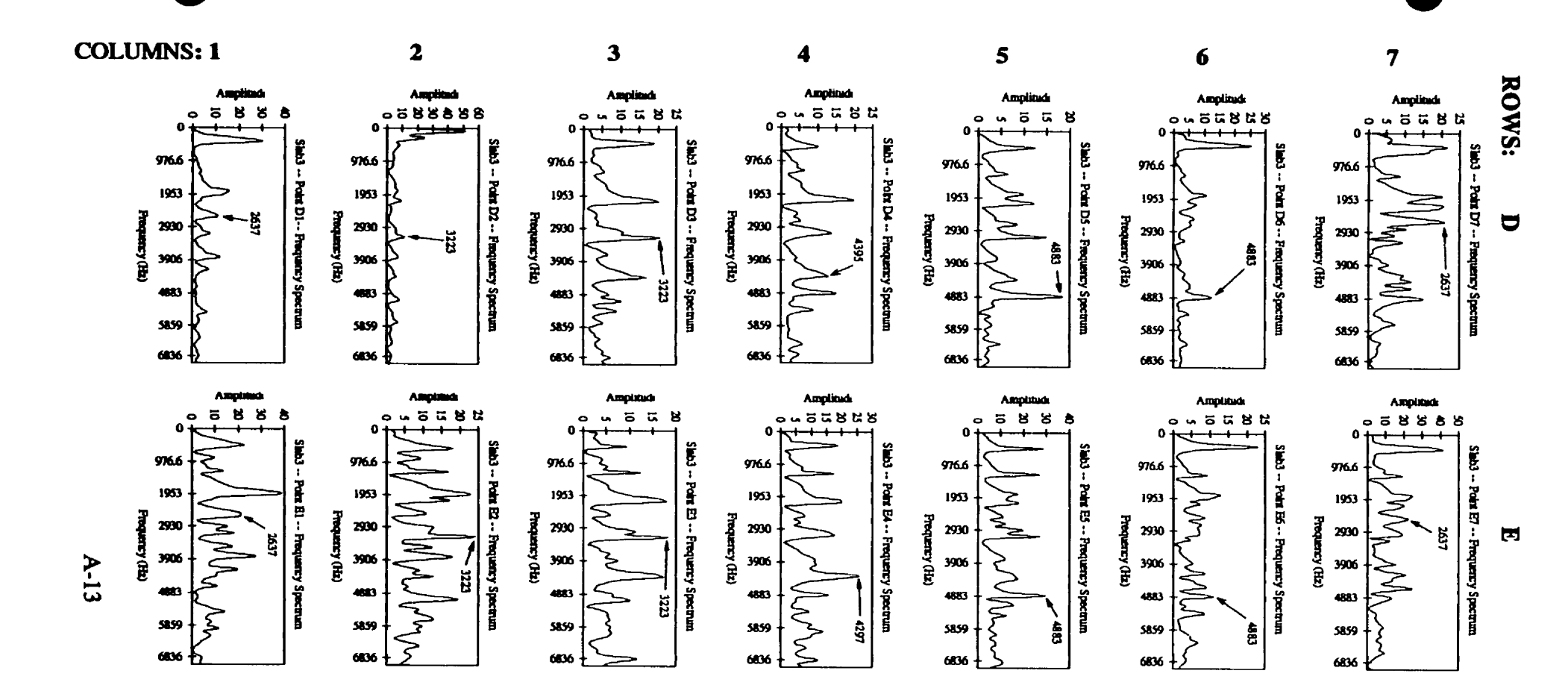


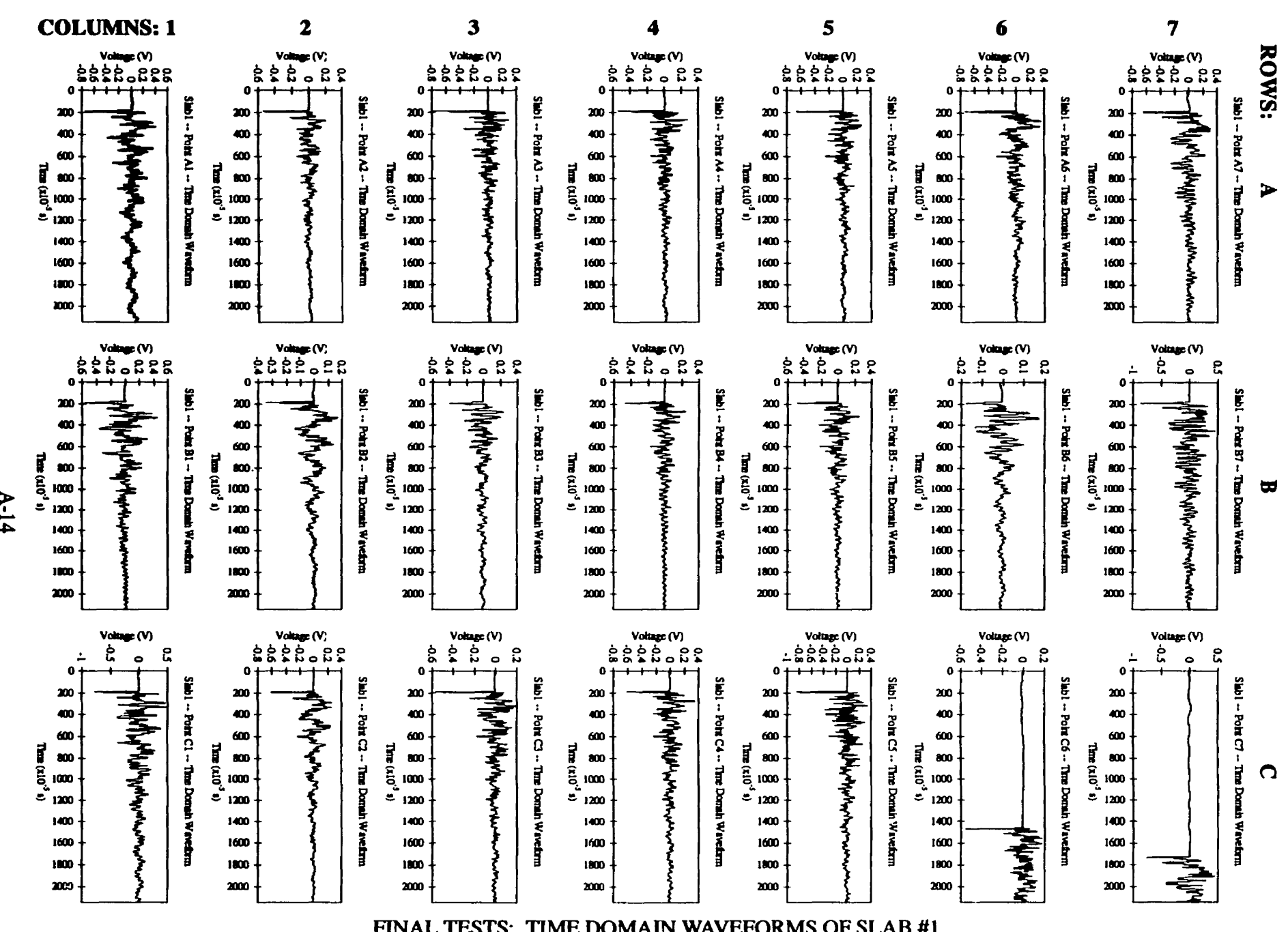
INITIAL TESTS: TIME DOMAIN WAVEFORMS OF SLAB #3 30 DEGREES PLASTIC BUBBLE WRAP ROWS A TO C



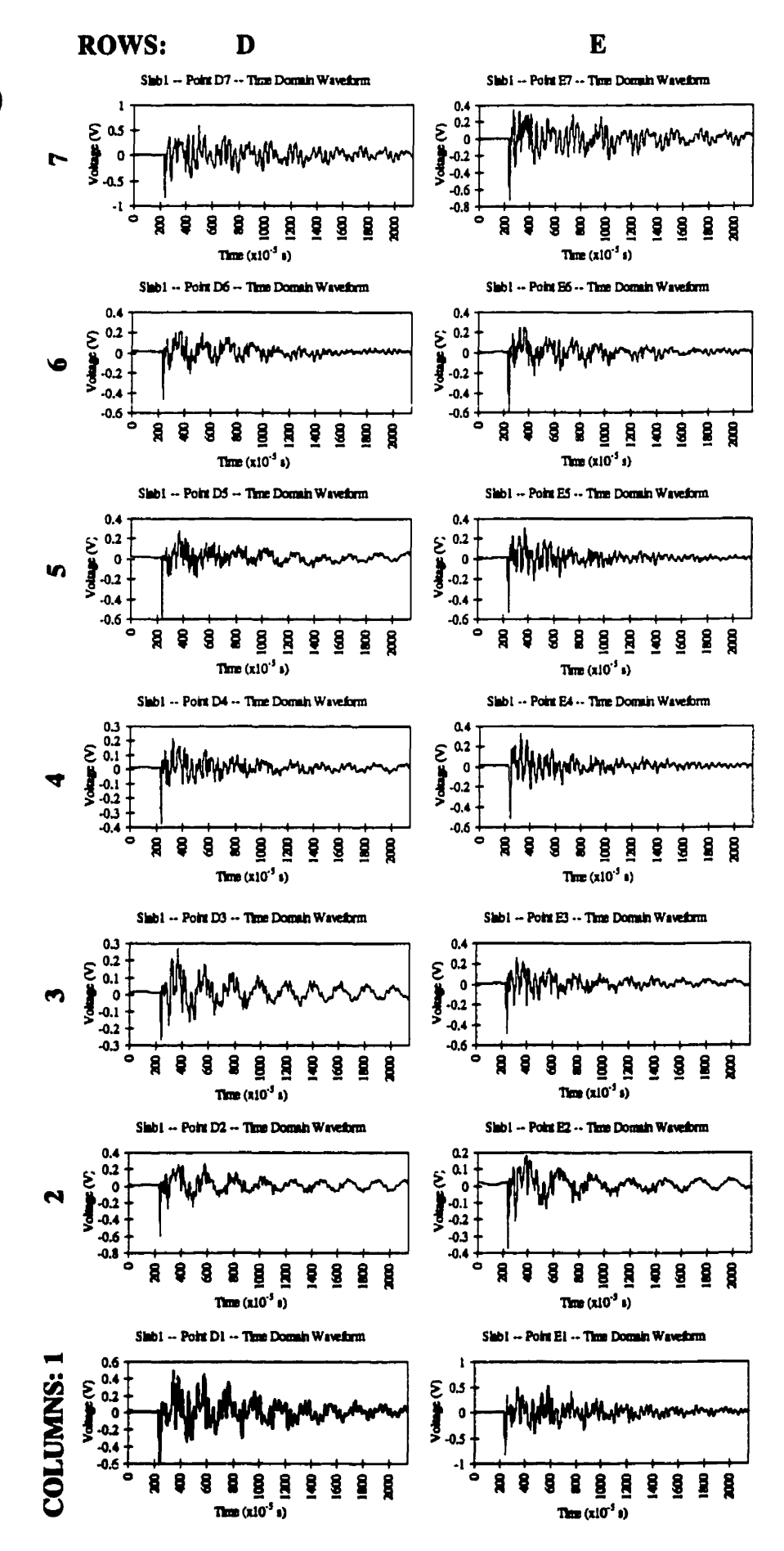


INITIAL TESTS: FREQUENCY SPECTRUMS OF SLAB #3 30 DEGREES PLASTIC BUBBLE WRAP: ROWS A TO C

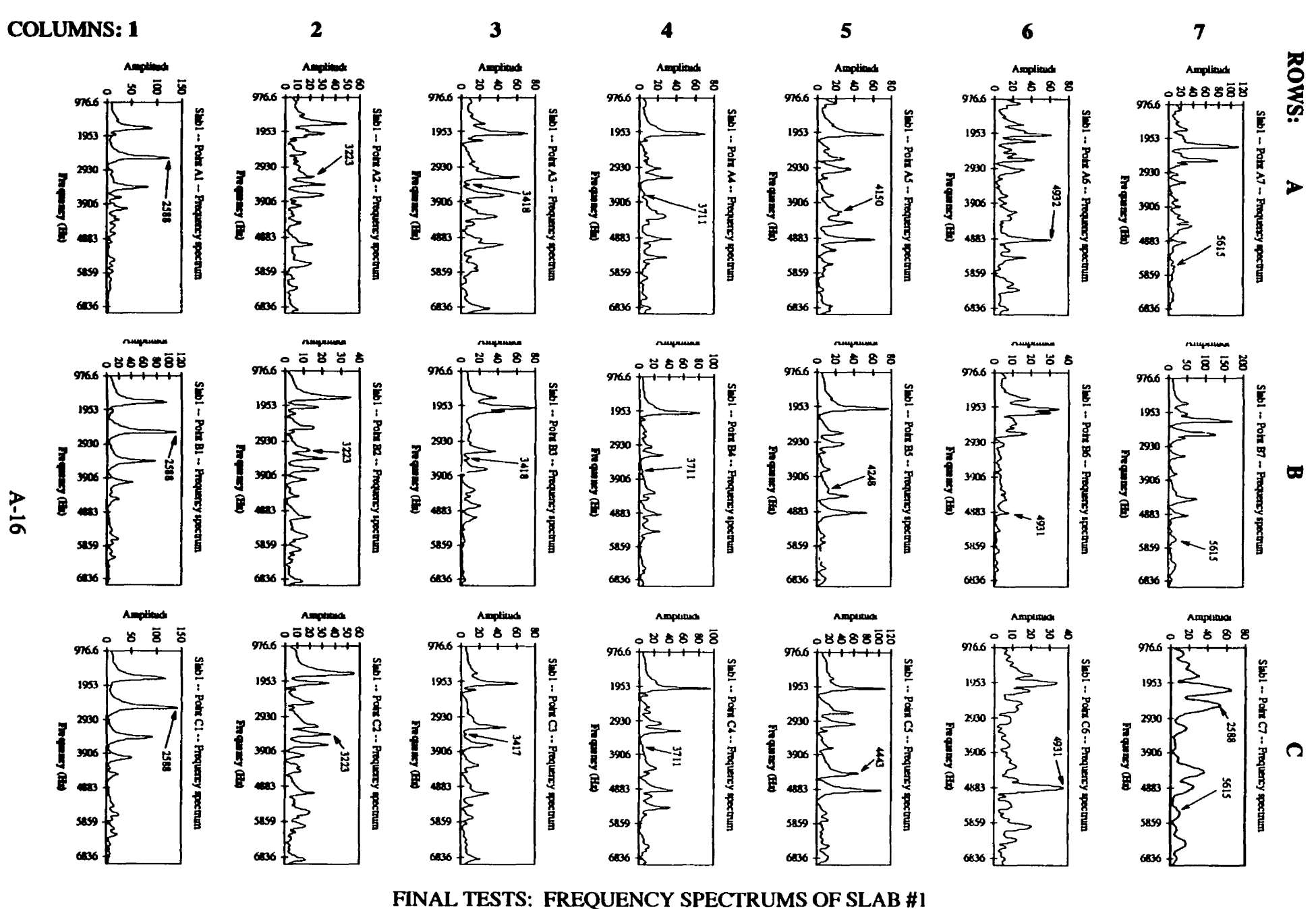




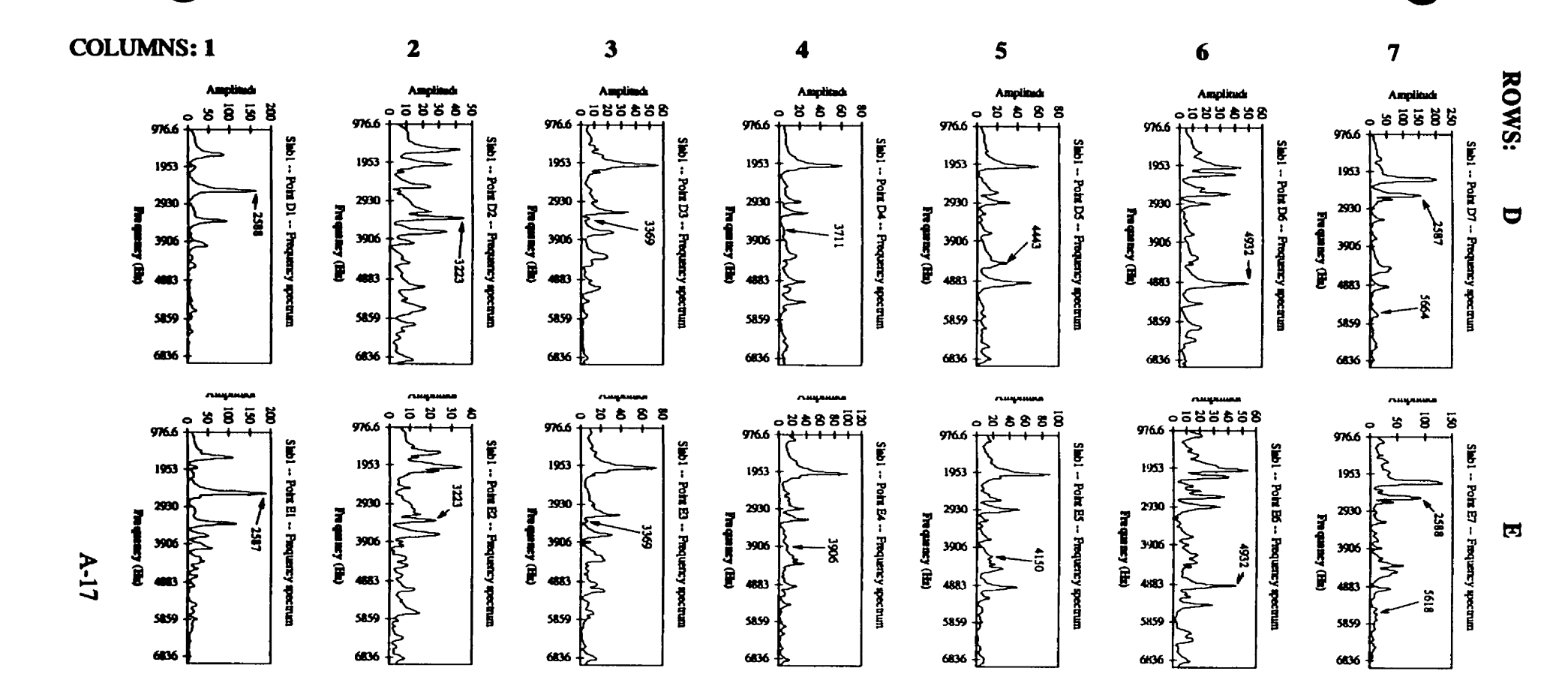
FINAL TESTS: TIME DOMAIN WAVEFORMS OF SLAB #1 30 DEGREES PLASTIC SHEET: ROWS A TO C



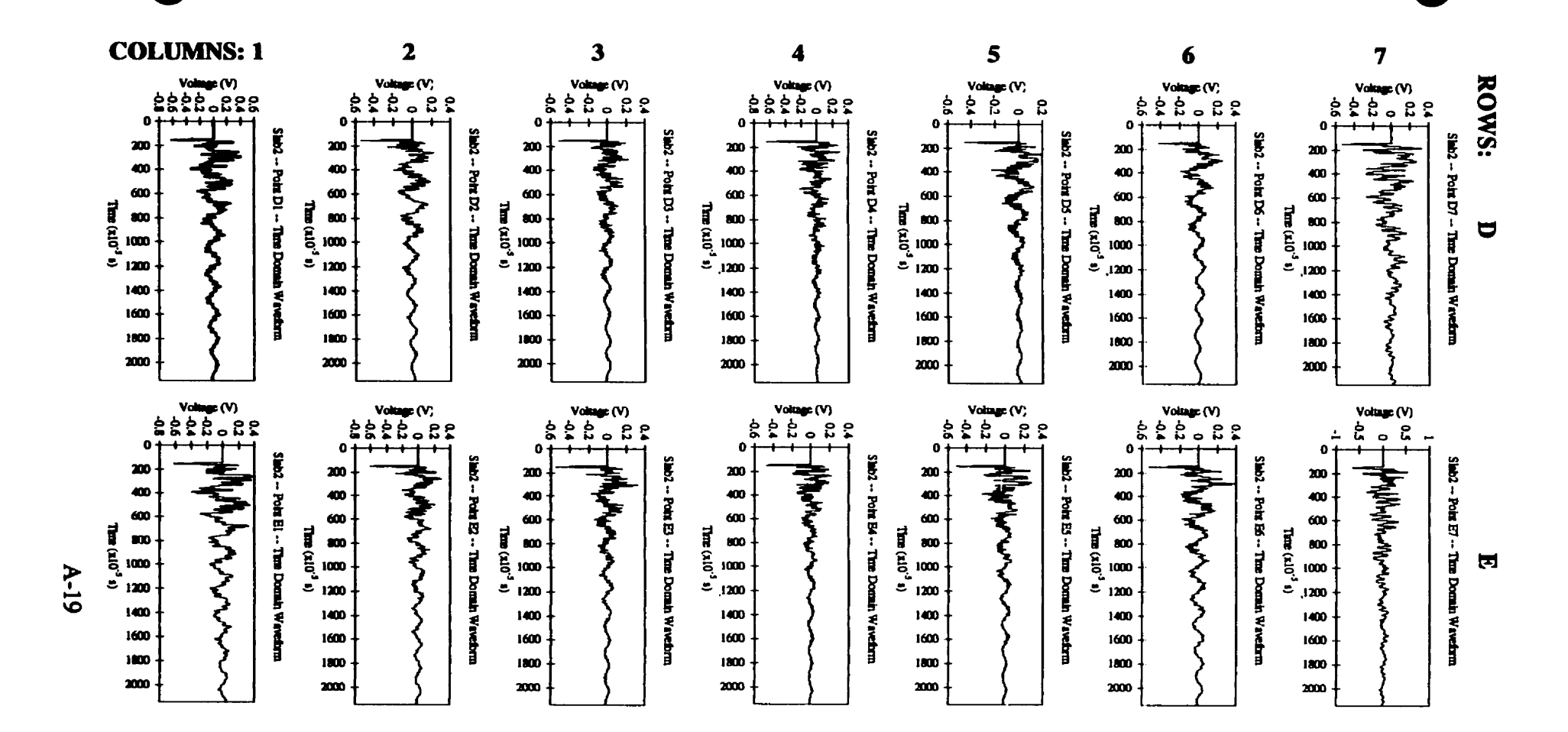
A-15

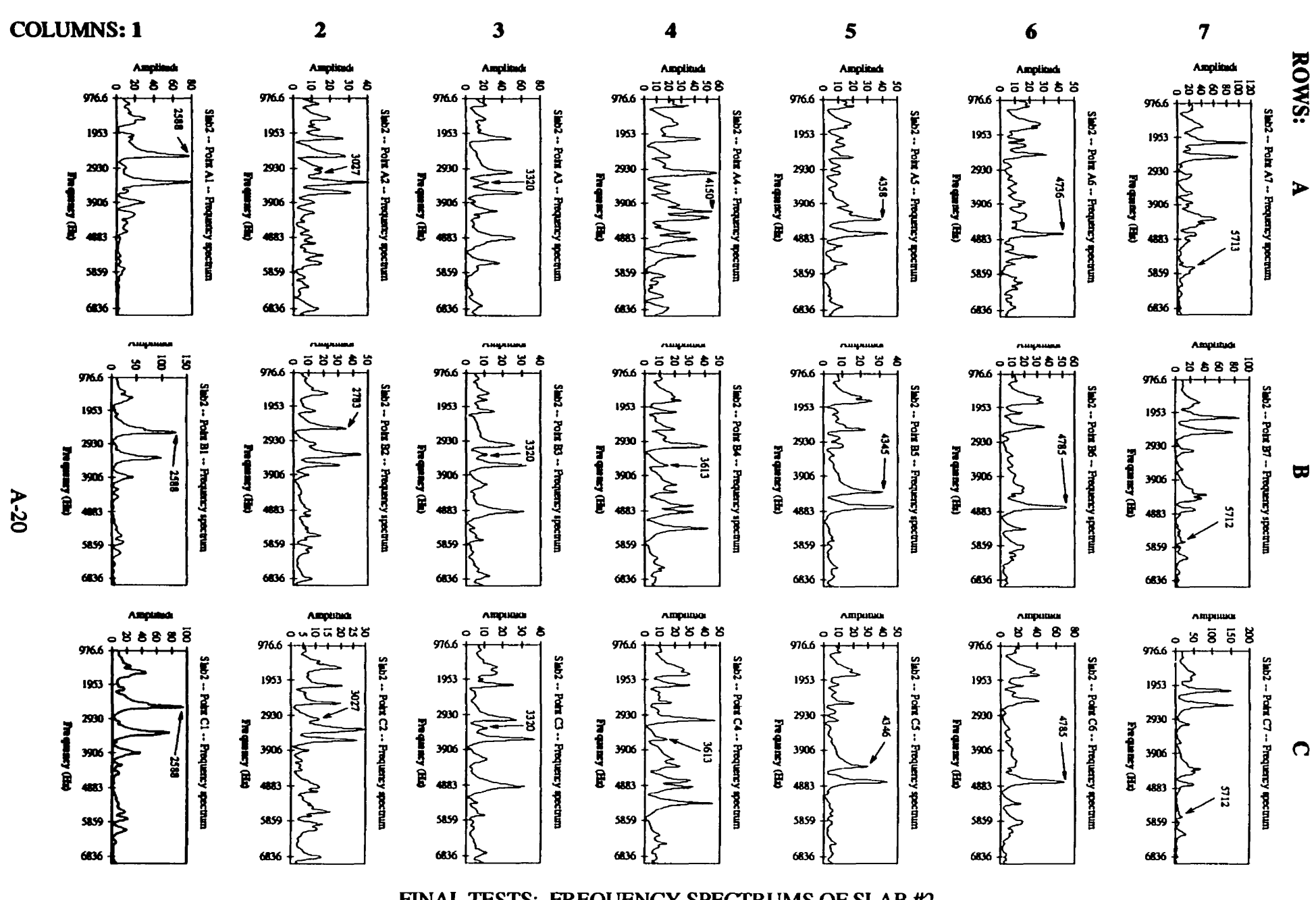


INAL TESTS: FREQUENCY SPECTRUMS OF SLAB #1
30 DEGREES PLASTIC SHEET: ROWS A TO C



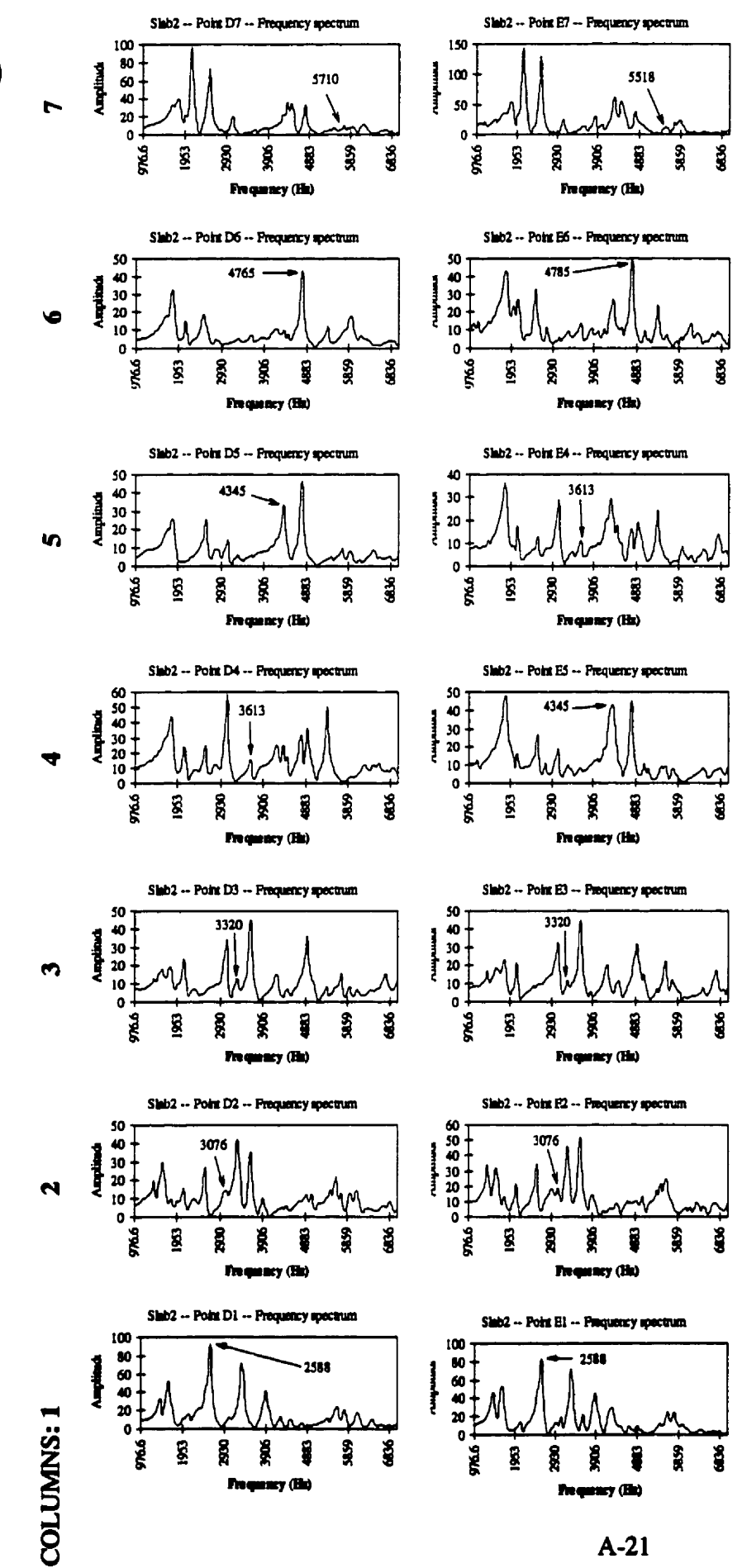
FINAL TESTS: TIME DOMAIN WAVEFORMS OF SLAB #2 30 DEGREES PLASTIC CARPET: ROWS A TO C

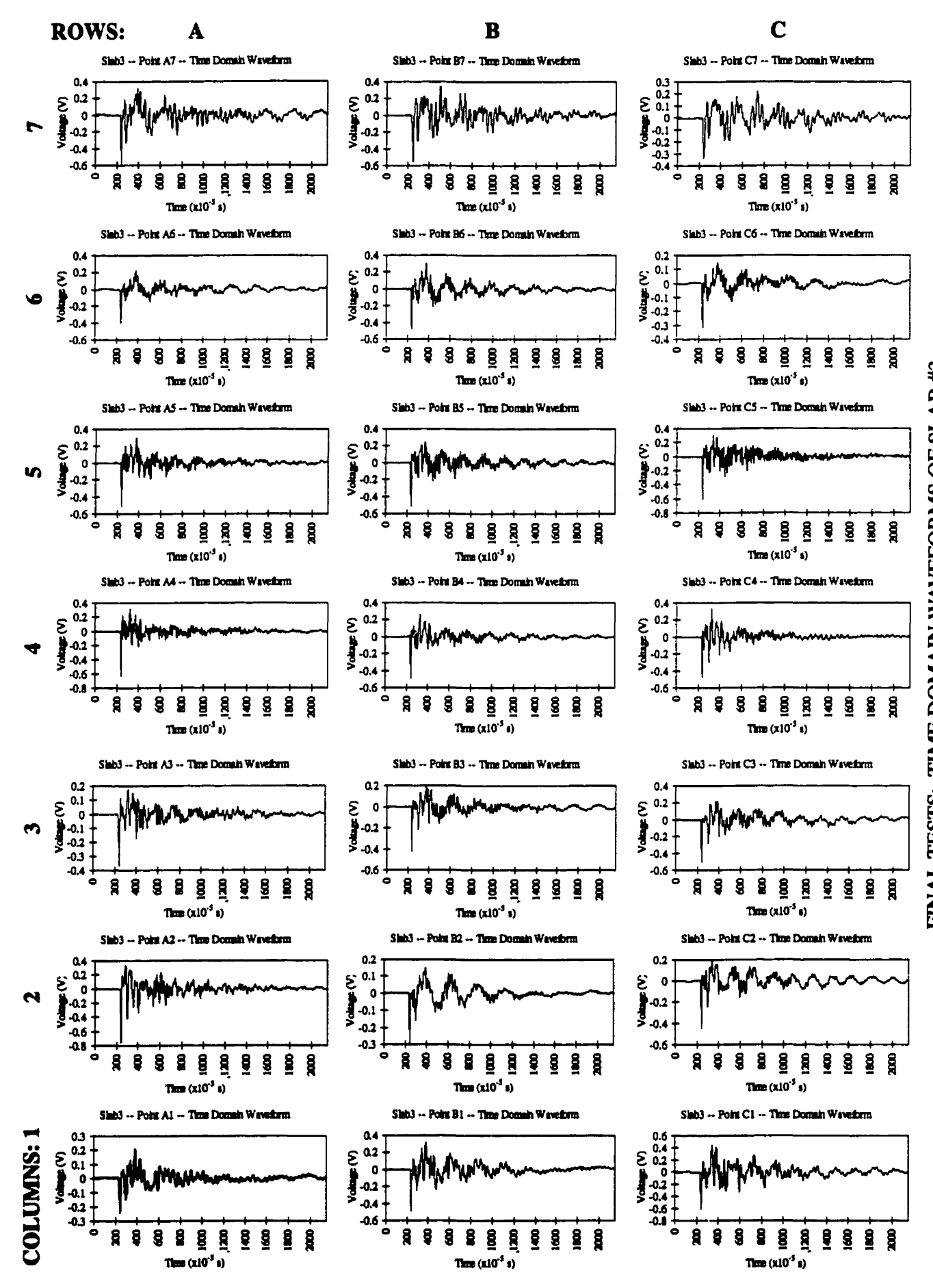




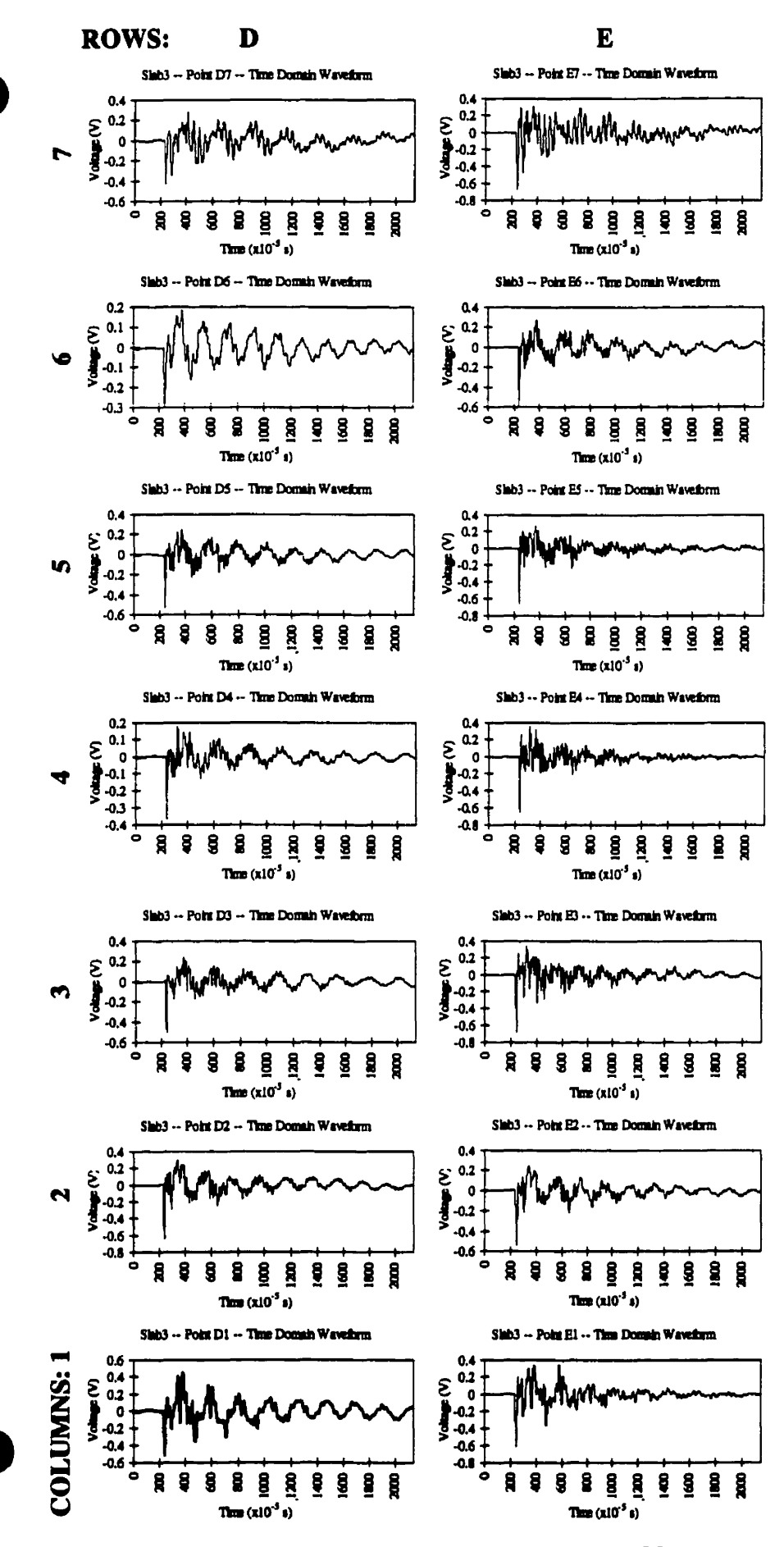
FINAL TESTS: FREQUENCY SPECTRUMS OF SLAB #2 30 DEGREES PLASTIC CARPET: ROWS A TO C

E





A-22



A-23

FINAL TESTS: FREQUENCY SPECTRUMS OF SLAB #3 30 DEGREES PLASTIC BUBBLE WRAP: ROWS A TO C

